



รายงานวิจัยฉบับสมบูรณ์

โครงการ: การจัดเรียงตัวและสมบัติทางแสงของอนุพันธ์พอลิไธโอฟืน

ในสภาวะแวดล้อมต่าง ๆ

โดย ผศ.ดร. รักชาติ ไตรผล

รายงานวิจัยฉบับสมบูรณ์

โครงการ: การจัดเรียงตัวและสมบัติทางแสงของอนุพันธ์พอลิไธโอฟิน

ในสภาวะแวดล้อมต่าง ๆ

ผู้วิจัย

สังกัด

ผศ.ดร. รักชาติ ไตรผล

ภาควิชาเคมี คณะวิทยาศาสตร์ มหาวิทยาลัยนเรศวร

สนับสนุนโดยสำนักงานคณะกรรมการการอุดมศึกษา

และสำนักงานกองทุนสนับสนุนการวิจัย

(ความเห็นในรายงานนี้เป็นของผู้วิจัย สกอ. และ สกว. ไม่จำเป็นต้องเห็นด้วยเสมอไป)

กิตติกรรมประกาศ

งานวิจัยนี้ได้รับการสนับสนุนทุนวิจัยจาก สำนักงานคณะกรรมการการอุดมศึกษาและ สำนักงานกองทุนสนับสนุนการวิจัย ผู้วิจัยขอขอบคุณหน่วยสร้างเสริมศักยภาพทางนาโนศาสตร์ และนาโนเทคโนโลยี มหาวิทยาลัยมหิดล ที่ให้การสนับสนุนเครื่องมือ AFM พร้อมทั้งอุปกรณ์อื่นๆ ในการทำงานวิจัย โดยเฉพาะอย่างยิ่ง ผศ.ดร.เติมศักดิ์ ศรีคิรินทร์ ผศ.ดร.ธีรเกียตริ์ เกิดเจริญ และ ผศ.ดร.ธนากร โอสถจันทร์ ที่ให้คำแนะนำในการใช้เครื่องมือสำหรับการทำงานวิจัยและให้ความ สะดวกในการให้ใช้สถานที่ในการทำวิจัย ซึ่งมีส่วนสำคัญในการทำให้งานวิจัยนี้สำเร็จลุล่วงไปด้วยดี รหัสโครงการ: RMU5380017

ชื่อโครงการ: การจัดเรียงตัวและสมบัติทางแสงของอนุพันธ์พอลิไธโอฟีนในสภาวะแวดล้อมต่างๆ

ชื่อนักวิจัย: ผศ.ดร. รักชาติ ไตรผล E-mail Address: rakchartt@nu.ac.th

ระยะเวลาโครงการ: 15 มิถุนายน 2553 ถึง 14 มิถุนายน 2556

บทคัดย่อ

ปัจจัยระดับโมเลกุล เช่นการเข้าจับกันภายในหรือระหว่างโมเลกุลและรูปร่างของโมเลกุล มี ผลอย่างมากต่อสมบัติของคอนจูเกตพอลิเมอร์ ในการศึกษานี้ได้ทำการเหนี่ยวนำให้ regioregular poly(3-octylthiophene) (rr-P3OT) เกิดการเปลี่ยนแปลงรูปร่างด้วยการใช้ตัวทำละลายที่ไม่ดี คือ ไซโคลเฮกเซนและเฮกเซน เมื่อสายโซ่แบบยืดออกของ *rr*-P3OT ในคลอโรเบนซีนเปลี่ยนไปเป็น แบบม้วนตัวในไซโคลเฮกเซน พบว่ามีผลทำให้เกิดการลดลงของความยาวของการเกิดคอนจูเกชั่น เทียบเท่ากับการสั้นลงของหน่วยไธโอฟีนประมาณ 6 ถึง 9 หน่วย ส่วนในเฮกเซนนั้นสายโซ่พอลิ เมอร์เกิดการเข้าซ้อนทับกันภายในโมเลกุล(intrachain aggregates) ส่งผลทำให้ความยาวของการ เกิดคอนจูเกชั่นมีค่าสูงขึ้น นอกจากนี้ยังได้ทำการศึกษาสมบัติทางแสงของ *rr*-P3OT aggregates ในระบบอื่นๆด้วย ผลจากศึกษาแสดงให้เห็นว่า aggregates ที่คายแสงไม่ได้ จะเกิดขึ้นเมื่อสายโซ่ พอลิเมอร์เข้ามาจับกันในช่วงแรก การลดลงของความสามารถในการละลายทำให้พอลิเมอร์จับกันได้ แน่นมากขึ้น ซึ่งส่งผลทำให้เกิด aggregates ที่คายแสงได้ สเปกตราการคายแสงของ aggregates ชนิดนี้จะเกิดขึ้นที่ช่วงพลังงานต่ำกว่าของโมเลกุลเดี่ยว สมบัติการดูดกลืนแสงของ aggregates ทั้ง สองชนิดนี้มีลักษณะแตกต่างกันเล็กน้อย นอกจากนี้ยังพบอีกว่าปริมาณและสมบัติของ aggregates ขึ้นอยู่กับเงื่อนไขของการเตรียมเช่นชนิดของตัวทำละลาย เป็นต้น ในส่วนสุดท้ายของการศึกษานี้ ได้ทำการเตรียมอนุภาคนาโนของคอนจูเกตพอลิเมอร์ในน้ำด้วยวิธี reprecipitation ซึ่งการเตรียมใน วิธีนี้เกี่ยวข้องกับการฉีดสารละลายพอลิเมอร์ในตัวทำละลายอินทรีย์ เข้าไปในตัวกลางน้ำที่มีปริมาณ มากเกินพอ การศึกษานี้แสดงให้เห็นว่าความสามารถในการละลายน้ำของตัวทำละลายเริ่มต้นเป็น ปัจจัยหลักที่มีผลต่อกลไกการเกิดอนุภาคนาโนของคอนจูเกตพอลิเมอร์ จากการใช้ไดคลอโรมีเทน และเตตระไฮโดรฟิวเรนเป็นตัวทำละลายเริ่มต้นนั้น พบว่ามีผลทำให้ได้อนุภาคนาโนของคอนจูเกต พอลิเมอร์ที่มีขนาดและสมบัติที่แตกต่างกันอย่างมาก

คำหลัก: conformation; conjugated polymer; photophysics; chain organization; solvent effect; nanoparticles

Project Code: RMU5380017

Project Title: Chain organization and photophysical properties of polythiophene derivatives

in different local environments

Investigator: Asst. Prof. Dr. Rakchart Traiphol

E-mail Address: rakchartt@nu.ac.th

Project Period: 15 June 2010 to 14 June 2013

Abstract

Molecular parameters such as interchain/intrachain aggregation and individual chain conformation affect the properties of conjugated polymers significantly. In this study, the conformational change of regionegular poly(3-octylthiophene) (rr-P3OT) is induced using cyclohexane and hexane as poor solvents. When the extended rr-P3OT chain in chlorobenzene transforms into coiled conformation in cyclohexane, the decrease of conjugation length is comparable to the shortening of 6 to 9 thiophene units. In hexane, the dense packing of thiophene units causes intrachain aggregation, resulting in the increase of conjugation length. We also explore the photophysical properties of rr-P3OT aggregates in different systems. Our results show that the non-emissive aggregates form in the early stage of interchain association, resulting in the formation of three redshift peaks in absorption spectrum. Further decrease of solvent quality forces dense packing of polymeric segments within the aggregates, which in turn causes the formation of emissive aggregates. The PL emission of this aggregate occurs at lower energy region compared to that of the non-aggregated chains. The non-emissive and emissive aggregates exhibit slightly different absorption bands. The amount and photophysical properties of aggregates also depend on the preparing condition such as the initial solvent. In the last part of this study, we prepare conjugated polymer nanoparticles (CPN) in water via reprecipitation technique, involving the injection of polymer solution in organic solvents into an excess amount of water. We demonstrate that water solubility of the initial solvent is a major factor dictating mechanism of the CPN formation. The use of dichloromethane and tetrahydrofuran as initial solvents provides the CPN with different sizes and properties.

Keywords: conformation; conjugated polymer; photophysics; chain organization; solvent effect; nanoparticles

คำนำ

เนื้อหาที่ได้จากโครงการวิจัยนี้ ผู้วิจัยได้ทำการจัดเตรียมเป็น manuscript ทั้งหมดแล้ว และ ได้รับการตีพิมพ์แล้วบางส่วน ซึ่ง manuscript แต่ละเรื่องนั้นมืองค์ประกอบของบทความทาง วิชาการที่ครบถ้วน และ มีการนำเสนอผลการทดลองที่ได้รวมทั้งการวิเคราะห์ผลอย่างละเอียดและ เป็นระบบ ดังนั้นเพื่อที่จะคงรูปแบบการนำเสนอผลงานวิจัยที่ได้ให้มีแบบแผนเช่นเดิม ผู้วิจัยจึงได้ นำเนื้อหาของแต่ละ manuscript มารวมกันไว้ในรายงานวิจัยฉบับนี้ ซึ่งในแต่ละส่วนก็จะมีเนื้อหาที่ จบในตัวเองพร้อมทั้งเอกสารอ้างอิง

(ผศ.ดร. รักชาติ ไตรผล) ผู้จัดทำ

บทที่ 1

Conformational Change, Intrachain Aggregation and Photophysical Properties of Regioregular Poly(3-octylthiophene) in Alkanes

Ruttayapon Potai¹, Anothai Kamphan¹, Rakchart Traiphol^{1,2*}

¹Laboratory of Advanced Polymers and Nanomaterials, Department of Chemistry and Center for Innovation in Chemistry, Faculty of Science, Naresuan University, Phitsanulok 65000, Thailand

²NANOTEC-MU Excellence Center on Intelligent Materials and Systems, Faculty of Science, Rama 6 Road, Ratchathewi, Bangkok 10400, Thailand

*Corresponding Author: Rakchart Traiphol; e-mail: rakchartt@nu.ac.th

Add cyclohexane Add hexane Intrachain aggregate Increase conjugation length Decrease conjugation length

Abstract

This study explores the role of segmental solubility of regionegular poly(3octylthiophene) (rr-P3OT) on chain organization and its photophysical properties. In good solvent chlorobenzene, rr-P3OT chain adopts an extended conformation, allowing long conjugation length of π -electrons. Cyclohexane is a good solvent for octyl side chain but a poor solvent for the thiophene backbone. The selective segmental interactions of rr-P3OT with this solvent induce conformational change of the polymer. Addition of cyclohexane into the chlorobenzene solution leads to chain coiling, which in turn causes significant decrease of the conjugation length. Absorption and photoluminescence spectra of the rr-P3OT in cyclohexane exhibit a blue shift of about 16 nm compared to those of the chlorobenzene solution. The change of chain conformation is also detectable by monitoring the variation of quantum yield upon increasing cyclohexane ratio. The quantum yield drops from 0.17 ± 0.01 to 0.11 ± 0.01 when the extended rr-P3OT chain transforms into coiled conformation. Hexane is a nonsolvent for rr-P3OT due to its relatively low solubility parameter. The addition of hexane into rr-P3OT solution in cyclohexane forces dense packing of thiophene rings within the coiled chain. An intrachain aggregation occurs in this system, leading to the appearance of three distinct red-shift peaks in absorption spectra and the drastic drop of quantum yield. Correlation between the growth of red-shift peaks and the decrease of quantum yield is clearly observed.

Keywords: conformation; conjugated polymer; photophysics; chain organization; solvent effect

INTRODUCTION

Structural-property relationship of conjugated polymers has been a subject of interest in the past few decades. This is mainly due to their potential applications in various advanced technologies such as organic light-emitting diodes^{1,2}, plastic solar cells^{3,4}, and organic field-effect transistors.^{5,6} Poly(3-alkylthiophene)s (P3ATs) is one class of conjugated polymer that receives tremendous attention. Advantages of the P3AT include high environmental stability and well-ordered semicrystalline structure.^{7,8} The close packing of conjugated backbone in their crystalline domains allows the overlap of π -orbitals, promoting charge carrier mobility.^{9,10} This characteristic is particularly important for plastic solar cell application where high degree of charge separation upon photo-irradiation is desired.^{3,4,11} The presence of alkyl side chains also allows high solubility in common organic solvents, which facilitates the fabrication of P3AT thin films in the devices via wet processes.^{7,8}

It has been demonstrated that properties of conjugated polymers can be controlled by structural modification of main chain and/or side chains. $^{8,9,11-13}$ To optimize efficiency of the aforementioned devices, tremendous effort has been dedicated for synthesizing new classes of conjugated polymers. However, other molecular parameters such as inter/intrachain aggregation and individual chain conformation also affect their properties significantly. 9,10 The stacking of conjugated backbone within aggregates promotes the overlap of π -orbitals, which in turn facilitates inter-segmental delocalization of π electrons. The aggregation of conjugated polymers normally leads to the formation of new electronic species with lower HOMO-LUMO energy gap compared to that of the isolated chain. Since the existence of aggregates strongly affects important properties of

conjugated polymers such as charge carrier mobility^{9,10,14}, photo/electroluminescence intensity and color^{1,9}, it is essential to understand molecular and experimental parameters dictating the aggregate formation. Previous studies reported by different groups have shown that the aggregation of P3AT leads to the growth of three distinct red-shift peaks in absorption spectrum.¹⁵⁻²¹ The quantum yield also decreases significantly.¹⁶

The change of individual chain conformation affects π electron delocalization along conjugated backbone. Roles of chain conformation on photophysical properties have been extensively investigated in the system of well-known poly[2-methoxy-5-(2'ethylhexyloxy)-1,4-phenylenevinylene] (MEH-PPV). 22-27 In good solvent, the conjugated polymer normally prefers extended conformation owning to its rigid backbone. ^{24,25} The conjugated chain folds or collapses in poor solvent to minimize local interactions. The presence of physical defects or kinks along the conjugated backbone of collapsed chain interrupts the delocalization of π electrons. ^{26,27} In other words, the conjugation length decreases when conjugated chain adopts folded or collapsed conformation, causing a blue shift in absorption and photoluminescence (PL) spectra. In previous studies by one of the authors, the blue shift of absorption spectrum as much as 60 nm is detected when the extended MEH-PPV chain is forced to collapse in very poor solvent.²⁷ In the system of P3AT, however, the blue shift of absorption and PL spectra is never detected in poor solvent. The decrease of solvent quality normally leads to the growth of new red-shift peaks, arising from inter-and/or intrachain aggregation. ^{10,15,19-21} Some authors also suggest the planarization of each individual chain in poor solvent. 18,28

In this study, we systematically induce conformational change of regionegular poly(3-octylthiophene) (*rr*-P3OT) using cyclohexane and hexane as poor solvents. The

solubility parameters (δ) of these solvents are much lower than that of rr-P3OT (see Table 1). However, the δ values are close to that of the octyl side chain, providing selective local polymer-solvent interactions. The hexane can only dissolve a trace amount of the polymer. The solubility of rr-P3OT increases significantly in cyclohexane, attributed its higher δ value. Therefore, cyclohexane can be used to induce chain coiling without intrachain aggregation. Atomic force microscopy (AFM) is used to follow conformational change in each system. In our study, we detect a significant blue shift in absorption and PL spectra.

TABLE 1 Properties of Solvents and Polymers 31,32,63,64

Sample	Dielectric constant	$\delta (J^{1/2} cm^{-3/2})$
Chlorobenzene	5.7	19.6
Pyridine	13.3	21.8
Cyclohexane	2.0	16.8
<i>n</i> -Hexane	1.8	14.9
n-Octane	1.9	15.5
Thiophene	2.7	20.2
rr-P3OT	-	18.2

EXPERIMENTAL

The rr-P3OT was purchased from Sigma–Aldrich. The number average molecular weight (M_n) determined by gel permeation chromatography (GPC) with polystyrene standard is 58,300 g/mol $(M_w/M_n = 2.3)$. It has been known that the GPC measurement of

rigid rod polymer usually overestimates the absolute molecular weight by a factor of about 2-2.3. 29,30 By comparing the M_n of GPC with MALDI-TOF data, the contour length of rr-P3OT in this study is approximately 51 nm. ²⁹ The regionegularity of P3OT provided by the supplier is about 98%. Solutions of rr-P3OT were prepared by dissolving powder sample in chlorobenzene (CRB) and pyridine (PRD), assisted by mechanical stirring and ultrasonication. All solvents used in this study are analytical grade. In PRD solvent, the polymer solution was stirred for several days to achieve complete dissolution. The solution appears clear to naked eyes. To vary local polymer-solvent interactions, poor solvents were added into the systems. In this study, the dissolved polymer solutions in solvents were injected into a mixture of solvent-nonsolvent under stirring. Concentration of the polymer was kept constant at 0.001 mg/mL. An inner-filtered effect is negligible at this concentration. When cyclohexane was used as a poor solvent, the ratio of the cyclohexane was varied from 0 to 100 %v/v. In this system, the properties of solution are independent of aging time. To induce larger extent of chain coiling, a nonsolvent, hexane, was added into the rr-P3OT solution in cyclohexane. Ratio of the hexane was increased up to 90 % v/v. When the hexane ratio was above 50 % v/v, it was important to use freshly prepared solutions to avoid the polymer precipitation. Absorption spectra of polymer solutions were recorded by using Analytica Specord 100 UV/vis spectrometer with 4 and 10 cm thick quartz cuvettes, depending on the polymer concentration. The measurements of photoluminescence emission (PL) spectra were carried out on Perkin-Elmer LS55 spectrometer.

The quantum yield of rr-P3OT (Φ_X) was measured by using 0.1 M NaOH aqueous solution of fluorescien (Φ_{ST} =0.79) as a standard. A series of solution exhibiting

absorbance less than 0.1 was used. The calculation was performed by using the following equation.

$$\Phi_{X} = \Phi_{ST} \left(\frac{slope_{X}}{slope_{ST}} \right) \left(\frac{\eta_{X}^{2}}{\eta_{ST}^{2}} \right)$$

The slopes ($slope_X$ and $slope_{ST}$) were obtained from the plots between integrated area of PL spectra and absorbance at the excitation wavelength. The refractive indices of solvent (η_X) and standard (η_{ST}) were taken into account in the calculation. In the system of mixtures, refractive indices were estimated by interpolation from those of the pure solvents.

Samples for AFM measurement were prepared by drop casting from 0.05 mg/mL solutions. The solution droplet was allowed to dry in a clean atmosphere under ambient condition. Three samples were prepared for each condition. Polished silicon wafer, used as a substrate, was freshly cleaned prior to the deposition. The substrate was soaked in a piranha solution (7:3 v/v of conc. H₂SO₄ and 30% H₂O₂) at 80 °C for 1 h. It was rinsed by using deionized water and dried with nitrogen gas. Morphology of self-assembled *rr*-P3OT films was explored by AFM (SPI3800N Nanoscope II, Seiko Instrument Inc., Japan) operating in a dynamic contact mode. The cantilever was fabricated from Si₃N₄ with a spring constant of about 15 N/m. At least three areas were scanned for each sample. To minimize the line broadening effect due to a finite shape of AFM tip, the width of nanostructures was measured as full width at half height.

RESULTS AND DISCUSSION

Conformational Change in Cyclohexane

Solubility parameters (δ) and dielectric constant of all solvents and rr-P3OT are listed in Table 1. The comparison of these δ values can provide an insight about local interactions between the solvent and each segment of rr-P3OT.^{18,31-33} The difference between solubility parameters of CRB and rr-P3OT is relatively small. This suggests strong polymer-solvent interactions, resulting in high solubility. PRD is a more polar solvent with higher δ value. Therefore, the PRD is a poorer solvent compared to the CRB. The weaker polymer-solvent interaction in PRD system is indicated by the decrease of polymer solubility. Cyclohexane is a non-polar solvent. It is a poor solvent for thiophene group due to the large difference of their δ values. However, the octyl side chain of rr-P3OT has strong dispersion interaction with this solvent. The disparity of these segmental interactions leads to the change of chain conformation.

Absorption and PL spectra of rr-P3OT in pure CRB and their mixtures with cyclohexane are shown in Figure 1(a,b). In good solvent CRB, the rr-P3OT chain adopts an extended conformation where dihedral angles between thiophene rings are relatively small. This allows large extent of π orbital overlapping along conjugated backbone, resulting in relatively long conjugation length. Absorption spectrum of rr-P3OT in this solvent exhibits a broad pattern with λ_{max} at 454 nm, assigned to π - π transition within conjugated backbone of the isolated chain. The PL spectrum exhibits a peak at 574 nm accompanied with vibronic shoulder at about 615 nm. When the cyclohexane is added into this system, local environment around rr-P3OT chain is altered. The absorption and PL spectra systematically shift to high energy region upon increasing the cyclohexane

ratio. The change takes place in a continuous fashion while the shape of spectra remains the same. The blue shift of about 16 nm is detected when the cyclohexane ratio reaches 100%. The position of maximum absorption and PL emission are at 438 nm and 558 nm, respectively. The variation of λ_{max} value as a function of cyclohexane ratio is shown in Figure 2. It is important to note that the blue shift of absorption and PL spectra in cyclohexane is not due to the change of dielectric constant of solvent. The use of non-polar toluene as a solvent for rr-P3OT does not provide the same result.

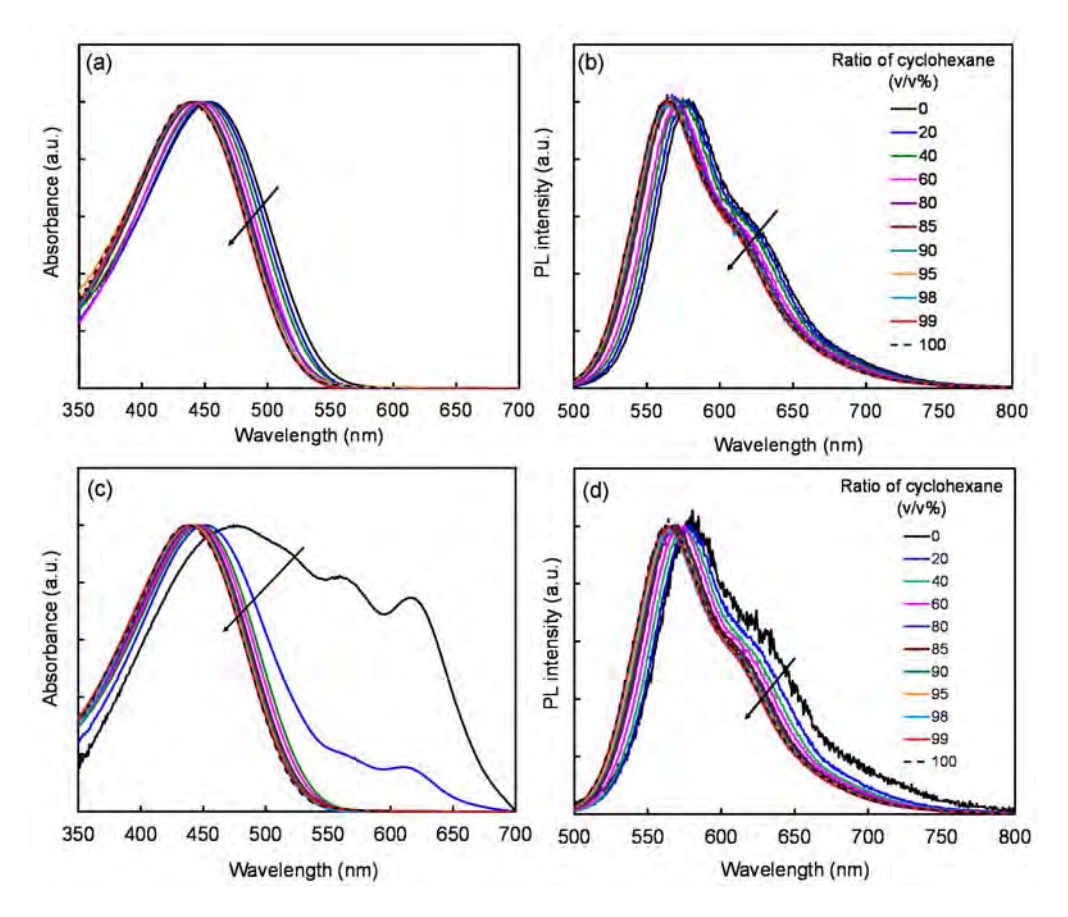


FIGURE 1 (left) Absorption and (right) PL spectra of 0.001 mg/mL *rr*-P3OT in (a, b) mixture of chlorobenzene and cyclohexane and (c, d) mixture of pyridine and cyclohexane. Arrows indicate the change of spectra upon increasing ratio of cyclohexane. All spectra are normalized for clarity.

The blue shift of absorption and PL spectra is attributed to the conformational change of rr-P3OT in cyclohexane. Previous studies by Kiriy et.al suggest that rr-P3OT can form helical conformation in the system of mixed chloroform/hexane. 39,40 In this structure, the octyl side chain extends toward the non-polar medium due to favorable dispersion interaction. The helical conformation also minimizes contact between the polar thiophene backbone and non-polar hexane. In contrast to our result, the authors observed the growth of three distinct red-shift peaks in absorption spectra upon increasing the hexane concentration. Since the red-shift peaks were still observed at extremely low polymer concentration, it was concluded that the planarization of rr-P3OT backbone occurred at a single-molecule level, resulting in the increase of conjugation length. However, the possibility of intrachain aggregation was not considered in their discussion. We believe that the rr-P3OT chain also forms helical conformation in cyclohexane. The twisting of thiophene group in the helix interrupts π -electron delocalization, causing the decrease of conjugation length. Since the solubility of rr-P3OT in cyclohexane is higher than that of the hexane, the magnitude of chain coiling and segmental packing along helical axis are expected to be lesser. Therefore, the intrachain aggregation along helical axis and/or planarization does not occur in this system.

Conjugated polymer in solution is a semiflexible chain. The chain can twist and fold causing physical defects or kinks along the conjugated backbone. Small angle neutron scattering measurements reveal that poly(3-butylthiophene) in nitrobenzene is a semiflexible chain with persistence length of about 14 thiophene units.⁴¹ Study of poly(2,5-dinonyl-*p*-phenyleneethynylene) in toluene also observes the chain bending in

dilute concentration.⁴² Since the presence of physical defects interrupts π electron delocalization, an effective conjugation length (ECL) of conjugated polymer is normally much shorter than the contour length. To further analyze our result, the ECL of *rr*-P3OT in each solvent is estimated by utilizing optical properties of its oligomers.⁴³⁻⁴⁶ Bidan et.al demonstrate that the absorption energy of regionegular oligo(3-octylthiophene)s (n = 1 to 6) varies linearly with reciprocal of the number of thiophene rings (n).⁴³ The obtained linear relationship is shown in equation (1).

$$E_{(eV)} = 2.54 + \frac{3.15}{n} \tag{1}$$

The ECL of rr-P3OT in chlorobenzene and cyclohexane is estimated by substituting the absorption energy (in eV unit) into (1). This calculation yields ECL of rr-P3OT in chlorobenzene and cyclohexane equivalent to about 17 and 11 thiophene units. However, several studies have shown that deviation from linear equation (1) occurs when the size of oligomers becomes relatively long. Meier suggests an exponential relationship between absorption energy and n as shown in equation (2), which takes into account the convergent behavior of λ_{max} of the long oligomers.

$$\lambda_{\max}(n) = (\lambda_{\infty} - \lambda_1)e^{-b(n-1)}$$
 (2)

The λ_1 , $\lambda_{max}(n)$ and λ_{∞} are the maximum absorption wavelength of monomer, oligomers and polymer, respectively. The convergent factor b can be obtained by fitting optical properties of oligomers⁴³ and rr-P3OT ($\lambda_{\infty} = 454$ nm), which provides the b value of 0.308 (regression coefficient = 0.99). The ECL is estimated by substituting b value into equation (3).

$$n_{ECL} = \frac{\ln(\lambda_{\infty} - \lambda_{1})}{h} + 1 \tag{3}$$

The ECL of rr-P3OT in chlorobenzene is equivalent to 18 thiophene units. For cyclohexane system, the ECL is estimated by substituting $\lambda_{max}(n) = 438$ nm into equation (2), which yields n = 9 thiophene units. These data analysis demonstrates significant decrease of ECL in cyclohexane due to the conformational change of rr-P3OT.

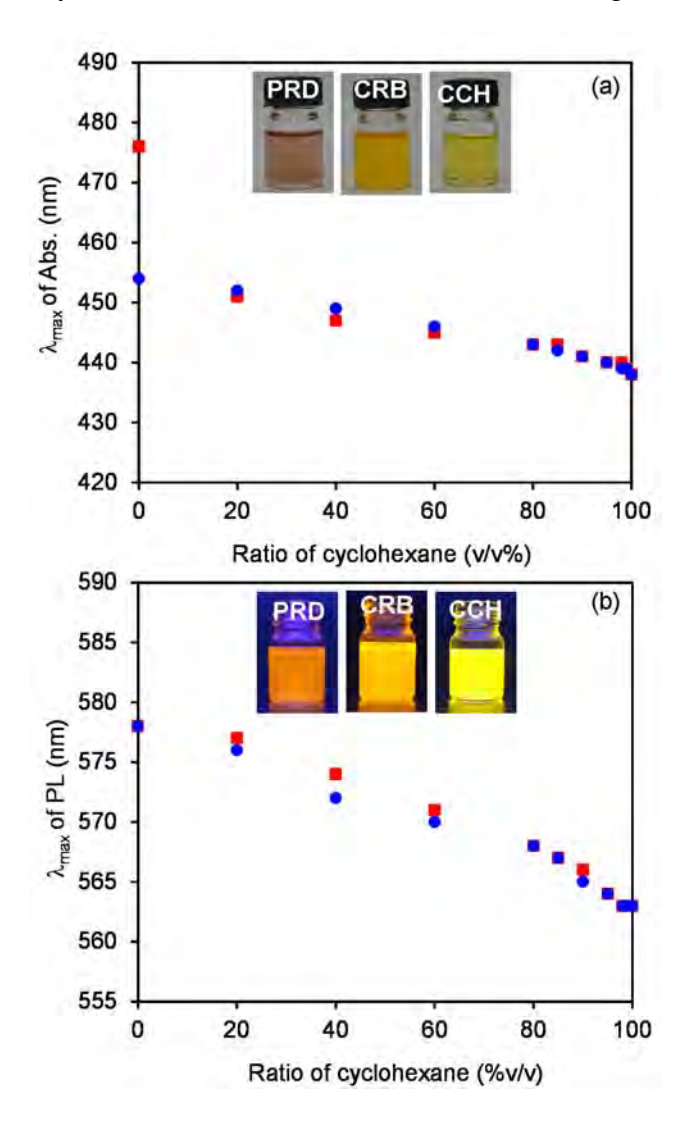


FIGURE 2 Variation of (a) λ_{max} of absorption and (b) PL spectra upon increasing ratio of cyclohexane (CCH) in rr-P3OT solutions. The initial solvents are (circle) chlorobenzene (CRB) and (square) pyridine (PRD). Insets show photographs of rr-P3OT in the pure solvents taken in (a) ambient condition and (b) under UV light irradiation.

In the system of pyridine, the polymer-solvent interactions are relatively weak. The rr-P3OT chains are forced to assemble into aggregates, indicated by the presence of three red-shift peaks at about 515 nm, 560 nm and 616 nm in absorption spectrum (see Figure 1c). Previous studies suggests that the improved π - π stacking causes the increase of conjugated length within aggregates. 9,24,26,29,47 The PL intensity also drops significantly compared to that of the chlorobenzene system. However, the shape and peak position of PL spectrum still resemble those of the isolated chain. This result suggests that the aggregates of rr-P3OT in pyridine are the non-emissive species. This type of aggregates was also observed in the system of poly(9,9-di(2-ethylhexyl)fluorene).⁴⁸ When a small amount of cyclohexane is added into the system, the red-shift peaks in absorption spectrum decrease significantly. The λ_{max} also shifts from 476 nm to 452 nm. This observation indicates that the enhanced dispersion interaction between octyl side chain of rr-P3OT and cyclohexane leads to the dissociation of aggregates. At 40 %v/v of cyclohexane, the red-shift peaks disappear and the shape of absorption spectrum is similar to that of the chlorobenzene system. At this stage, the rr-P3OT chains separate from each other. The systematic blue shift of absorption and PL spectra occurs upon increasing cyclohexane ratio to 99 %v/v, indicating the conformational change. The decrease of λ_{max} is comparable to the system of chlorobenzene (see Figure 2). Therefore, the polarity of initial solvent hardly affects the magnitude of conformational change of rr-P3OT.

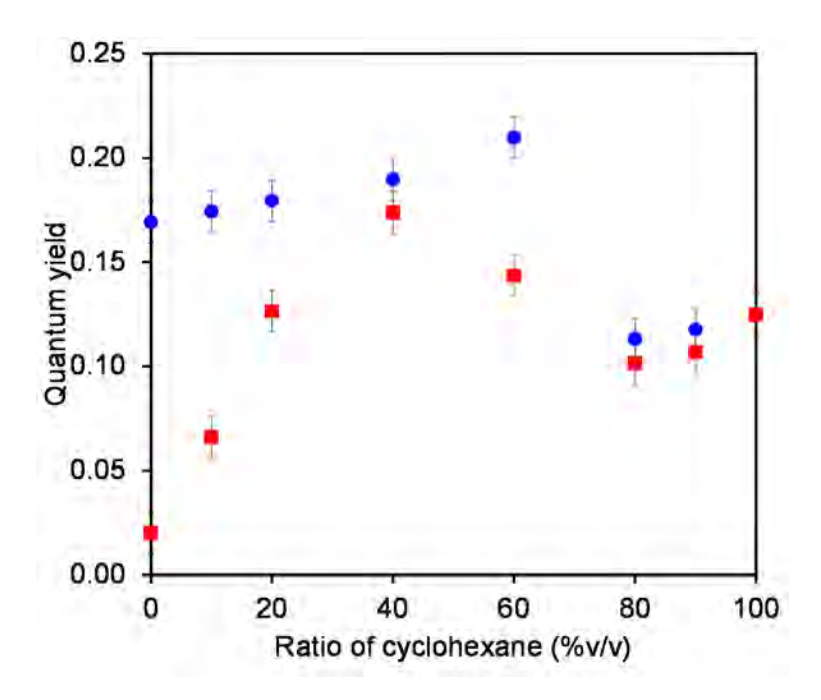


FIGURE 3 Variation of quantum yield of *rr*-P3OT in mixed solutions. (circle) Mixtures of chlorobenzene/cyclohexane and (square) mixtures of pyridine/cyclohexane.

The change of chain conformation significantly affects the quantum yield of rr-P3OT. The extended chain in chlorobenzene exhibits a quantum yield of about 0.17±0.01. The addition of cyclohexane ratio up to 60 % v/v leads to continuous increase of quantum yield to 0.21±0.01 (see Figure 3). This is probably due to the change of local polymer-solvent interactions and conformational change of rr-P3OT, affecting the radiative de-excitation pathways of excited π electrons. However, it is not trivial to separate these two effects because they are closely related. Interestingly, significant drop of quantum yield to 0.11±0.01 occurs upon increasing the cyclohexane ratio to 80% v/v. The discontinuous change of quantum yield indicates an abrupt increase of non-radiative de-excitation processes within the system. This behavior can not be attributed to the

change of solvent composition because the quantum yield remains roughly constant at higher cyclohexane ratio. We believe that the magnitude of chain coiling or shrinking at this stage is relatively large, causing intrachain-segmental interactions. This leads to the drop of quantum yield similar to the effect of inter/intrachain aggregation. However, the strength of segmental interactions within aggregates is much stronger, leading to the growth of new absorption peaks and further drop of quantum yield. The presence of aggregates in pyridine system causes the decrease of quantum yield to about 0.02 ± 0.01 . The aggregates dissociate upon increasing cyclohexane ratio, leading to systematic increase of quantum yield as shown in Figure 3. At 40 %v/v of cyclohexane, the chains are in isolated conformation. Therefore, the quantum yield of rr-P3OT at this stage is comparable to that of the chlorobenzene system. The significant drop of quantum yield is detected at higher cyclohexane ratio.

AFM is utilized to investigate the conformational change of rr-P3OT. Samples are prepared by drop-casting from different solutions onto flat SiO_x/Si substrate where the isolated chains assemble into large domains. Although the AFM does not directly reveal the conformation of isolated chain, morphology of the assembled domains can reflect the conformation of individual chains. The self-assembling from pure chlorobenzene leads to the formation of nanoribbons and clusters (see Figure 4a). It has been observed in different types of conjugated polymers that their rigid rod nature drives the formation of nanoribbons. $^{18,50-52}$ In this structure, the main chains arrange parallel to each other perpendicular to the nanoribbon axis. $^{7,47,53-57}$ The width of nanoribbons is defined by contour length of conjugated backbone. The nanoribbons of rr-P3OT in this study exhibit a width of about 60.2 ± 7.5 nm, consistent with its contour length. When the

sample is prepared from pyridine solution, spherical nanoparticles with large size distribution are observed as shown in Figure 4b. We believe that these nanoparticles form in solution due to relatively weak polymer-solvent interactions. The segmental aggregation occurs within these nanoparticles. We note that micron-size particles are also detected in some areas of the sample. The addition of 50% v/v cyclohexane into chlorobenzene solution leads to the formation of flat sheet-like structure with homogeneous thickness of about 11.7 ± 1.8 nm (see Figure 4d). Width of the nanosheets is in a micron range. We suggest that the rr-P3OT chains are still extended at this condition. These extended chains arrange into the nanosheets where their thickness depends on number of the stacked rr-P3OT layers. This hypothesis is parallel with molecular packing model suggested by previous works.⁵³⁻⁵⁷ The width of nanosheets is much larger than that of the nanoribbons, attributed to the decrease of polymer solubility. In the system of pyridine and 50% v/v cyclohexane, we also observe the formation of nanosheets (see Figure 4e). The sheet thickness, however, increases to about 17.7 ± 2.2 nm. Some nanoparticles are still detected. This result indicates that the addition of 50% v/v cyclohexane causes the dissociation of aggregates. The chains also become extended prior to the assembling into nanosheets.

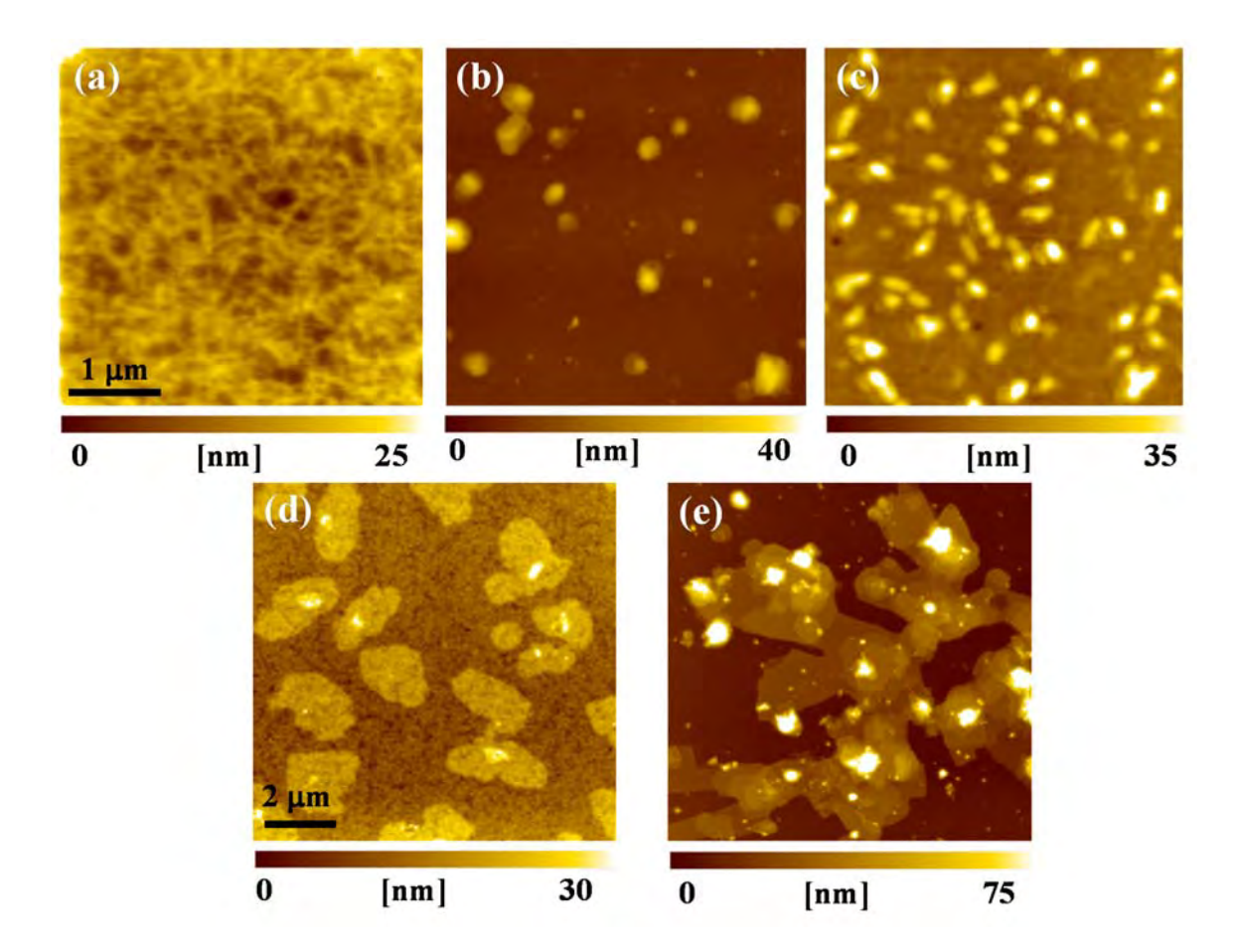


FIGURE 4 AFM topography images of *rr*-P3OT on silicon wafer prepared by drop casting from 0.05 mg/mL solution in (a) chlorobenzene, (b) pyridine, (c) cyclohexane, (d) mixed chlorobenzene/cyclohexane (50:50 v/v%) and (e) mixed pyridine/cyclohexane (50:50 v/v%). Scale bars are 1 μ m for (a,b,c) and 2 μ m for (d,e).

The preparation of thin films from rr-P3OT solution in pure cyclohexane provides rather different morphology. We observe the formation of dot-like and rod-like structures (see Figure 4c). The width and thickness of these structures are quite uniform, about 135 \pm 6.8 nm and 21.8 \pm 3.3 nm, respectively. Some of the dots also arrange into nanorods. Previous studies by Kiriy et. al observe one dimensional aggregation of rr-P3OT and rr-

P3HT in the mixtures of chloroform and hexane, yielding micron-long nanorods.^{39,40} Based on the width of nanorods, the authors suggest that helical coils of the polymers aggregate in one dimensional direction. The width of nanorods in this study is much larger than that of the previous studies. It cannot be attributed to the diameter of single helical coil. However, we still observe the aggregation of nanodots in one dimensional direction. We suggest that multiple helical coils assemble to form the nanodots and nanorods in this study. The formation of helical coil aggregates has been observed in the systems of polythiophene derivatives.⁵⁸⁻⁶⁰ It is important to note that the self-assembling of *rr*-P3OT in a random fashion will lead to the formation of nanoparticles as detected in the system of pure pyridine.

Intrachain Aggregation in Hexane/Cyclohexane

In this section, the conformational change of rr-P3OT is further induced by addition of hexane into the cyclohexane solution. From Table 1, the solubility parameters (δ) of rr-P3OT, cyclohexane and hexane are 18.2, 16.8 and 14.9 J^{1/2} cm^{-3/2}, respectively. In general, the solubility of polymer in solvent is reduced when the difference between their δ values is large.³¹ The δ value of hexane is 1.9 J^{1/2} cm^{-3/2} lower than that of the cyclohexane, which leads to the reduction of rr-P3OT solubility. Therefore, the magnitude of helical coiling is expected to increase upon increasing the hexane ratio. Absorption and PL spectra of rr-P3OT in cyclohexane/hexane mixtures are shown in Figure 5. The addition of 30% v/v hexane does not cause the blue shift of absorption and PL spectra, indicating that the conjugation length of rr-P3OT still remains the same. An increase of hexane ratio to 40% v/v leads to the growth of red-shift peaks. The

absorbance of these new peaks increases systematically upon increasing the hexane ratio. At 90% v/v hexane, the red-shift peaks are at about 525 nm, 558 nm and 605 nm. Since the red-shift peaks are still detected at extremely low concentration of the polymer (see Figure 6), this phenomenon is likely to occur at a single-molecule level. Kiriy et.al suggests that the formation of helical coil causes planarization of the conjugated backbone, which in turn results in the increase of conjugation length. 39,40 Their computational study shows that the dense packing of thiophene rings along helical axis limits the dihedral SCCS angle to about 1 to 6 °C. They also observe that it takes about 12 thiophene units to complete one turn of the helix. However, our calculation by utilizing equation (1) indicates that the fully extended rr-P3OT chain (n = ∞) yields λ_{max} of about 488 nm. This number is much lower than the detected λ_{max} values in mixed cyclohexane/hexane. Therefore, the backbone planarization is not a sole factor causing the growth of red-shift peaks in absorption spectra. We suggest that the intrachain aggregation also contributes to the increase of conjugation length. The decrease of solvent quality forces the packing of main chain along helical axis, allowing the overlap of π orbitals. The enhanced π electron delocalization leads to the formation of new electronic species with lower HOMO-LUMO gap. 61,62 The transition between two distinct electronic species is indicated by the observation of isosbestic point in Figure 5. However, it is not trivial to separate the effects from those two phenomena. This is mainly because the conjugated backbones become planar when they stack on top of each other to form aggregates. 18,21,56

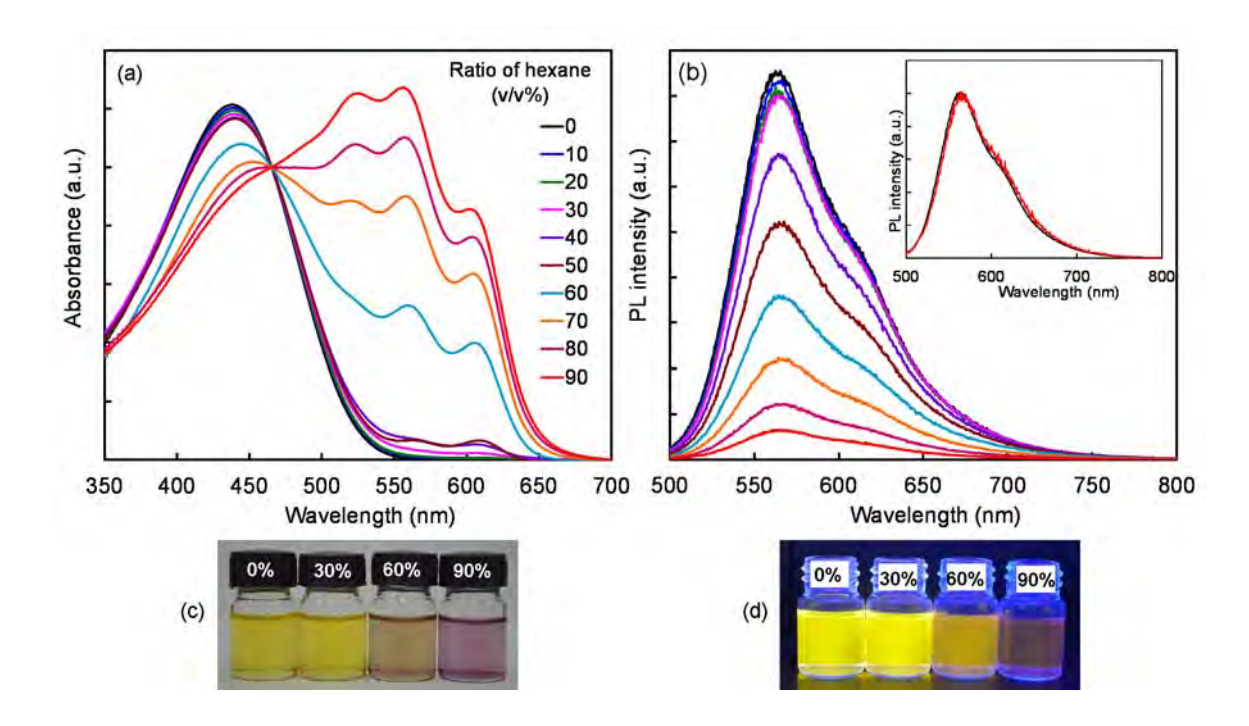


FIGURE 5 (a) Absorption and (b) PL spectra of 0.001 mg/mL *rr*-P3OT in mixtures of cyclohexane and hexane. The inset compares PL spectra of *rr*-P3OT in pure cyclohexane and mixture with 90 %v/v hexane. Photographs of *rr*-P3OT in mixtures of cyclohexane and hexane in (c) ambient condition and (d) under UV light irradiation.

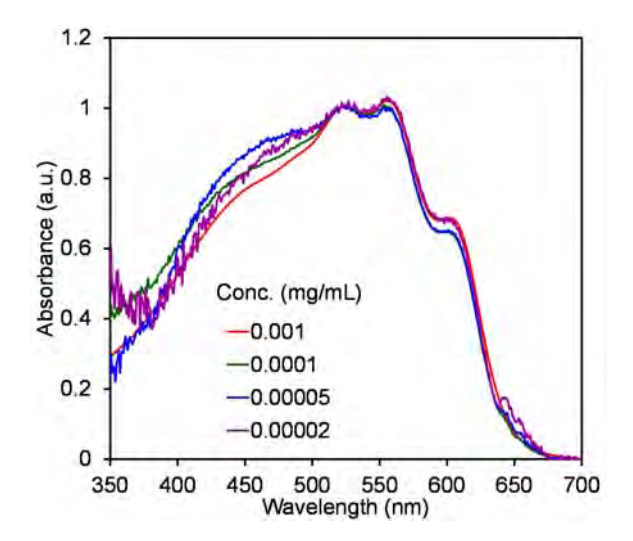


FIGURE 6 Normalized absorption spectra of rr-P3OT in mixture of cyclohexane and 90 %v/v hexane. Polymer concentration ranges from 1 x 10⁻³ to 2 x 10⁻⁵ mg/mL.

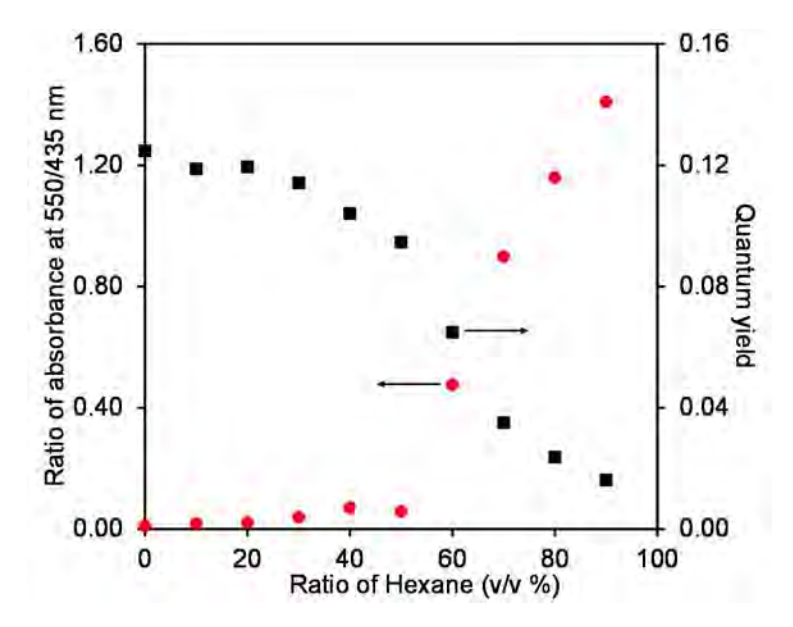


FIGURE 7 Variation of absorbance at 550/435 nm and quantum yield upon increasing hexane ratio. The error bars of quantum yield are omitted for clarity of presentation.

The intrachain aggregation is also indicated by the decrease of quantum yield. Figure 5b shows systematic decrease of PL intensity upon increasing the hexane ratio. Correlation between the growth of red-shift peaks and quantum yield of *rr*-P3OT is illustrated in Figure 7. The ratio of absorbance at 550/435 nm reflects the aggregate fraction within the system. An increase of hexane ratio to 30% v/v hardly affects the absorption spectra and quantum yield of *rr*-P3OT. The appearance of small red-shift peaks at 50% v/v hexane causes slight decrease of the quantum yield. The aggregate fraction increases abruptly at higher hexane ratio, which in turn causes a sharp drop of quantum yield. At 90% v/v hexane, the quantum yield of *rr*-P3OT is comparable to the system of pure pyridine, also containing large aggregate fraction. AFM measurements also show supporting results (see Figure 8). When the sample is prepared from the

solution containing 40%v/v hexane, we observe sheet-like structure with thickness of about 8.1 ± 1.0 nm. Some nanoparticles are also detected. At 60%v/v hexane, the amount of these nanoparticles increases significantly. They assemble into large clusters in the thin film. We believe that the intrachain aggregation takes place within these nanoparticles. The formation of large cluster is an indication of sudden decrease of the polymer solubility. It is worthwhile to note that one dimensional aggregation is not observed in our system. This is probably due to the difference of solvent used in the previous study.

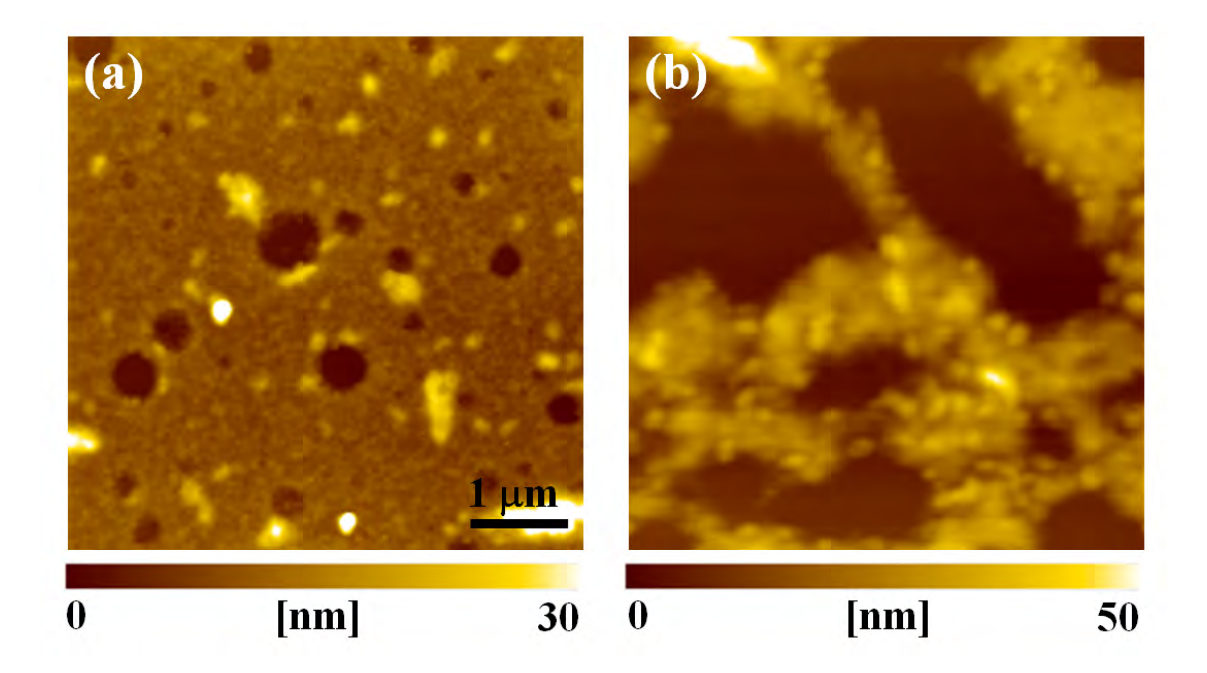


FIGURE 8 AFM topography images of rr-P3OT on silicon wafer prepared by drop casting from 0.05 mg/mL solution in (a) mixed cyclohexane/hexane (60:40 v/v%) and (b) mixed cyclohexane/hexane (40:60 v/v%).

The PL pattern hardly changes upon increasing the hexane ratio (see inset of Figure 5b). This is in contrast to the results from absorption spectra, which detect a significant red-shift. The PL spectrum of rr-P3OT solution containing 90% v/v hexane still exhibits λ_{max} at about 558 nm, which is the same as that of the pure cyclohexane system. This observation indicates that the aggregates in this system are the non-emissive species. The observed PL intensity arises from the photoemission of non-aggregated segments within the system. We also observe that PL spectrum of rr-P3OT in pyridine is detected at lower energy region compared to the system of mixed cyclohexane/hexane. The λ_{max} is detected at 574 nm. This λ_{max} value is equal to that of the extended rr-P3OT chain is pure chlorobenzene. Therefore, the conformation of non-aggregated chain does not change in the pyridine. In system of cyclohexane/hexane, the chain form helical coil, resulting in the decrease of conjugation length, before the intrachain aggregation takes place.

CONCLUSION

In this study, we have shown that conformational change of *rr*-P3OT chain occurs in cyclohexane solution. The unfavorable interaction between thiophene conjugated backbone and the non-polar solvent induces chain coiling, which in turn causes the decrease of effective conjugation length (ECL). When the extended *rr*-P3OT chain in chlorobenzene transforms into coiled conformation in cyclohexane, the decrease of ECL is comparable to the shortening of about 6 to 9 thiophene units. The chain coiling in cyclohexane also causes the drop of quantum yield. The extent of chain coiling is further induced by addition of a nonsolvent hexane. The dense packing of thiophene units within

the coiled chain allows intrachain aggregation, which is responsible to appearance of three red-shift peaks in absorption spectrum and the drastic drop of quantum yield. We also observe that the intrachain aggregates are the non-emissive species. Our study clearly distinguishes the effects of individual chain conformation and segmental aggregation on photophysical properties of polythiophene derivative.

ACKNOWLEDGMENTS

This research is financially supported by the Thailand Research Fund, Ministry of Higher Education and Naresuan University (Grant RMU5380017). RP thanks the Office of Higher Education Commission for supporting her Ph.D. scholarship under the program Strategic Scholarships for Frontier Research Network. This work has partially been supported by the Nanotechnology Center (NANOTEC), Ministry of Science and Technology, Thailand, through its program of center of Excellence Network. RT thanks Center for Innovation in Chemistry (PERCH-CIC) for supporting some research facilities.

REFERENCES AND NOTES

- 1. Y. Chen, D. Ma, J. Mater. Chem. 2012, 22, 18718-18734.
- R. R. Søndergaard, M. Hösel, F. C. Krebs, J. Polym. Sci. Part B: Polym. Phys.
 2013, 51, 16–34.
- 3. W. Cai, X. Gong, Y. Cao, Sol. Energy Mater. Sol. Cells **2010**, 94, 114-127.
- 4. S. Günes, H. Neugebauer, N. S. Sariciftci, Chem. Rev. 2007, 107, 1324-1338.
- 5. C. Wang, H. Dong, W. Hu, Y. Liu, D. Zhu, Chem. Rev. 2011, 112, 2208-2267.

- S. Kola, J. Sinha, H. E. Katz, J. Polym. Sci. Part B: Polym. Phys. 2012, 50, 1090-1120.
- 7. R. D. McCullough, *Adv. Mater.* **1998**, *10*, 93-116.
- 8. I. Osaka, R. D. McCullough, Acc. Chem. Res. 2008, 41, 1202-1214.
- F. J. M. Hoeben, P. Jonkheijm, E. W. Meijer, A. P. H. J. Schenning, *Chem. Rev.* 2005, 105, 1491-1546.
- O. A. Gus'kova, P.G. Khalatur, A. R. Khokhlov, *Macromol. Theory Simul.* 2009, 18, 219–246.
- 11. A. Facchetti, *Chem. Mater.* **2011**, *23*, 733-758.
- 12. Z. B. Henson, K. Müllen, G. C. Bazan, Nature Chem. **2012**, *4*, 699-704.
- M. Theander, O. Inganäs, W. Mammo, T. Olinga, M. Svensson, M. R. Andersson,
 J. Phys. Chem. B 1999, 103, 7771-7780.
- 14. J. D. Myers, J. Xue, *Polym. Rev.* **2012**, *52*, 1-37.
- S. D. D. V. Rughooputh, S. Hotta, A. J. Heeger, F. Wudl, J. Polym. Sci. Part B: Polym. Phys. 1987, 25, 1071-1078.
- G. Rumbles, I. D. W. Samuel, L. Magnani, K. A. Murray, A. J. DeMello, B. Crystall, S. C. Moratti, B. M. Stone, A. B. Holmes, R. H. Friend, Synth. Met. 1996, 76, 47-51.
- 17. R. Potai, R. Traiphol, *J. Colloid Interface Sci.* (2013), http://dx.doi.org/10.1016/j.jcis.2013.04.022
- S. Samitsu, T. Shimomura, S. Heike, T. Hashizume, K. Ito, *Macromolecules* 2008, 41, 8000-8010.

- Y. D. Park, H. S. Lee, Y. J. Choi, D. Kwak, J. H. Cho, S. Lee, K. Cho, Adv. Funct. Mater. 2009, 19, 1200-1206.
- S. Sun, T. Salim, L. H. Wong, Y. L. Foo, F. Boey, Y. M. Lam, J. Mater. Chem.
 2011, 21, 377-386.
- 21. C. Scharsich, R. H. Lohwasser, M. Sommer, U. Asawapirom, U. Scherf, M. Thelakkat, D. Neher, A. Köhler, J. Polym. Sci. Part B: Polym. Phys. 2012, 50, 442-453.
- 22. T.-Q. Nguyen, I. B. Martini, J. Liu, B. J. Schwartz, *J. Phys. Chem. B* **1999**, *104*, 237-255.
- R. Traiphol, R. Potai, N. Charoenthai, T. Srikhirin, T. Kerdcharoen, T. Osotchan,
 J. Polym. Sci. Part B: Polym. Phys. 2010, 48, 894-904.
- 24. P. Kumar, A. Mehta, S. M. Mahurin, S. Dai, M. D. Dadmun, B. G. Sumpter, M. D. Barnes, *Macromolecules* 2004, 37, 6132-6140.
- B. G. Sumpter, P. Kumar, A. Mehta, M. D. Barnes, W. A. Shelton, R. J. Harrison,
 J. Phys. Chem. B 2005, 109, 7671-7685.
- R. Traiphol, N. Charoenthai, T. Srikhirin, T. Kerdcharoen, T. Osotchan, T. Maturos, *Polymer* 2007, 48, 813-826.
- R. Traiphol, P. Sanguansat, T. Srikhirin, T. Kerdcharoen, T. Osotchan,
 Macromolecules 2006, 39, 1165-1172.
- 28. W. Xu, L. Li, H. Tang, H. Li, X. Zhao, X. Yang, J. Phys. Chem. B 2011, 115, 6412-6420.
- 29. J. Liu, R. S. Loewe, R. D. McCullough, *Macromolecules* **1999**, *32*, 5777-5785.
- 30. J. A. Merlo, C. D. Frisbie, *J. Phys. Chem. B* **2004**, *108*, 19169-19179.

- 31. A. F. M. Barton, *Chem. Rev.* **1975**, *75*, 731-753.
- 32. A. Zen, M. Saphiannikova, D. Neher, U. Asawapirom, U. Scherf, *Chem. Mater.* **2005**, *17*, 781-786.
- 33. L. Xue, X. Yu, Y. Han, Colloid Surf. A: Physicochem. Eng. Asp 2011, 380, 334-340.
- 34. P. V. Shibaev, K. Schaumburg, T. Bjornholm, K. Norgaard, *Synth. Met.* **1998**, *97*, 97-104.
- 35. D. Curcó, C. Alemán, J. Comput. Chem. **2007**, 28, 1743-1749.
- 36. M. Moreno, M. Casalegno, G. Raos, S. V. Meille, R. Po, *J. Phys. Chem. B* **2010**, *114*, 1591-1602.
- 37. X. Qiao, X. Wang, Z. Mo, Synth. Met. 2001, 118, 89-95.
- 38. R. Palacios, P. Barbara, J. Fluoresc. **2007**, 17, 749-757.
- N. Kiriy, E. Jähne, H.-J. Adler, M. Schneider, A. Kiriy, G. Gorodyska, S. Minko,
 D. Jehnichen, P. Simon, A. A. Fokin, M. Stamm, *Nano Lett.* 2003, 3, 707-712.
- 40. N. Kiriy, E. Jähne, A. Kiriy, H.-J. Adler, *Macromol. Symp.* **2004**, *210*, 359-367.
- 41. J. P. Aimé, F. Bargain, M. Schott, H. Eckhardt, G. G. Miller, R. L. Elsenbaumer, *Phys. Rev. Lett.* **1989**, *62*, 55-58.
- 42. D. Perahia, X. Jiao, R. Traiphol, *J. Polym. Sci. Part B: Polym. Phys.* **2004**, 42, 3165-3178.
- 43. G. Bidan, A. De Nicola, V. Enée, S. Guillerez, *Chem. Mater.* **1998**, *10*, 1052-1058.
- 44. C.-G. Wu, C.-Y. Lai, N.-L. Hsiao, Eur. Polym. J. 2009, 45, 879-887.
- 45. H. Meier, Angew. Chem. Int. Ed. 2005, 44, 2482-2506.

- L. Zhang, N. S. Colella, F. Liu, S. Trahan, J. K. Baral, H. H. Winter, S. C. B. Mannsfeld, A. L. Briseno, J. Am. Chem. Soc. 2013, 135, 844-854.
- 47. J. Liu, Y. Sun, X. Gao, R. Xing, L. Zheng, S. Wu, Y. Geng, Y. Han, *Langmuir* 2011, 27, 4212-4219.
- 48. R. Traiphol, N. Charoenthai, P. Manorat, T. Pattanatornchai, T. Srikhirin, T. Kerdcharoen, T. Osotchan, *Synth. Met.* **2009**, *159*, 1224-1233.
- 49. B. Valeur, In Molecular Fluorescence: Principles and Applications; Wiley-VCH: Weinheim, **2001**; pp 8-11.
- 50. R. Traiphol, D. Perahia, *Thin Solid Films* **2006**, *515*, 2123-2129.
- H. Dong, S. Jiang, L. Jiang, Y. Liu, H. Li, W. Hu, E. Wang, S. Yan, Z. Wei, W. Xu, X. Gong, J. Am. Chem. Soc. 2009, 131, 17315-17320.
- R. Traiphol, N. Charoenthai, T. Srikhirin, D. Perahia, *Synth. Met.* 2010, 160, 1318-1324.
- P. Arosio, M. Moreno, A. Famulari, G. Raos, M. Catellani, S. V. Meille, *Chem. Mater.* 2009, 21, 78-87.
- 54. M. Brinkmann, P. Rannou, *Macromolecules* **2009**, *42*, 1125-1130.
- 55. N. Kayunkid, S. Uttiya, M. Brinkmann, *Macromolecules* 2010, 43, 4961-4967.
- 56. M. Brinkmann, J. Polym. Sci. Part B: Polym. Phys. **2011**, 49, 1218-1233.
- 57. C. Melis, L. Colombo, A. Mattoni, *J. Phys. Chem. C* **2011**, *115*, 576-581.
- S. Haraguchi, Y. Tsuchiya, T. Shiraki, K. Sugikawa, K. Sada, S. Shinkai, *Chem. Eur. J.* 2009, 15, 11221-11228.
- J. D. Ripoll, A. Serna, D. Guerra, A. Restrepo, J. Phys. Chem. A 2010, 114, 10917-10921.

- J. Torras, C. Sanchez-Navas, O. Bertran, C. Aleman, *Phys. Chem. Chem. Phys.* 2012, 14, 1881-1891.
- 61. S. Siddiqui, F.C. Spano, Chem. Phys. Lett. 1999, 308, 99-105.
- 62. S. Tretiak, A. Saxena, R.L. Martin, A.R. Bishop, *J. Phys. Chem. B* **2000**,104, 7029-7037.
- 63. C. L. Yaws; K. Y. Li, In Thermophysical Properties of Chemicals and Hydrocarbons; C. L. Yaws, Eds.; William Andrew: Norwich, New York, 2008; Chepeter 13.
- 64. C. Wohlfarth, In CRC Handbook of Chemistry and Physics; Internet Version 2005; D. R. Lide, Eds.; http://www.hbcpnetbase.com; CRC Press: Boca Raton, Florida, **2005**; Section 6.

บทที่ 2

On the formation and photophysical properties of emissive and nonemissive aggregates of regionegular poly(3-octylthiophene) in different local environments

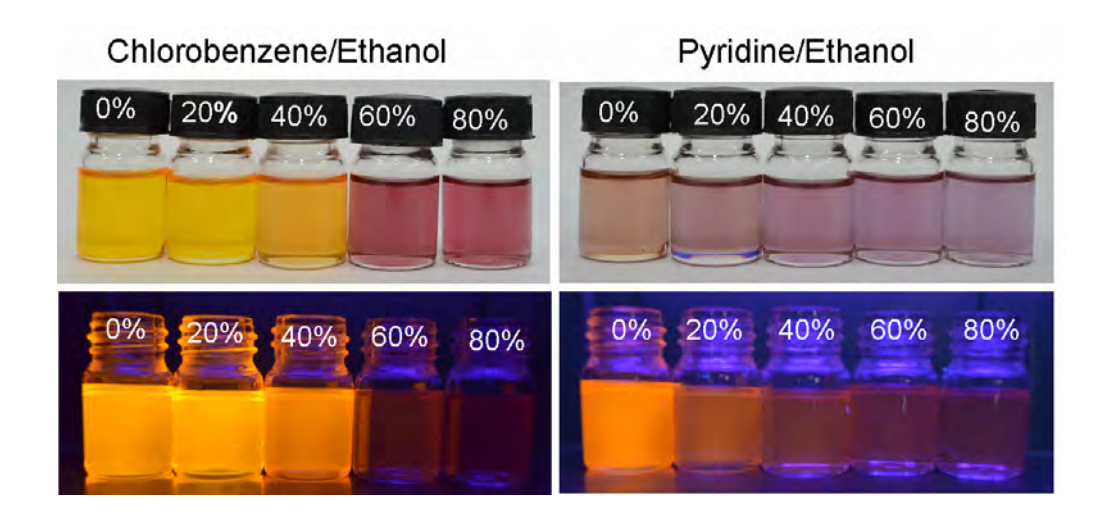
Ruttayapon Potai^a, Anothai Kamphan^a, Rakchart Traiphol^{a,b*}

^aLaboratory of Advanced Polymers and Nanomaterials, Department of Chemistry and Center for Innovation in Chemistry, Faculty of Science, Naresuan University, Phitsanulok 65000, Thailand

^bNANOTEC-MU Excellence Center on Intelligent Materials and Systems, Faculty of Science, Rama 6 Road, Ratchathewi, Bangkok 10400, Thailand

*Corresponding Author: Rakchart Traiphol; e-mail: rakchartt@nu.ac.th

Tel: +66 55963451 Fax. +66 55261025



Abstract

This contribution explores the aggregation behaviors of regionegular poly(3octylthiophene) (rr-P3OT) in solvent-nonsolvent systems. The photophysical properties of aggregates in different states are characterized by using UV/vis absorption, photoluminescent emission (PL) and photoluminescent excitation (PLE) spectroscopy. The rr-P3OT chains are dispersed in different solvents, including chlorobenzene and pyridine. At this state, polymer chains are isolated or associated, depending on local polymer-solvent interactions. The polymer chains are forced to densely pack by adding a poor solvent, ethanol. Ratio of poor solvent ranges from 0 to 99 v/v%. We have found that the formation of aggregates results in the appearance of distinct red-shift peaks in absorption spectra. In addition, the measurements of PL and PLE spectra indicate the existence of two types of aggregates, non-emissive and emissive species. The formation of these two aggregates depends on segmental packing. The early stage of interchain association results in the non-emissive species. When the chain segments are forced to densely pack within the aggregates, emissive species forms. The change of initial solvent also affects the amount of type of aggregates. The aggregates formed in the chlorbenzene and pyridine systems exhibit rather different absorption pattern.

Keywords: chain conformation; conjugated polymer; photophysics; aggregates

1. Introduction

Poly(3-alkylthiophene) (P3AT) is a class of conjugated polymer that is known to exhibit interesting opto-electronic properties and high charge transport. These characteristics are suitable for the utilization in advanced organic electronic technologies such as organic solar cells (OSC) [1,2], organic field-effect transistors (OFET) [3,4] and organic light emitting diode (OLED) [5,6]. It has been known that segmental aggregation of conjugated polymers strongly affect their electroluminescence and photoconductivity, which in turn dictates the performance of aforementioned devices.[7,8] Therefore, it is important to get a full understanding about molecular and experimental parameters that control the chain organization of conjugated polymers in different states. For example, the aggregation of conjugated polymers leads to the increase of charge carrier mobility while photoluminescence intensity is reduced.[3,6,9] These properties are desirable in OSC application. The OLED device, on the other hand, prefers less amount of aggregate to maximize its brightness. In the past decade, aggregation of various conjugated polymers has been extensively investigated. It has been observed that the change of experimental parameters such as concentration, temperature, or quality of solvent can lead to the formation of aggregates.

An early work by Rughooputh et.al [10] shows that aggregation of regioregular poly(3-hexyllthiophene) (*rr*-P3HT) in mixtures of methyltetrahydrofuran/acetonitrile leads to the growth of three distinct red-shift peaks in absorption spectrum. Rumbles et.al [11] observe similar results in the system of regioregular poly(3-dodecylthiophene) (*rr*-P3DDT) where the aggregation is induced by varying ratio of toluene/methanol mixtures. The aggregation also causes red shift peaks in PL spectrum and the drop of quantum

yield. Many research groups have investigated molecular parameters that influence the aggregation behaviors of P3AT. The main chain of regioregular P3AT possesses a more planar-like structure compared to that of the regiorandom one [12-14]. Therefore, it is more favorable for *rr*-P3AT to form aggregates where appropriate interchain stacking is required. The increase of chain length also promotes the aggregation. Recent study by Scharsich et al [15], investigating *rr*-P3HT with molecular weights of 5 kDa, 11 kDa and 19 kDa, observes the increase of aggregate fraction upon increasing molecular weight. The change of side chain length affects photophysical properties of the aggregates. Magnani et.al [16] observe that absorption peaks of *rr*-P3DDT aggregates occur at lower energy region compared to those of *rr*-P3HT with shorter side chain length.

In recent studies by several research groups, the aggregation of rr-P3AT in solvent-nonsolvent has been utilized to grow various types of nanostructures. The self assembling of rr-P3AT in this system often leads to the formation of nanofiber [17,18], nanowire [19,20] and nanowhisker [21,22]. For example, Samitsu et al.[17] prepare P3AT nanofiber by adding anisole into the polymer solution in a good solvent. The formation of nanofiber originate from one dimensional crystallization of P3AT, driven by strong π - π interaction between thiophene backbone and the crystallization of alkyl side chains. Xu et al.[21] control solvent composition and aging time to induce the formation of rr-P3DDT nanowhiskers with different dimensions. They suggest that conformational change from coil to rod occurs prior to the assembling process. Park et al.[23] observe similar results in the system of rr-P3HT. The random coils of rr-P3HT in chloroform assemble into order aggregates upon adding poor solvent acetonitrile. The dimension of aggregation also depends on polymer concentration. Kiriy et al. [24,25] investigate

different types of poor solvents used to induce the aggregation of *rr*-P3AT. They observe the variation of aggregation behaviors depending on properties of the poor solvent. The use of methanol, a non-solvent for both alkyl side group and aromatic backbone, provides 3 dimensional (3D) aggregates. The P3AT chain in hexane, which is a good solvent for the alkyl side chain but poor solvent for the thiophene backbone, undergoes helical coil formation followed by 1D aggregation.

In these previous works, the authors have noticed the variation of aggregation behaviors as well as photophysical properties in different systems. However, detailed study exploring the origins of these discrepancies is rather limited. Therefore, we look closely into nature and photophysical properties of regioregular poly(3-octylthiophene) (rr-P3OT) aggregates in this study. We systematically induce the aggregation by varying properties of solvents. Mixed solvents are also used for fine tuning the strength of local polymer-solvent interactions. The photophysical change of rr-P3OT in different states is followed by utilizing uv/vis absorption, steady state photoluminescence (PL), photoluminescence excitation (PLE) and site selective PL spectroscopy. Atomic force microscopy (AFM) is also used to probe the nanostructure of assembled rr-P3OT chains. We have observed the formation non-emissive and emissive aggregates depending on strength local segmental packing. The amount of each aggregate can also be controlled by varying type of the solvents.

2. Experimental

The rr-P3OT was purchased from Sigma-Aldrich. The molecular weight (M_n) determined by gel permeation chromatography (GPC) in tetrahydrofuran (THF) with

polystyrene standard is 58,300 g/mol ($M_w/M_n = 2.3$). According to previous reports, the GPC tends to overestimate the molecular weight of rr-P3AT by a factor of 2-2.3 [15,26,27]. By comparing the M_n obtained from GPC with MALDI-TOF data, the M_n of rr-P3OT in this study is approximately 26,850 g/mol [27]. The solvents used in this study are analytical grade. The solutions of rr-P3OT were prepared by dissolving powder sample in chlorobenzene (CRB) and pyridine (PRD) assisted by mechanical stirring and ultrasonication. In the pyridine system, the polymer solution was stirred for several days to allow complete dissolution. The resultant solution appears clear to naked eyes. To vary local polymer-solvent interactions, a poor solvent ethanol (EtOH) was added into the polymer solutions. Ratio of the ethanol was increased to 99 v/v%. Concentration of the rr-P3OT was kept constant at 0.001 mg/mL. An inner-filtered effect is negligible at this concentration. In these systems, freshly prepared solutions were used to avoid the polymer precipitation. Absorption spectra of the solutions were recorded by using Analytica Specord 100 UV/vis spectrometer with a 4 cm thick quartz cuvette. The measurements of PL and PLE spectra were carried out on Perkin-Elmer LS55 spectrometer.

Morphology of the aggregated *rr*-P3OT was explored by atomic force microscopy (AFM) (SPI3800N Nanoscope II, Seiko Instrument Inc., Japan) operating in a dynamic contact mode. The cantilever was fabricated from Si₃N₄ with a spring constant of about 15 N/m. The samples were prepared by drop cast from 0.05 mg/mL *rr*-P3OT solutions on a flat silicon wafer. The substrates were cleaned by soaking in a mixture of conc. H₂SO₄ and 30% H₂O₂ (7:3, v/v) at 80°C for 1 h. The substrates were rinsed by using deionized water several times and dried with nitrogen gas. The droplet of polymer solution was

allowed to dry in a clear atmosphere under ambient condition. Three samples were prepared for each condition.

3. Result and Discussion

3.1. Formation of non-emissive and new emissive species

In this section, we focus on the nature and photophysical properties rr-P3OT aggregates in mixtures of CRB/EtOH and PRD/EtOH. The small difference between solubility parameter (δ) of CRB (19.6 J^{1/2} cm^{-3/2}) [28] and rr-P3OT (18.2 J^{1/2} cm^{-3/2}) [29] suggests that CRB is a good solvent for the rr-P3OT chain. Studies have shown that polymer can dissolve in a solvent at relatively high concentration when the difference of their solubility parameters is less than 2 J^{1/2}cm^{-3/2} [30]. Absorption and PL spectra of rr-P3OT in CRB exhibit λ_{max} at 454 nm and 574 nm, respectively (see Fig. 1). The addition of EtOH ($\delta = 26.5 \text{ J}^{1/2} \text{ cm}^{-3/2}$), a poor solvent for both thiophene backbone and alkyl side chain, results in systematic change of the absorption and PL spectra. The presence of 40 %v/v EtOH in the system hardly affects the pattern of absorption and PL spectra, indicating that the rr-P3OT chains remain well-dissolved and isolated. The absorption spectrum change significantly when the EtOH ratio is increased to 60 %v/v. The growth of three redshift peaks at about 515, 555 and 605 nm is clearly observed. The pattern and absorbance of these redshift peaks hardly change when the EtOH ratio is further increased to 99 %v/v. These redshift peaks are attributed to the aggregation of rr-P3OT chains, minimizing the unfavorable polymer-solvent interactions. The stacking of conjugated backbone within aggregates allows the overlap of π orbitals and also induces planarization of thiophene rings, which in turn results in the increase of conjugation length [15,17-23]. The photophysical change of *rr*-P3OT in mixed CRB/EtOH can be observed via naked eyes as shown in Fig. 1c where the solution color changes from bright orange to pink-purple.

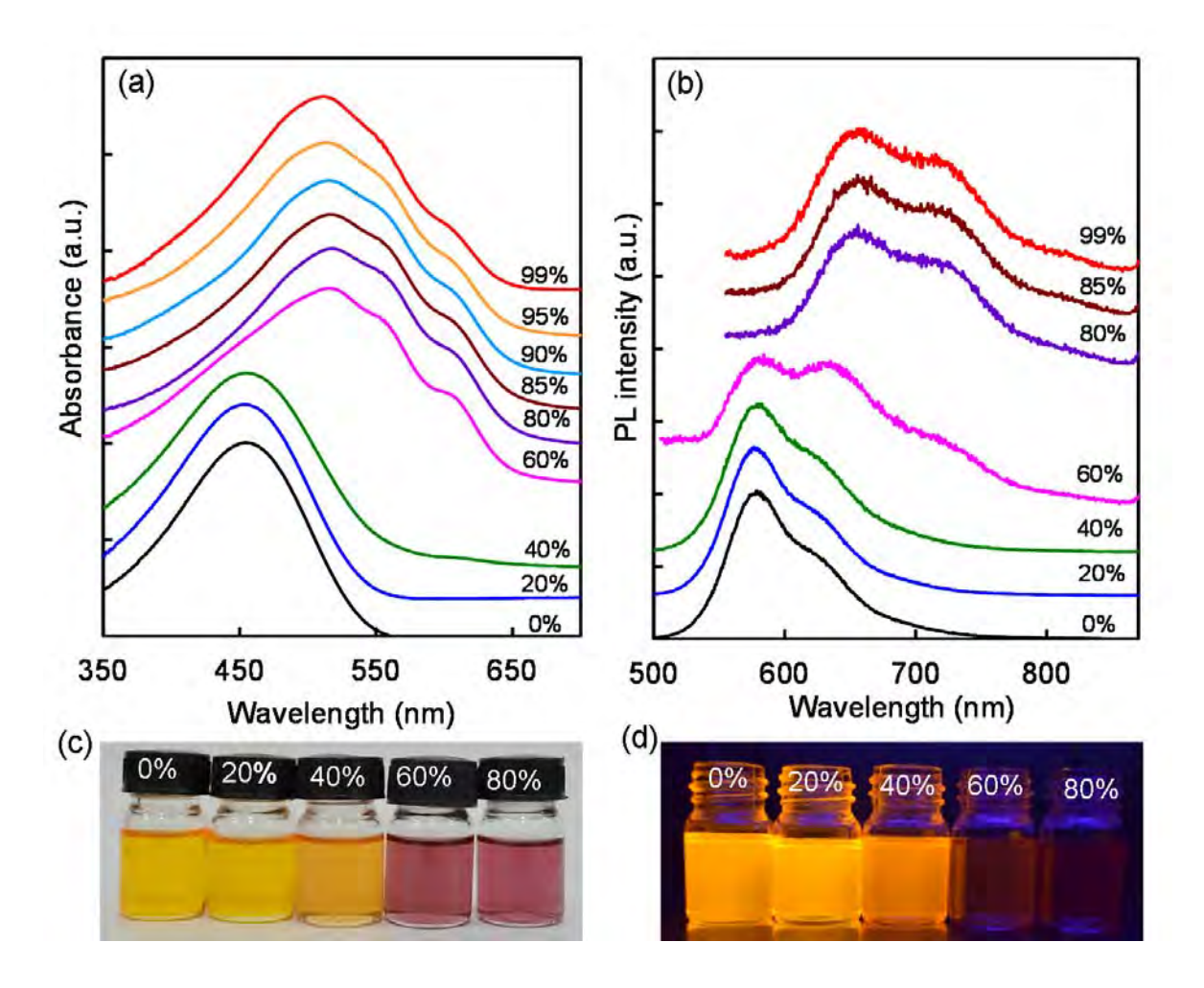


Figure 1 (a) Absorption and (b) PL spectra of 0.001 mg/mL *rr*-P3OT in mixtures of chlorobenzene and ethanol. Ratios of ethanol in %v/v are shown on the right side of each spectrum. Photographs of *rr*-P3OT in mixture of chlorobenzene and ethanol in (c) ambient conditions and (d) under UV light irradiation

The PL pattern of rr-P3OT in mixed CRB/EtOH changes accordingly (see Fig. 1b). The addition of 60 % v/v EtOH causes the growth of redshift peak at about 638 nm, indicating the formation of new emissive species with lower HOMO-LUMO energy gap. The quantum yield also decreases significantly at this condition due to the aggregation of rr-P3OT chains (see Fig. 1d). When the EtOH ratio is increased to 80 % v/v, PL peak of the non-aggregated chains at 574 nm disappears. The PL spectrum of rr-P3OT at this state constitutes peak and shoulder at about 658 nm and 720 nm, respectively. Further increase of EtOH ratio to 99 %v/v does not affect the PL pattern. This observation indicates that the dense packing of rr-P3OT chains within the aggregates results in new type of emissive species. Our result is consistent with previous studies of rr-P3HT, rr-P3DDT where the new emissive species also form upon increasing the alcohol ratio [11,16,31]. The PL spectra of rr-P3OT aggregates in condensed phases such as thin film and nanoparticles also exhibit pattern similar to this study [32]. However, our recent study in the system of cyclohexane/hexane does not detect the formation of emissive species [33]. Although an increase of the poor solvent ratio, hexane, causes the growth of three redshift peaks in absorption spectra, the PL pattern remains the same. Therefore, the aggregates detected in the cyclohexane/hexane system are designated as non-emissive aggregates. It is worthwhile to note that the absorption pattern of aggregates is this study is quite different from that of cyclohexane/hexane system. Our results indicate that the photophysical properties of rr-P3OT aggregates depend significantly on local chain arrangement.

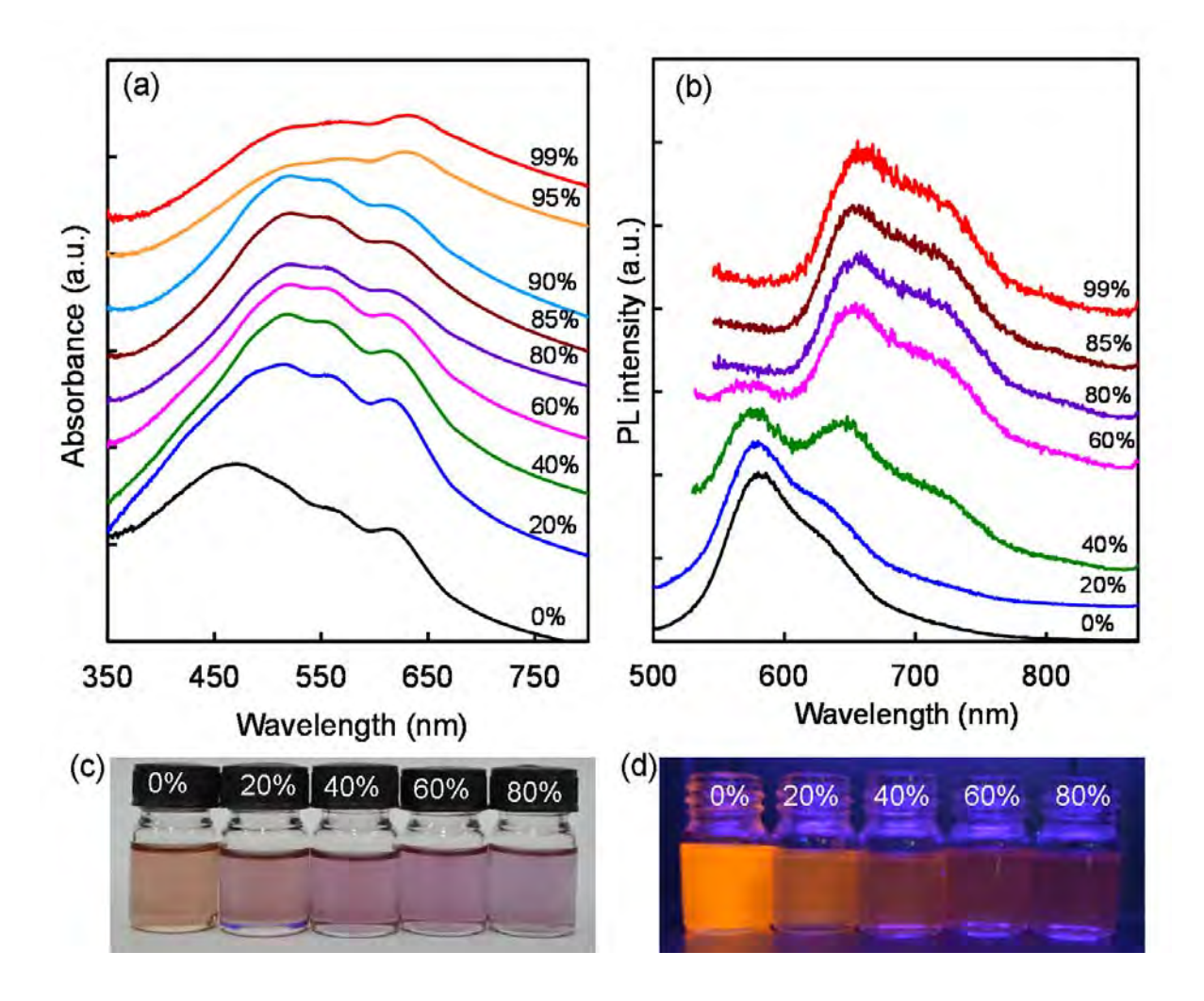


Figure 2 (a) Absorption and (b) PL spectra of 0.001 mg/mL *rr*-P3OT in mixture of pyridine and ethanol. Ratios of ethanol in %v/v are shown on the right side of each spectrum. Photographs of *rr*-P3OT in mixture of pyridine and ethanol in (c) ambient conditions and (d) under UV light irradiation

We further investigate the nature of non-emissive and emissive aggregates by using PRD as an initial solvent. The PRD is a more polar solvent with higher solubility parameter ($\delta = 21.8 \text{ J}^{1/2}\text{cm}^{-3/2}$) compared to those of the CRB and rr-P3OT. Therefore,

the rr-P3OT chains aggregate in this solvent. The absorption spectrum of rr-P3OT in PRD solution shows λ_{max} at about 470 nm, accompanied with three redshift peaks at about 515 nm, 560 nm and 616 nm (see Fig. 2a). The pattern of these redshift peaks is similar to that of the CRB/EtOH system. The absorbance of redshift peaks in the PRD solution is rather strong, indicating the existence of large aggregated fraction. However, we do not detect any drastic change in the photoemission pattern. Fig. 2b shows that the PL spectrum of rr-P3OT in PRD is still very similar to that of the isolated chain in pure CRB solution. While the color of PRD solution is pink-purple in ambient condition, the PL emission shows relatively bright orange color (see Fig. 2c,d). This result indicates that the rr-P3OT aggregates in PRD solution are the non-emissive species. We suggest that the observed PL spectrum arises from the non-aggregated segments, which may exist as isolated chain and/or associated particles. The PLE and site selective PL spectra in the following section provide supportive results. Since the association of rr-P3OT chains in this system occurs in a random fashion, some conjugated segments or chromophores may not stack on top of each other, a requirement for aggregate formation [34,35]. Therefore, the photophysical properties of these non-aggregated segments remain unaltered. Detail discussion of this topic is given in our previous report, investigating the well-known poly[2-methoxy-5-(2'-ethylhexyloxy)-1,4-phenylenevinylene] (MEH-PPV) [36,37].

The addition of 20 %v/v EtOH causes significant growth of the redshift peaks in absorption spectrum, corresponding to the increase of aggregated fraction. The PL pattern, however, is still the same. The further increase of EtOH ratio to 40 and 60 %v/v hardly affect the absorption pattern. Interestingly, we detect drastic growth of redshift peaks in PL spectra. The absorption and PL pattern are not affected by increasing EtOH

ratio to 90 %v/v. At these conditions, the PL spectra constitute a peak and shoulder at about 658 nm and 720 nm, respectively. In this system, the increase of EtOH ratio causes the decrease of solvent quality, which in turn forces dense packing of rr-P3OT chains within aggregates. Our observation indicates that the dense packing of rr-P3OT segments leads to the formation of new emissive species with lower HOMO-LUMO energy gap. Similar behavior is observed in the system of poly(9,9-di(2-ethylhexyl)fluorene) in mixtures of chloroform/methanol [38]. Previous studies have shown that the crystalline rr-P3OT in solid state can exist in the so called Form I and Form II [34,35,39-41]. The interlayer distance is slightly larger in the Form II crystal. Thermal annealing of the Form II above T_g causes the decrease of interlayer distance, resulting in the formation of Form I crystal. We suggest that similar structural transformation occurs upon increasing EtOH ratio in our system. The shift of segment along chain axis, affecting the overlap of π orbitals, may also occurs [39,40]. We note that this emissive species does not belong to excimers. The discussion of this topic is presented in following section.

The structural transformation is still detected upon increasing EtOH ratio to 95 and 99 %v/v, indicated by the growth of a redshift peak at about 616 nm in absorption spectra. Since the growth of this peak is independent from the other peaks at 515 and 560 nm, we suggest that this band belongs to different type of aggregates. The formation of this electronic species probably requires different packing parameters of the conjugated backbone. This result is in contrast to the CRB/EtOH system where the absorption pattern remains the same at EtOH ratio ranging from 80 to 99 %v/v. The drastic discrepancy of absorption pattern in the two systems is illustrated in Fig. 3a. At 99 %v/v of EtOH ratio, local environments in the PRD/EtOH and CRB/EtOH systems is roughly the same but the

photophysical properties of aggregates are quite different. Our results demonstrate that the segmental arrangements within the aggregates vary with the preparation conditions and largely dictate its photophysical properties. This observation is consistent with our previous reports on the systems of MEH-PPV in solvent/nonsolvent [42] and rr-P3OT nanoparticles [32] where the amount of aggregates also depends on type of the initial solvent. However, the PL spectra of rr-P3OT at 99% v/v EtOH of the two systems still show similar pattern indicating the presence of same emissive species (see Fig. 3b). Therefore, segmental rearrangements in the PRD/EtOH system only affect the amount and nature of non-emissive aggregates.

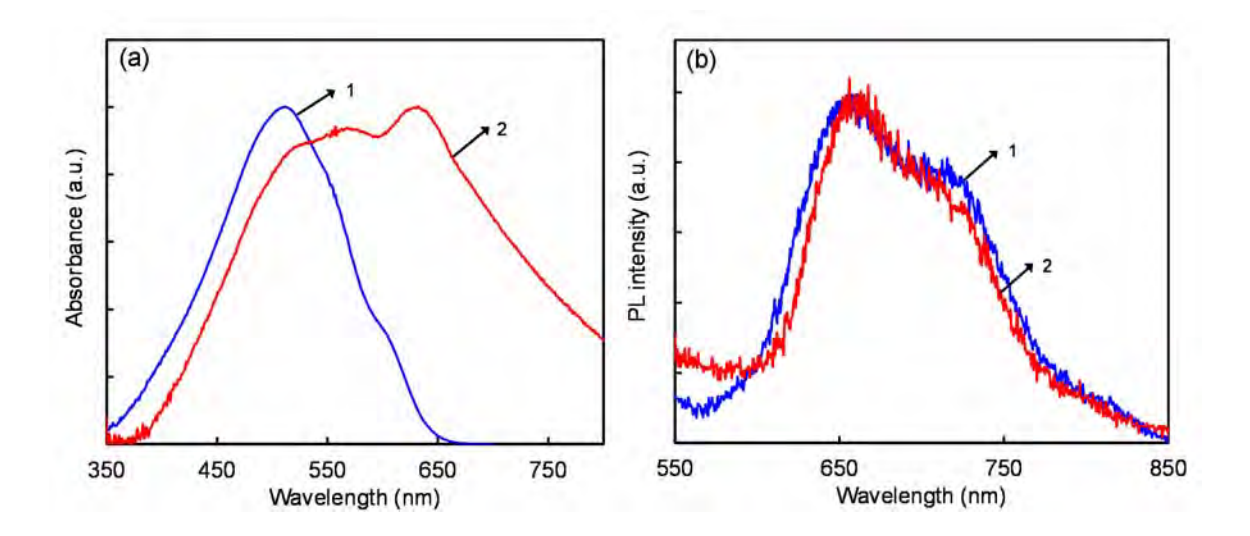


Figure 3 (a) Absorption and (b) PL spectra of 0.001 mg/mL *rr*-P3OT in mixtures of (1) chlorobenzene and 99 v/v% ethanol and (2) pyridine and 99 v/v% ethanol

AFM is utilized to explore the aggregation behaviors of *rr*-P3OT chains in the mixed CRB/EtOH and PRD/EtOH systems. Samples are prepared by drop casting from solutions onto flat-surface silicon wafer. Although the AFM can not directly reveal the

molecular packing within the aggregates, morphologies of the samples provide an insight into the assembling behaviors of individual chains. The AFM topography images of rr-P3OT films in Fig. 4 show that the addition of EtOH causes the formation of large assembled particles. In CRB/EtOH system, the addition of 50 %v/v EtOH yields flat sheet-like structure with thickness of about 12.7 ± 2.1 nm. Some polymeric particles also randomly disperse on the sample. Previous studies have shown that the sheet-like structure forms by parallel stacking of conjugated backbone, where its dimensions correspond to chain length and number of the stacked layers [33]. We suggest that large fraction of rr-P3OT chains is still isolated and extended in the mixed CRB/EtOH solvents. The assembling of these extended chains into sheet-like aggregates takes place during the evaporation of solvent. The aggregation of some rr-P3OT chains in the solution probably causes the formation of polymeric particles. When the samples are prepared from the PRD/EtOH system containing 50% v/v EtOH, the assembled domains in thin film mostly exhibit irregular shapes. Their thicknesses are also inhomogeneous. Since the polymer-solvent interactions are less favorable in the PRD/EtOH system, large polymer fraction at this state aggregates in solution, corresponding to the absorption spectrum. At 90 % v/v EtOH ratio, the drastic decrease of solvent quality forces the rr-P3OT chains to densely pack into nanoparticles in solution state. Interestingly, primary size of the rr-P3OT nanoparticles obtained from the CRB/EtOH system appears to be much smaller compared to that of the PRD/EtOH one. The high magnification AFM image reveals that the large domains detected in Fig. 4c consists of small size nanoparticles. The large domains observed in the PRD/EtOH system, on the other hand, exhibit homogeneous surface and do not constitute any smaller internal structure. These discrepancies of *rr*-P3OT morphologies reflect the difference of segmental packing within the two systems, resulting in the variation of absorption pattern and PL spectra. It is worthwhile to note that our recent study also detect the variation of *rr*-P3OT nanoparticle size and their photophysical properties, depending on type of the initial solvent [32].

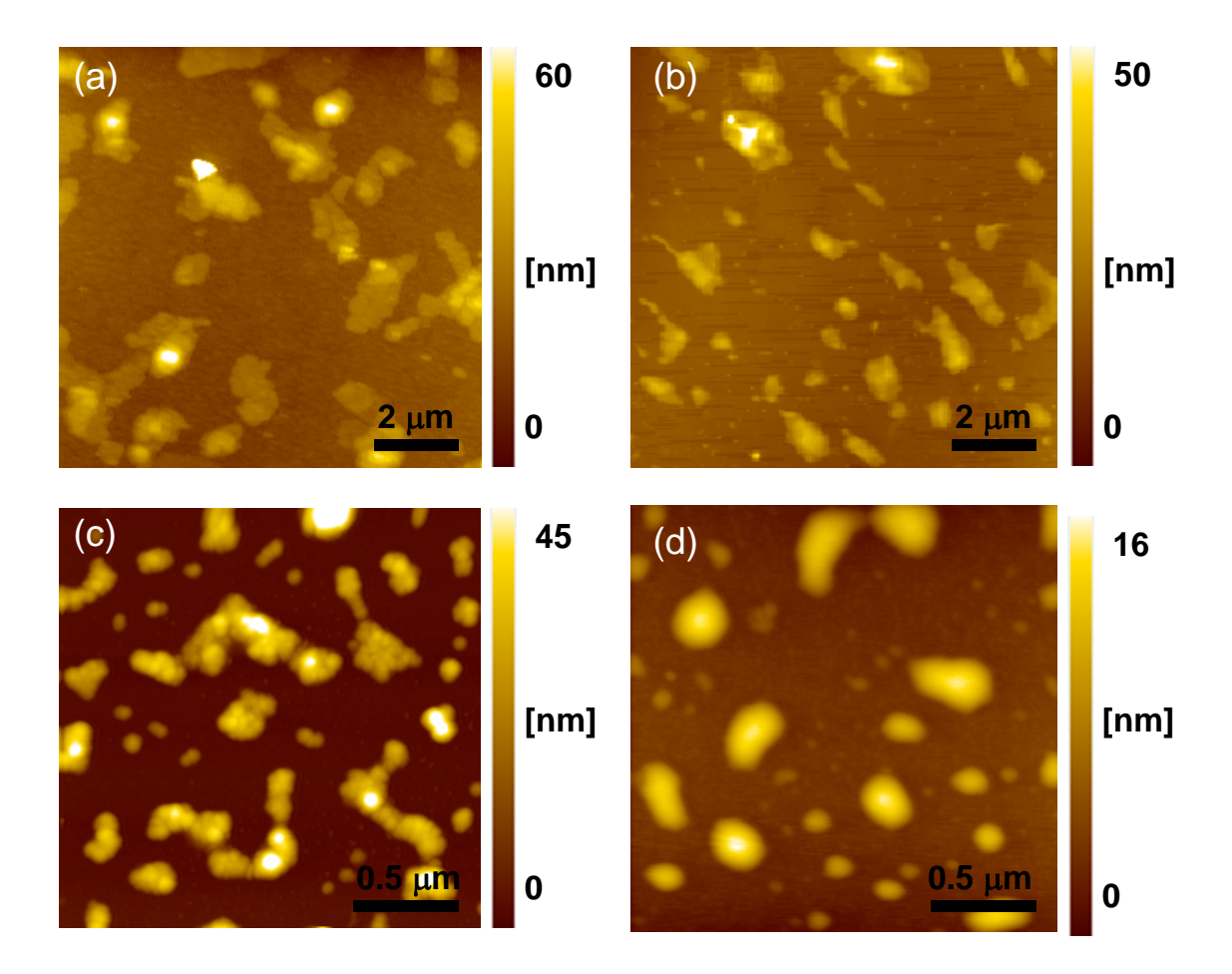


Figure 4 AFM topography images of rr-P3OT thin films on silicon wafer prepared by drop casting from 0.05 mg/mL in mixed solvents; (a) chlorobenzene:ethanol (50:50 v/v%), (b) pyridine:ethanol (50:50 v/v%), (c) chlorobenzene:ethanol (10:90 v/v%) and (d) pyridine:ethanol (10:90 v/v%).

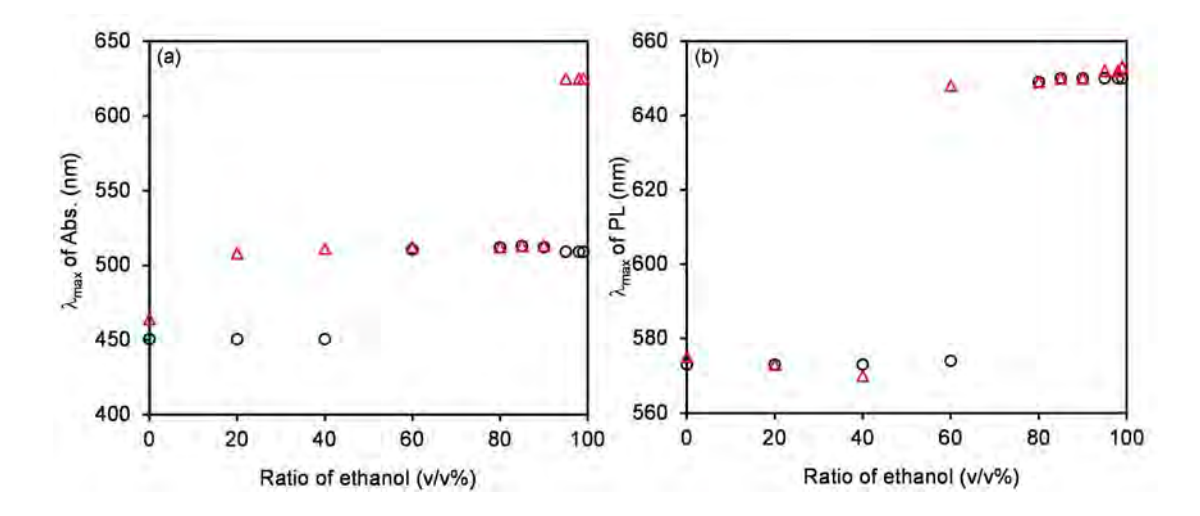


Figure 5 Variation of λ_{max} of (a) absorption and (b) PL spectra of *rr*-P3OT in mixtures solutions upon increasing the ratio of ethanol. Solvents are chlorobenzene (circle) and pyridine (triangle).

The photophysical change of rr-P3OT in CRB/EtOH and PRD/EtOH is summarized in Fig. 5 where λ_{max} of absorption and PL spectra are plotted as a function of EtOH ratio. In the CRB/EtOH system, an abrupt increase of absorption λ_{max} from 450 nm to 512 nm occurs when the aggregation takes place at about 60 %v/v EtOH. Large aggregate fraction already exists in pure PRD solution. The increase of EtOH ratio to 20 %v/v in the PRD/EtOH system causes the shift of absorption λ_{max} to 512 nm, corresponding to the increase of aggregated fraction. The λ_{max} of PL spectra, however, is still similar to that the isolated chain in pure CRB. Therefore, most of the aggregates at this stage are the non-emissive species. When the EtOH ratio is increased to 90 %v/v, the absorption λ_{max} in both systems remains the same while the λ_{max} of PL spectra abruptly increases from 574 nm to 648 nm. At this condition, the decrease of solvent quality

causes segmental rearrangement of small aggregated fraction, which in turn results in the formation of new emissive species. The further increase of EtOH ratio to 99 %v/v causes segmental rearrangement of aggregates in PRD/EtOH system, indicated by the shift absorption λ_{max} to 625 nm. However, the PL spectra are not affected, indicating that these additional aggregates are the non-emissive species.

Relationship between the growth of redshift peaks in absorption and PL spectra is further investigated in more details. The value of absorbance ratio at 605/450 nm reflects the amount of aggregates while the increase of PL intensity ratio at 650/575 nm indicates the formation of new emissive species (see Fig. 6). The absorbance and PL ratios are relatively small in mixed CRB/EtOH system containing 0, 20 and 40 %v/v of EtOH, which corresponds to the presence of isolated chains. At 60% v/v EtOH, the absorbance ratio increases abruptly due to the rr-P3OT aggregation. The amount of aggregates remains approximately the same at the higher EtOH ratios. The fraction of new emissive species (i.e. PL ratio at 650/575 nm), however, continuously increase upon increasing EtOH ratio to 85 %v/v. The absorbance ratio is quite high in the PRD/EtOH system containing 0, 20% v/v EtOH. The PL ratio, on the other hand, is still comparable to that of isolated chain in pure CRB. The absorbance ratio steadily increases with EtOH ratio and remains roughly constant at EtOH ratio ranging from 80 to 90 % v/v. Further increase of EtOH to 95 and 99 %v/v causes significant increase of the absorbance ratio. The PL ratio shows continuously increase upon increasing the EtOH ratio similar to the CRB/EtOH system. These plots illustrate that there is no clear correlation between the growth of redshift peaks in absorption and PL spectra. The non-emissive aggregates form in the early stage of interchain association. The increase of EtOH ratio forces dense segmental packing within these aggregates resulting in the formation of new emissive species. The formation of these emissive species hardly affects the absorption pattern.

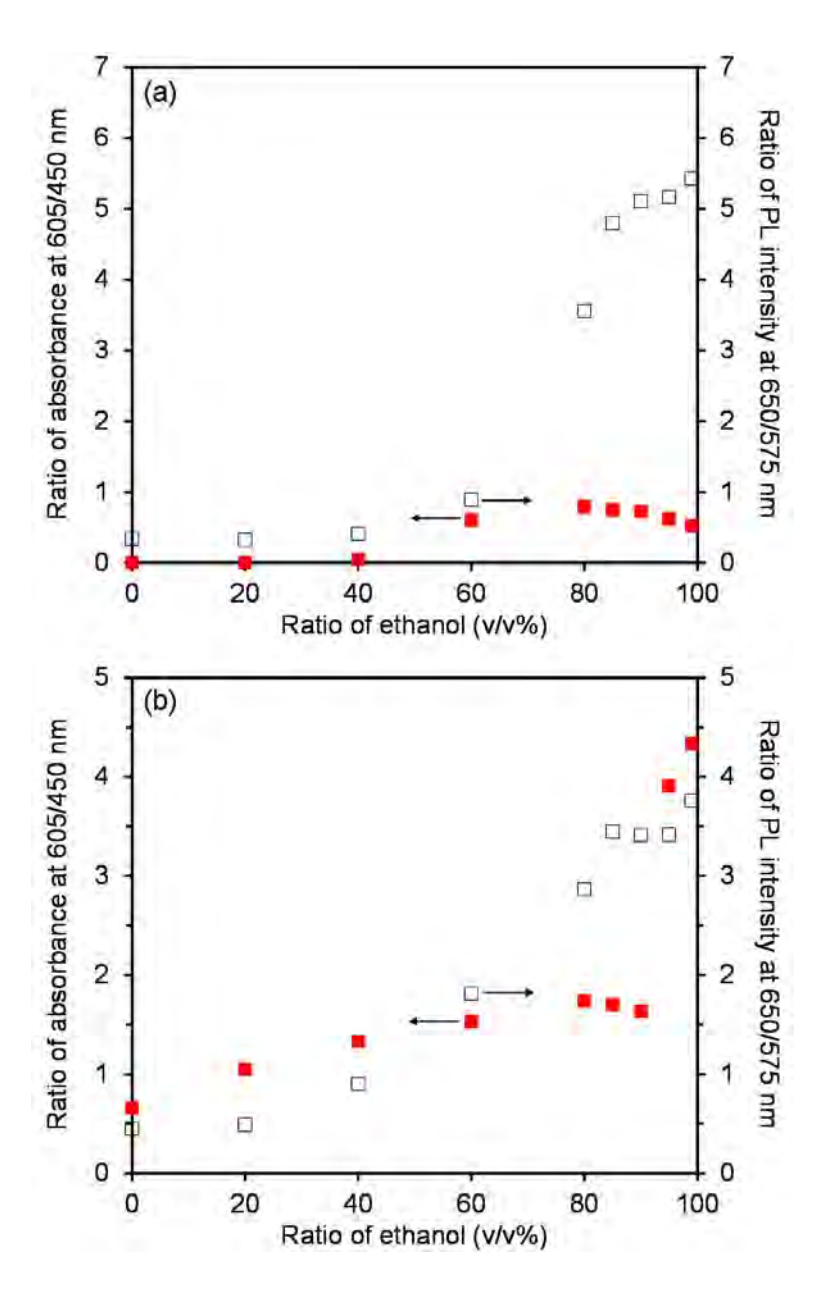


Figure 6 Ratio of (fill square) absorbance at 605/450 nm and (open square) PL intensity at 650/575 nm of 0.001 mg/mL *rr*-P3OT in mixtures of (a) chlorobenzene/ethanol and (b) pyridine/ethanol

3.2. Emissive aggregates or excimer

The new emissive species discussed in previous section may belong to aggregates or excimer. The formation of excimer takes place in the excited state. It dissociates during the relaxation processes back to ground state. Therefore, absorption band of the excimer does not exist. To get a more understanding about the origin of new emissive species, we measure the site selective PL and PLE spectra by varying excitation and emission wavelengths, respectively. The results obtained from CRB/EtOH and PRD/EtOH systems are shown in Fig. 7,8. The PL pattern of isolated chain in pure CRB is independent of the excitation wavelength (see Fig. 7a). The variation of excitation wavelength from 450 nm to 525 nm, exciting chromophores with different conjugation length, yields the same PL pattern. The result indicates the presence of only one type of emitting species. The measurements of PLE spectra detected at different emission wavelengths provide consistent results. The PLE spectra represent absorption band of emissive species within the system. In this case, the pattern of PLE spectra is similar to that of the corresponding absorption spectra. Studies have shown that conjugated chain consists of multiple chromophores with various conjugation lengths [36-38]. However, the PL emission process usually takes place via the chromorphores with the lowest HOMO-LUMO energy gap (i.e. longest conjugation length) [43-45]. This is mainly due to the high efficiency of intrachain energy transfer process. In this system, the excited chromophores effectively transfer energy to the one with lowest energy before the PL emission process occurs. The PL spectra of rr-P3OT in pure PRD solution are also independent of the excitation wavelength as shown in Fig. 8a. Although the absorption spectrum constitutes strong redshift peaks, the use of 450 nm and 525 nm excitation wavelength yields the same PL pattern, which is similar to that of the isolated chain in pure CRB. The PLE spectra obtained from both PRD and CRB solutions also exhibit similar pattern, indicating that both systems contain the same type of emitting species. The results from PL and PLE spectra confirm that the *rr*-P3OT aggregates in PRD solution is a non-emissive species. Only the non-aggregated segments contribute to the PL emission.

Significant change is detected in PLE and PL patterns when 60 %v/v EtOH is added into the CRB solution. The PL pattern of rr-P3OT in this system varies upon increasing the excitation wavelength as shown in Fig. 7b. Using excitation wavelength at 450 nm, which is at maximum absorption of the non-aggregated chains, yields PL spectra with two peaks at 575 nm and 625 nm. As discussed in previous section, the first peak relates to PL emission of non-aggregated segments while the second one arises from new emissive species. An increase of excitation wavelength to 500 nm results in the suppression of PL peak at 575 nm. Moving the excitation wavelength to 525 nm, which mostly excites the aggregated chromophores, provides PL spectrum with peak and shoulder at about 645 nm and 715 nm, respectively. This result indicates that two types of emitting species exist in the system. The PLE measurements also reveal that these emissive species absorb energy at different regions. When the emission wavelength is fixed at 580 nm, the PLE spectrum exhibits a peak at 450 nm, consistent with absorption λ_{max} of non-aggregated chains. The increase of emission wavelength to 650 nm and 690 nm causes systematic growth of redshift band in PLE spectra. The detection the redshift band in PLE spectra indicates that the new emissive species belong to aggregates.

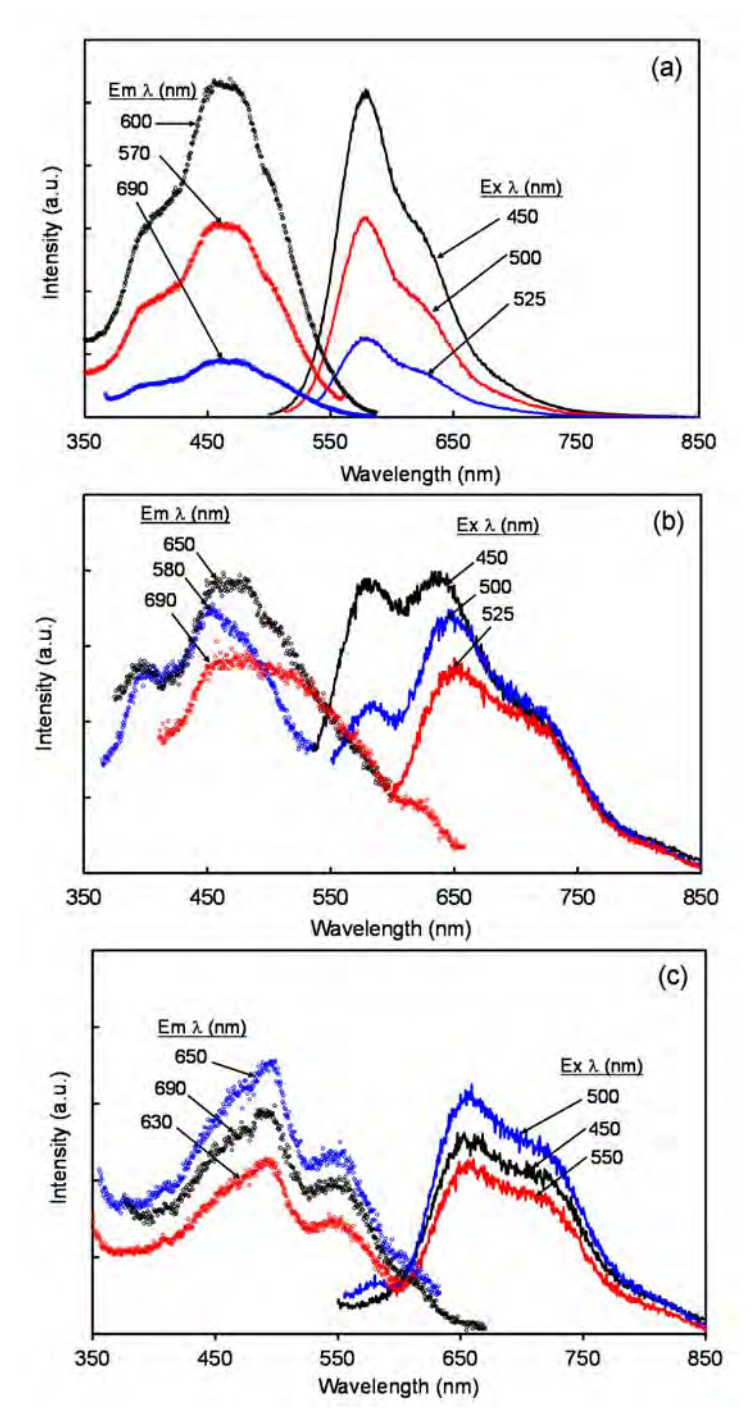


Figure 7 PLE spectra (symbol) and PL spectra (solid line) of 0.001 mg/mL rr-P3OT in mixtures of chlorobenzene and ethanol. The ratios of ethanol are (a) 0, (b) 60 and (c) 99 v/v%, respectively. The spectra were measured at different emission wavelengths (Em λ) and excitation wavelengths (Ex λ).

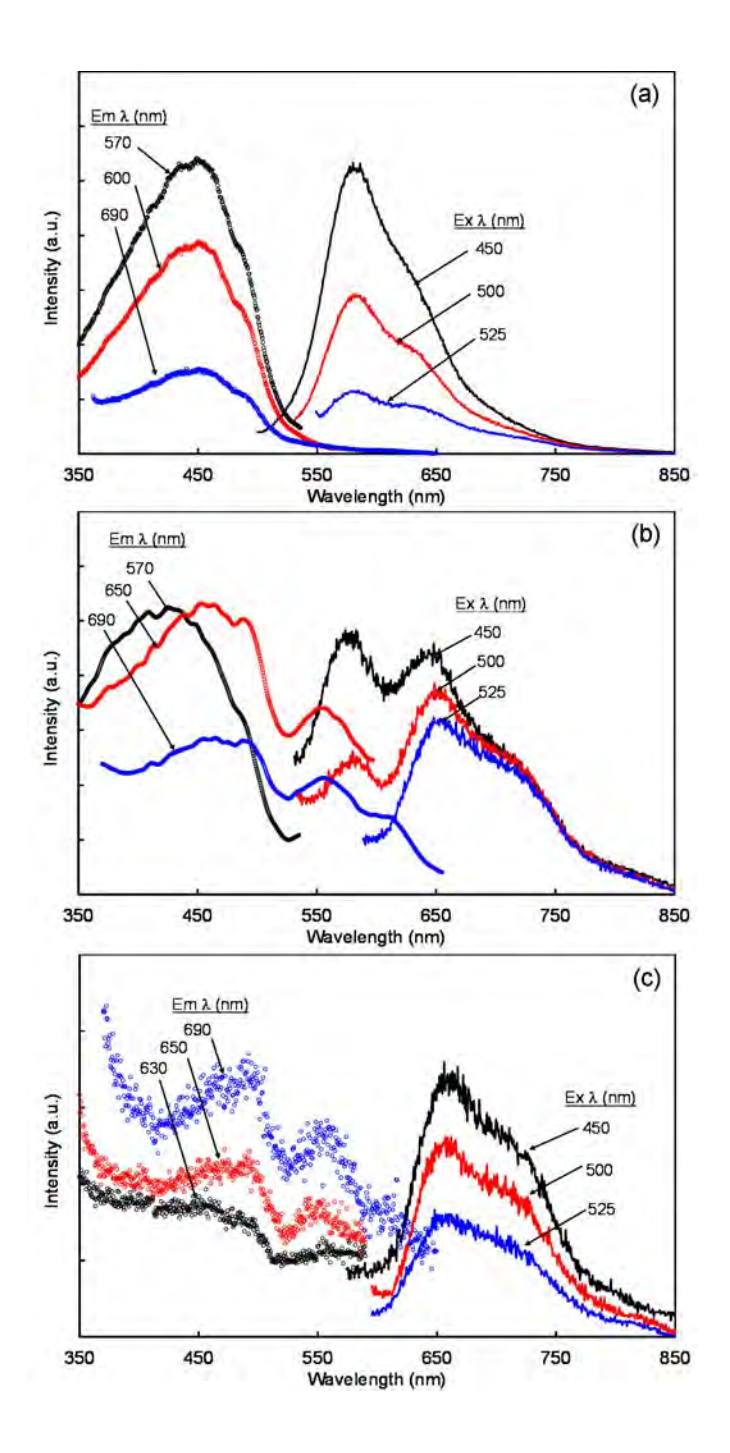


Figure 8 PLE spectra (symbol) and PL spectra (solid line) of 0.001 mg/mL rr-P3OT mixtures of pyridine and ethanol. The ratios of ethanol are (a) 0, (b) 40 and (c) 99 v/v%, respectively. The spectra were measured at different emission wavelengths (Em λ) and excitation wavelengths (Ex λ).

The measurements of PLE spectra in CRB/EtOH containing 99 %v/v EtOH clearly reveal the absorption band of the emissive aggregates (see Fig. 7c). In this system, the PL spectrum is independent of excitation wavelength. The use of excitation wavelengths at 450 nm, 500 nm, and 550 nm, which excites both non-aggregated and aggregated segments, provides the same PL pattern, constituting a peak and shoulder at about 650 nm and 715 nm, respectively. The dense segmental packing in this unfavorable environment of the nonsolvent promotes the efficiency of energy transfer processes. Therefore, the PL emission only occurs via aggregated chromophores with lowest HOMO-LUMO energy gap. The PLE spectra measured at different emission wavelengths show the same pattern, constituting three peaks at about 500 nm, 555 nm and 605 nm. The redshift peaks observed in absorption spectrum are at about 515 nm, 555 nm and 605 nm (see Fig. 1a). This comparison shows that the absorption λ_{max} of emissive aggregates is slightly shorter than that of the non-emissive one. On other words, these aggregates possess different conjugation length. The measurements of PLE and PL of rr-P3OT in PRD/EtOH provide consistent results (see Fig. 8b,c). The variation of excitation wavelength causes the change of PL pattern, corresponding to the presence of two emitting species in the solution containing 40 %v/v EtOH. At 99 %v/v EtOH, three peaks are clearly observed in PLE spectra. The peak position is the same as that of the CRB/EtOH system, indicating that the same emitting species exist in both systems.

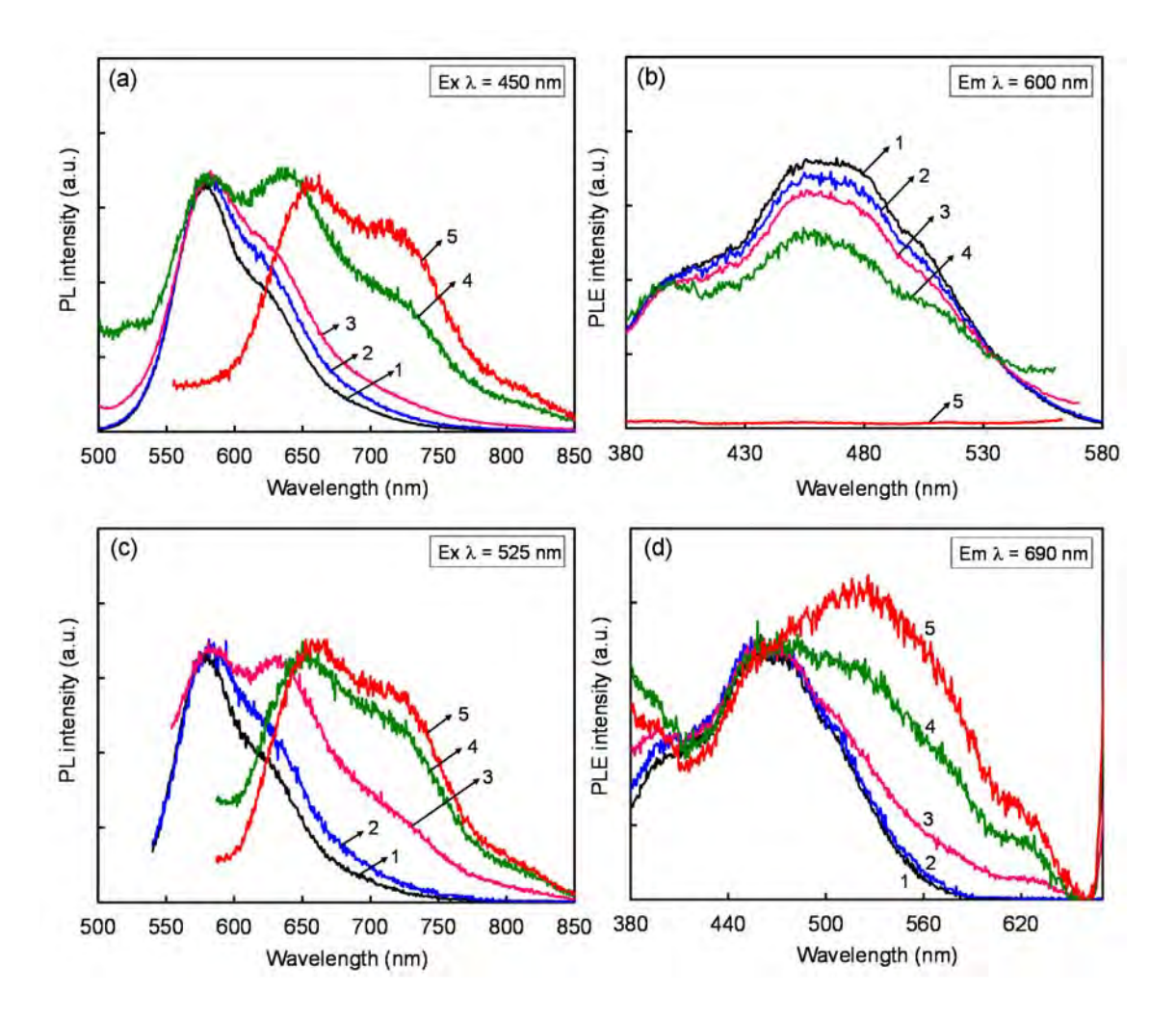


Figure 9 PL spectra (left) and PLE spectra (right) of 0.001 mg/mL rr-P3OT in mixtures of chlorobenzene and ethanol measured at excitation wavelengths (Ex λ) (a) 450 nm and (c) 525 nm and at emission wavelengths (Em λ) (b) 600 nm and (d) 690 nm, respectively. Ratios of ethanol are (1) 0 v/v%, (2) 40 v/v%, (3) 50 v/v%, (4) 60 v/v% and (5) 80 v/v%, respectively.

The change of PLE and PL spectra upon increasing EtOH ratio is summarized in Fig. 9. The PL spectra measured by using excitation wavelength at 450 nm show systematic growth of redshift peak upon increasing EtOH ratio to 60 %v/v, corresponding to the formation of emissive aggregates. At 80 %v/v EtOH, the emission of aggregates dominates the entire PL spectrum. The emission of aggregates is promoted when the excitation wavelength is increased to 525 nm (see Fig. 9c). The measurements of PLE spectra by fixing emission wavelength at 600 nm reveal absorption band of nonaggregated segments. The PLE spectra obtained from the solutions containing 0, 40, 50 and 60 %v/v EtOH show the same pattern (see Fig. 9b). This is due to the presence of relatively large fraction of non-aggregated segments in these systems. At 80 %v/v EtOH, PLE spectrum is not detectable because the emission processes only occurs via aggregated segments. When the emission wavelength is moved to 690 nm, systematic growth of redshift band in PLE is observed upon increasing EtOH ratio (see Fig. 9d). This corresponds to the increase emissive aggregates due to the dense packing of rr-P3OT segments.

4. Conclusion

In this study, we explore the nature and photophysical properties of *rr*-P3OT aggregates in solvent-nonsolvent system. We have found that the non-emissive aggregates form in the early stage of interchain association, resulting in the formation of three redshift peaks in absorption spectrum. The further decrease of solvent quality forces dense packing of polymeric segments within the aggregates, which in turn causes the formation of emissive aggregates. The PL emission of this aggregate occurs at lower energy region compared to that of the non-aggregated chains. The non-emissive and emissive aggregates also exhibit slightly different absorption

bands. We also observe that the amount and phtophysical properties of aggregates depend on the preparing condition such as the initial solvent. The use of PRD and CRB as initial solvent provide aggregates with rather different absorption pattern. Our results provide fundamental understanding about aggregation behaviors of conjugated polymers in different states. This knowledge is important for their utilization in advanced technologies.

Acknowledgments

This research is financially supported by the Thailand Research Fund, Ministry of Higher Education and Naresuan University (Grant RMU5380017). RP thanks the Office of Higher Education Commission for supporting her Ph.D. scholarship under the program Strategic Scholarships for Frontier Research Network. This work has partially been supported by the Nanotechnology Center (NANOTEC), Ministry of Science and Technology, Thailand, through its program of center of Excellence Network. RT thanks Center for Innovation in Chemistry (PERCH-CIC) for supporting some research facilities.

References

- 1. Brabec, C. J.; Sariciftci, N. S.; Hummelen, J. C. Adv. Funct. Mater. 2001, 11, 15-26.
- 2. Spanggaard, H.; Krebs, F. C. Sol. Energy Mater. Sol. Cells 2004, 83, 125-146.
- 3. Wang, C.; Dong, H.; Hu, W.; Liu, Y.; Zhu, D. Chem. Rev. 2011, 112, 2208-2267.
- 4. Kola, S.; Sinha, J.; Katz, H. E. J. Polym. Sci. Part B: Polym. Phys. 2012, 50, 1090-1120.
- 5. AlSalhi, M. S.; Alam, J.; Dass, L. A.; Raja, M. Int. J. Mol. Sci. 2011, 12, 2036-2054.
- 6. Chen, Y.; Ma, D. J. Mater. Chem. 2012, 22, 18718-18734.

- 7. Hoeben, F. J. M.; Jonkheijm, P.; Meijer, E. W.; Schenning, A. P. H. J. Chem. Rev. 2005, 105, 1491-1546.
- 8. Varghese, S.; Das, S. J. Phys. Chem. Lett. 2011, 2, 863-873.
- 9. Facchetti, A. Chem. Mater. 2011, 23, 733-758.
- 10. Rughooputh, S. D. D. V.; Hotta, S.; Heeger, A. J.; Wudl, F. J. Polym. Sci. Part B: Polym. Phys. 1987, 25, 1071-1078.
- 11. Rumbles, G.; Samuel, I. D. W.; Magnani, L.; Murray, K. A.; DeMello, A. J.; Crystall,
- B.; Moratti, S. C.; Stone, B. M.; Holmes, A. B.; Friend, R. H. Synth. Met. 1996, 76, 47-51.
- 12. Xu, B.; Holdcroft, S. Macromolecules 1993, 26, 4457.
- 13. Buvat, P.; Hourquebie, P. Macromolecules 1997, 30, 2685.
- 14. Lanzi, M.; Bertinelli, F.; Costa-Bizzarri, P.; Paganin, L.; Cesari, G. Eur. Polym. J. 2007, 43, 835-846.
- 15. Scharsich, C.; Lohwasser, R. H.; Sommer, M.; Asawapirom, U.; Scherf, U.;

Thelakkat, M.; Neher, D.; Köhler, A. J. Polym. Sci. Part B: Polym. Phys. 2012, 50, 442-453.

- 16. Magnani, L.; Rumbles, G.; Samuel, I. D. W.; Murray, K.; Moratti, S. C.; Holmes, A.
- B.; Friend, R. H. Synth. Met. 1997, 84, 899-900.
- 17. Samitsu, S.; Shimomura, T.; Heike, S.; Hashizume, T.; Ito, K. Macromolecules 2008, 41, 8000-8010.
- 18. Sun, S.; Salim, T.; Wong, L. H.; Foo, Y. L.; Boey, F.; Lam, Y. M. J. Mater. Chem. 2011, 21, 377-386.

- 19. Wu, P.-T.; Xin, H.; Kim, F. S.; Ren, G.; Jenekhe, S. A. Macromolecules 2009, 42, 8817-8826.
- 20. He, M.; Zhao, L.; Wang, J.; Han, W.; Yang, Y.; Qiu, F.; Lin, Z. ACS Nano 2010, 4, 3241-3247.
- 21. Xu, W.; Li, L.; Tang, H.; Li, H.; Zhao, X.; Yang, X. J. Phys. Chem. B 2011, 115, 6412-6420.
- 22. Chen, C.-Y.; Chan, S.-H.; Li, J.-Y.; Wu, K.-H.; Chen, H.-L.; Chen, J.-H.; Huang, W.-Y.; Chen, S.-A. Macromolecules 2010, 43, 7305-7311.
- 23. Park, Y. D.; Lee, H. S.; Choi, Y. J.; Kwak, D.; Cho, J. H.; Lee, S.; Cho, K. Adv. Funct. Mater. 2009, 19, 1200-1206.
- 24. Kiriy, N.; Jähne, E.; Adler, H.-J.; Schneider, M.; Kiriy, A.; Gorodyska, G.; Minko, S.; Jehnichen, D.; Simon, P.; Fokin, A. A.; Stamm, M. Nano Lett. 2003, 3, 707-712.
- 25. Kiriy, N.; Jähne, E.; Kiriy, A.; Adler, H.-J. Macromol. Symp. 2004, 210, 359-367.
- 26. Liu, J.; Loewe, R. S.; McCullough, R. D. Macromolecules 1999, 32, 5777-5785.
- 27. Merlo, J. A.; Frisbie, C. D. J. Phys. Chem. B 2004, 108, 19169-19179.
- 28. Barton, A. F. M. Chem. Rev. 1975, 75, 731-753.
- 29. Zen, A.; Saphiannikova, M.; Neher, D.; Asawapirom, U.; Scherf, U. Chem. Mater. 2005, 17, 781-786.
- 30. Xue, L.; Yu, X.; Han, Y. Colloid Surf. A: Physicochem. Eng. Asp 2011, 380, 334-340.
- 31. Huang, W. Y.; Huang, P. T.; Han, Y. K.; Lee, C. C.; Hsieh, T. L.; Chang, M. Y. Macromolecules 2008, 41, 7485-7489.
- 32. Potai, R.; Traiphol, R. J. Colloid Interface Sci. 2013, 403, 58-66.

- 33. Potai, R.; Kamphan, A.; Traiphol, R. J. Polym. Sci. Part B: Polym. Phys. 2013, DOI:
- 10.1002/polb.23326
- 34. Melis, C.; Colombo, L.; Mattoni, A. J. Phys. Chem. C 2011, 115, 576-581.
- 35. Brinkmann, M. J. Polym. Sci. Part B: Polym. Phys. 2011, 49, 1218-1233.
- 36. Traiphol, R.; Sanguansat, P.; Srikhirin, T.; Kerdcharoen, T.; Osotchan, T.

Macromolecules 2006, 39, 1165-1172...

- 37. Traiphol, R.; Charoenthai, N.; Srikhirin, T.; Kerdcharoen, T.; Osotchan, T.; Maturos,
- T. Polymer 2007, 48, 813-826.
- 38. Traiphol, R.; Charoenthai, N.; Manorat, P.; Pattanatornchai, T.; Srikhirin, T.;

Kerdcharoen, T.; Osotchan, T. Synth. Met. 2009, 159, 1224-1233.

- 39. Prosa, T. J.; Winokur, M. J.; McCullough, R. D. Macromolecules 1996, 29, 3654-3656.
- 40. Arosio, P.; Moreno, M.; Famulari, A.; Raos, G.; Catellani, M.; Meille, S. V. Chem. Mater. 2009, 21, 78-87.
- 41. Brinkmann, M. J. Polym. Sci. Part B: Polym. Phys. 2011, 49, 1218-1233.
- 42. Traiphol, R.; Potai, R.; Charoenthai, N.; Srikhirin, T.; Kerdcharoen, T.; Osotchan, T.
- J. Polym. Sci. Part B: Polym. Phys. 2010, 48, 894-904.
- 43. Barbara, P. F.; Gesquiere, A. J.; Park, S.-J.; Lee, Y. J. Acc. Chem. Res. 2005, 38, 602-610.
- 44. Palacios, R.; Barbara, P. J. Fluores. 2007, 17, 749-757.
- 45. Adachi, T.; Lakhwani, G.; Traub, M. C.; Ono, R. J.; Bielawski, C. W.; Barbara, P. F.; Vanden Bout, D. A. J. Phys. Chem. B 2012, 116, 9866-9872.

บทที่ 3

Controlling chain organization and photophysical properties of conjugated polymer nanoparticles prepared by reprecipitation method:

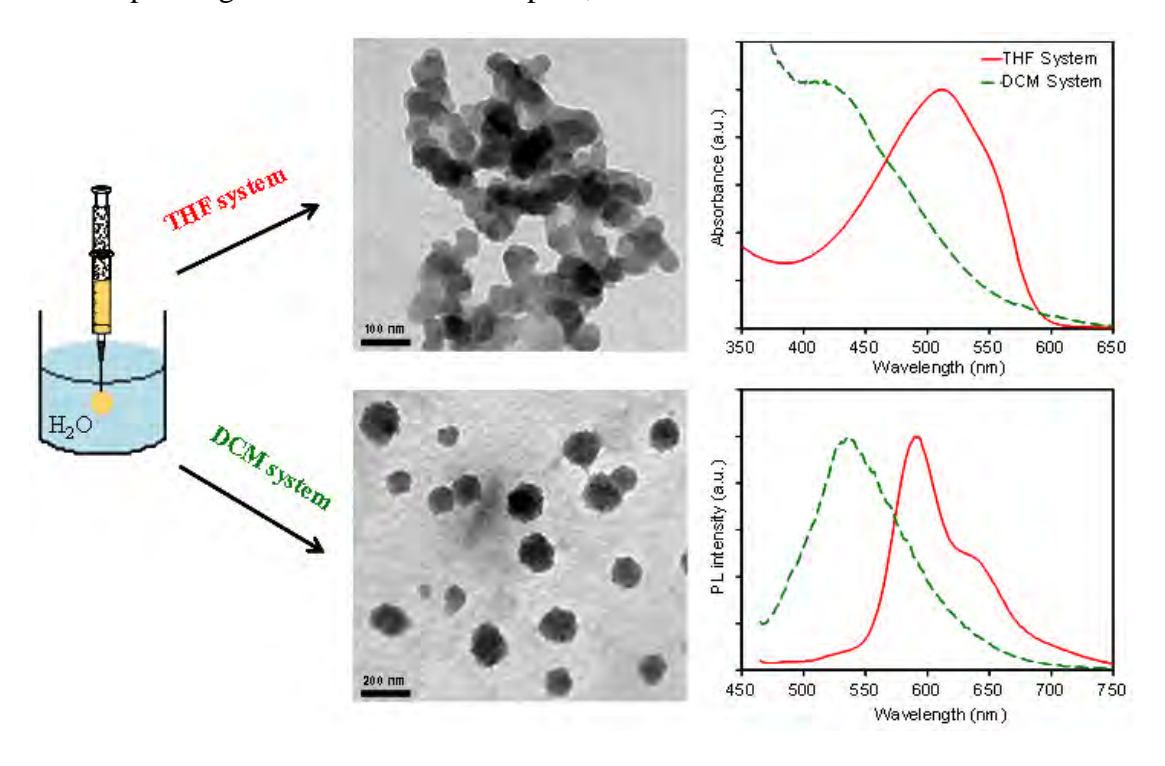
The effect of initial solvent

Ruttayapon Potai^a, Rakchart Traiphol^{a,b*}

^a Laboratory of Advanced Polymers and Nanomaterials, Department of Chemistry and Center for Innovation in Chemistry, Faculty of Science, Naresuan University, Phitsanulok 65000, Thailand

^bNANOTEC-MU Excellence Center on Intelligent Materials and Systems, Faculty of Science, Rama 6 Road, Ratchathewi, Bangkok 10400, Thailand

*Corresponding Author: Rakchart Traiphol; e-mail: rakchartt@nu.ac.th



Abstract

This study explores roles of initial solvent on the formation of conjugated polymer nanoparticles (CPNs) and their photophysical properties. Stable aqueous CPN dispersion of poly(2-methoxy-5-(2'-ethylhexyloxy)-1,4-phenylvinylene)(MEH-PPV) and regioregular poly(3-octylthiophene)(rr-P3OT) are prepared via reprecipitation technique. This preparation method involves the injection of polymer solution in organic solvents into an excess amount of water. We demonstrate that water solubility of the initial solvent is a major factor dictating mechanism of the CPN formation. Dichloromethane (DCM) and tetrahydrofuran (THF), possessing very different water solubility, are used as initial solvents in this work. The resultant CPNs exhibit quite different size and photophysical properties. The preparation of MEH-PPV nanoparticles from DCM solution provides average size of about 127 nm. Their absorption and photoluminescence (PL) spectra shift to higher energy region compared to those of the isolated chain. When the THF solution is used, opposite results are observed. Average size of the nanoparticles decreases to about 40 nm. Significant red shift of their absorption and PL spectra is also detected. Detailed data analysis indicates that the individual chain conformation and degree of segmental aggregation within the CPNs are quite different. This leads to drastic discrepancies of their photophysical properties. The use of DCM and THF as initial solvents provides the MEH-PPV nanoparticles with green ($\lambda_{max} = 535$ nm) and red (λ_{max} = 590 nm) photoemission, respectively. The investigation of rr-P3OT provides consistent results. Our study offers a new and simple route to control size and photophysical properties of CPNs by careful selection of the initial solvents.

Keywords: conformational change; aggregation; self-assembling; molecular packing

1. Introduction

Conjugated polymer is a class of material that has received tremendous attention from scientific community in the past few decades. Major applications of conjugated polymers, which exhibit electroluminescent and semiconducting properties, involve organic electronic technologies such as organic light emitting diode (OLED) [1,2], organic solar cell (OSC) [3,4] and organic field emission transistor [5,6]. Poly[2-methoxy-5-(2'-ethylhexyloxy)-1,4-phenylenevinylene] (MEH-PPV) and regioregular poly(3-alkylthiophenes) (*rr*-P3ATs) are well-known conjugated polymers that has been extensively studied. The presence of branched side chains in MEH-PPV causes high fraction of amorphous region in thin film, which in turn enhances the fluorescent intensity [7,8]. The *rr*-P3ATs, on the other hand, are more crystalline materials with relatively high charge carrier mobility while their fluorescent intensity in thin film is rather weak [9,10]. Therefore, the MEH-PPV is more suitable for OLED application while the *rr*-PATs are normally utilized as active materials in OSC [1,10].

Conjugated polymer is also a potential material for being utilized in biotechnologies such as fluorescent sensor [11,12], biological fluorescent imaging [13,14], and biological label [15,16]. To utilize conjugated polymers in these biotechnologies, the polymers are usually fabricated into nanoparticle form. Compared to other types of nanoparticles such as liposomes and micelles, conjugated polymer nanoparticles (CPNs) possess an increased colloidal stability and a better chemical resistance [17]. The fabrication process is usually easier as well. Moreover, the higher biocompatibility and less toxicity of CPNs compared to inorganic nanoparticles are desirable properties for using these materials in the biotechnologies [18,19]. Because

each CPN contains a number of chromophores, it normally exhibit higher brightness and better photostability compared to molecular dyes [13,20]. Their photoluminescent properties can also be tuned by varying particles size, composition and type of conjugated polymers [19].

CPNs can be prepared by using different methods such as oxidative polymerization, miniemulsion and reprecipitation. The oxidative polymerization process requires catalyst/oxidant such as FeCl₃/H₂O₂ and appropriate surfactants [21-24]. The polymerization of monomers is allowed to take place inside small droplets of the reaction medium stabilized by surfactant. The properties of CPNs can be optimized by varying the surfactant/oxidant/monomer ratio, polymer concentration, polymerization temperature, and reaction time [24-26]. However, there are several problems involving this method such as poor water-solubility of polymer, low oxidizing activity of catalysts, and extremely low conversion [21,26]. For miniemulsion method, the conjugated polymer dissolved in organic solvent is injected into an aqueous medium containing surfactant molecules [17]. The process generates stable-colloidal droplets of the polymer solution. The CPNs are obtained after evaporating the organic solvent. However, the surfactant molecules still remain in the system. The reprecipitation method can produce pure CNPs with controllable size [18,27]. The process requires the addition of small amount of dilute conjugated polymer solution into an excess volume of water. The sudden decrease of solubility drives the conjugated polymers to form nanoparticle The reprecipitation method is a popular technique because it is quite simple, cheap and does not require any surfactant or template. The particle size can be simply controlled by adjusting the polymer concentration [13,19,28]. Moreover, this method can be applied to a wide variety of conjugated polymers that are soluble in organic solvents.

The preparation and photophysical properties of CPNs have been reported by several research groups. McNeill and co-workers have prepared various CPNs by using reprecipitation method. The injection of a dilute solution of MEH-PPV in tetrahydrofuran (THF) into aqueous medium provides CPNs with particle size ranging from 5 to 10 nm [29]. The conjugated polyfluorene, use of other polymers such as polyphenyleneethynylene and their copolymers also yields the CPNs with similar size [13,19]. They have demonstrated in these studies that the photoluminescent (PL) color of CPNs varies with types of the conjugated polymers. The size of CPNs also affects their PL properties. The CPNs of 2,7-poly(9,9-dialkylfluorene-co-fluorenone) exhibit systematic shift of PL spectra to low-energy region when their size is increased from 5 to 500 nm [30]. The CPNs of polythiophene shows similar behavior. Their PL color changes from blue to red upon increasing the size from 12 to 51 nm [23].

In this work, we present a new and versatile method for controlling the photophysical properties of CPNs. Previous studies have shown that conjugated polymer such as MEH-PPV in solution adopts different conformation depending on the strength of local polymer-solvent interactions [31-35]. The MEH-PPV chain is extended in a good solvent, dichloromethane (DCM), while the chain forms collapsed coil in a poor solvent, THF [31,34]. The decrease of solvent quality by addition of nonsolvent forces the MEH-PPV chains into aggregated state, which in turn causes the red shift of absorption and PL spectra [33,35,36]. In our recent study, we observe that the variation of initial solvents affects the degree of segmental aggregation in the solvent-nonsolvent system [35]. Since

the preparation of CPNs via reprecipitation method also induces the assembling of polymer chains by decreasing solvent quality, the initial solvents are expected to play important role on their aggregation behavior. In this study, we use DCM and THF as initial solvents to prepare CPNs of MEH-PPV and regioregular poly(3-octylthiophene)(rr-P3OT) in aqueous medium. The difference of initial polymer conformations is expected to influence of chain packing within CPNs. In addition, the miscibility of DCM and THF with water is quite different [37] (see Table 1), which may also play important role on the formation of CPNs. In fact, the CPNs obtained by using the DCM and THF exhibit quite different photophysical properties. Our approach provides a simple method for controlling photophysical properties of CPNs without modifying chemical structure and/or composition of the conjugated polymer.

2. Experimental

The conjugated polymers, MEH-PPV and rr-P3OT, were purchased from Sigma-Aldrich. Number average molecular weight (M_n) and polydispersity (M_w/M_n) of the polymers determined by gel permeation chromatography (GPC) with polystyrene standard are 120,000 g/mol $(M_w/M_n = 4.3)$ for MEH-PPV and 58,300 g/mol $(M_w/M_n = 2.3)$ for rr-P3OT. THF was used as a solvent in the GPC measurement. The solvents, THF (anhydrous 99%) and DCM (AR grade), were purchased from Sigma-Aldrich. Physical properties of these solvents are shown in Table 1.

Table 1 Physical properties of solvents [37] and size of conjugated polymer nanoparticles prepared by using different solvents

Solvents	Boiling point (°C)	Dielectric constant	Solubility in water (g/L, 25°C)	Average particle size (nm)	
				MEH-PPV	rr-P3OT
THF	66.0	7.52	Miscible	49.1 ± 17.5	49.4 ± 13.1
DCM	39.8	8.93	17.6	127.2 ± 29.8	99.6 ± 64.5

Nanoparticles of all conjugated polymers were prepared by a reprecipitation method adapted from literature [13,14,19]. The conjugated polymers were fully dissolved in THF and DCM solvents and then diluted to concentration of 0.001 mg/mL. This concentration is lower than that of McNeill's study. However, the concentration is appropriate for the measurements of PL spectra with minimal influence of an innerfiltered effect. To prepare CPNs, each of 0.2 mL polymer solution was injected in a stepwise process into 32 mL of deionized water while the mixtures were under continuous ultrasonication at 60 °C. The 0.2 mL addition of solution is equivalence to 8.3 g/L concentration of the organic solvents in water. This concentration is still lower than their water solubility (see Table 1). The mixtures appeared clear to naked eyes indicating complete miscibility. The time interval between each step was about 2 minutes, allowing the evaporation of organic solvents. The sum volume of polymer solution was 8 mL requiring the addition time of about 1.5 hours. The ultrasonication process was continued for 30 minutes to ensure complete evaporation of the organic solvents. The resultant aqueous suspensions were filtered through 0.45 µm pore size cellulose acetate membrane. The CPN aqueous suspensions were clear and stable for months with no sign of agglomeration. Thin films of conjugated polymers were prepared by drop-casting from 1 mg/mL solution onto quartz slide. The solution droplet was allowed to dry in a clean atmosphere under ambient condition. Atomic force microscopy reveals that the films exhibit rough surface with thickness ranging from about 30 to 400 nm. Absorbance of all films is less than 0.1.

The UV-vis absorption spectra of CPNs were recorded by employing Analytic Specord 100 spectrometer with 10 cm thick quartz cuvette while the PL spectra were measured by using Perkin-Elmer LS55 spectrometer. Absorbance of the CPN aqueous suspensions is less than 0.4 (equivalence to 0.04 for 1 cm thick cuvette). Since the absorbance of conjugated polymer is very low, an inner-filtered effect in the PL measurement is negligible in all systems [38]. Morphology and size distribution of the CPNs were characterized by transmission electron microscopy (TEM, Tecnai 12, D291) and scanning electron microscopy (SEM, LEO 1455 VP). The samples for TEM were prepared by drop-casting from CPN aqueous suspensions onto copper grids coated with carbon film. For SEM samples, one drop of CPN aqueous suspensions was deposited on a polished silicon substrate. After the evaporation of water, the samples were coated with gold.

3. Results and discussion

3.1. Nanoparticles of MEH-PPV

Morphologies and size distribution of MEH-PPV nanoparticles revealed by TEM are shown in Fig. 1. The nanoparticles prepared from both THF and DCM solvents exhibit spherical shape. Their size, however, varies significantly with type of the solvents. The use of THF as an initial solvent provides the nanoparticles with smaller size. The majority of nanoparticles exhibit diameter of about 40 nm. When the DCM is used as an initial solvent, average size of the nanoparticles significantly increases to about 120 nm. Their size distribution also becomes much broader. Furthermore, the packing of polymer chains within nanoparticles are affected by the variation of initial solvents. The nanoparticles prepared from DCM exhibit a rougher surface compared to that of the THF system. The interior density of each nanoparticle is also less homogeneous in the DCM system. These results indicate that mechanism for the nanoparticle formation strongly depends on type of the initial solvent. We note that the nanoparticles prepared from THF can be filtered through 200 nm pore size cellulose acetate membrane. Therefore, the agglomeration of nanoparticles in Fig. 1a is likely to occur during the preparation process for TEM measurement. The SEM images also detect large fraction of isolated nanoparticles. The nanoparticles obtained in this study exhibit larger size compared to the previous reports [13,18,29]. This is attributed to the difference in preparation conditions such as power of the ultrasonication and volume of the added solution in each step.

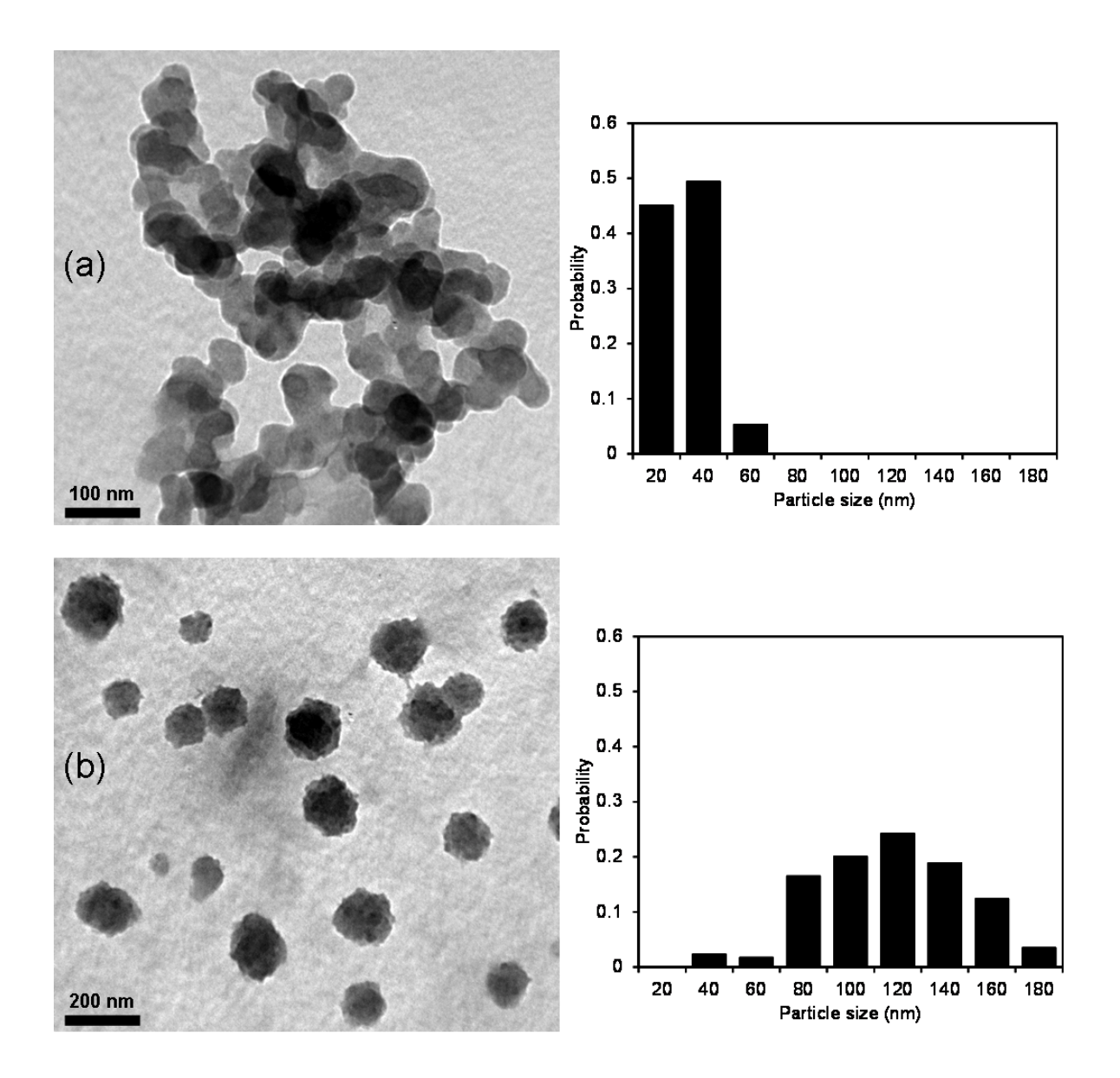


Fig. 1 TEM images of MEH-PPV nanoparticles prepared from different initial solvents, (a) THF and (b) DCM. Their size distributions are presented at the right side.

Photophysical properties of the MEH-PPV nanoparticles vary significantly with type of the initial solvent. Fig. 2 illustrates absorption and PL spectra of the MEH-PPV in different forms. The isolated chains in dilute THF solution exhibit a broad absorption spectrum with λ_{max} at about 504 nm. The broad pattern corresponds to electronic transition of various chromophores, possessing different conjugation length, within the conjugated chains. The photoemission process normally takes place via chromophores with the lowest HOMO-LUMO energy gap due to the high efficiency of energy transfer process [39-41]. The PL spectrum showing a well-defined pattern with λ_{max} and vibronic shoulder at about 554 nm and 594 nm, respectively, reflects energy levels of the longest chromophore within the system. When the MEH-PPV chains are forced to densely pack into nanoparticles by injecting the solution into an excess amount of water, the absorption and PL patterns change drastically. The absorption spectrum of nanoparticles prepared from THF solution shifts to lower energy region where the λ_{max} is detected at 515 nm. New red-shift peak is also observed at about 550 nm. The appearance of this red-shift peak indicates the formation of inter- and/or intrachain aggregates where some conjugated segments or chromophores stack on top of each other. The appropriate overlapping of π -orbitals within the aggregates allows the formation of new electronic species with lower HOMO-LUMO energy gap. PL spectrum of the nanoparticles, reflecting electronic energy levels of the aggregates, exhibit λ_{max} and vibronic shoulder at about 594 nm and 640 nm, respectively. It is important to note that some conjugated segments do not form aggregates within the nanoparticles. The packing of these segments during the addition of water occurs in a random fashion, which do not allow the overlapping of π -orbitals. Absorption spectra of these segments remain unaltered. Therefore, fraction of the aggregates within the system is proportional to the ratio of absorbance at 550/500 nm. Detailed discussion of this topic is given in our previous reports [33,35].

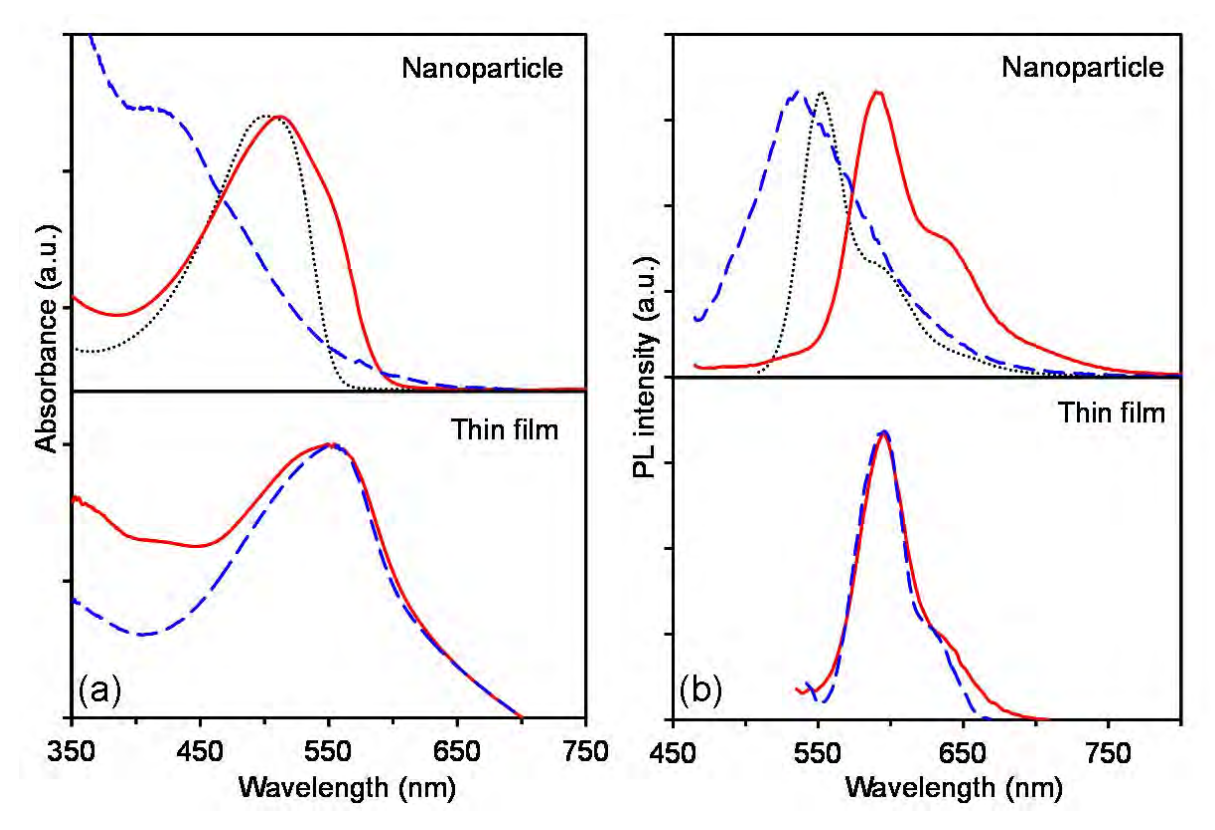


Fig. 2 (a) UV-vis absorption and (b) PL spectra of MEH-PPV in different forms, (top) nanoparticles and (bottom) drop-cast films. The samples were prepared by using (solid lines) THF and (dashed lines) DCM as initial solvents. The spectra of MEH-PPV dilute solution in THF (dotted lines) are included for comparison.

The MEH-PPV nanoparticles prepared by using DCM as an initial solvent exhibit quite different photophysical properties. Interestingly, the absorption spectrum shifts to higher energy region compared to that of the isolated chain. The absorbance at wavelength below 400 nm also rises significantly. Local λ_{max} is detected at about 420 nm.

The significant blue shift of absorption spectrum indicates the collapse of MEH-PPV chains within the nanoparticles [31-34]. The drastic shrinkage of conjugated chains introduces kinks or physical defects within the backbone, which in turn limit local delocalization of π electrons. In other words, the conjugation length of chromophores in the collapsed chain is reduced. Our previous studies have shown that the location of absorption spectra depends on the extent of chain collapse [42]. The absorption spectrum of isolated MEH-PPV chain systematically shifts to high-energy region upon increasing the polarity of alcohol solvents (i.e. decreasing solvent quality). In methanol, the MEH-PPV exhibits λ_{max} at about 445 nm. In this study, λ_{max} of the nanoparticles in water is detected at about 420 nm. This indicates higher magnitude of the chain collapse, which is attributed to the higher polarity of water medium. However, we also detect a broad shoulder at wavelength above 550 nm, corresponding to the aggregation of some chromophores within the nanoparticles. The measurement of PL spectrum indicates the collapse of MEH-PPV chain as well. The PL spectrum shifts to high-energy region and exhibits a featureless pattern. The PL peak is detected at about 535 nm while the vibronic shoulder is not observed. The absence of the vibronic shoulder suggests that the vibrational energy levels of this system are not well-defined. We also prepare the MEH-PPV nanoparticles by using polymer concentration at 1×10^{-2} mg/mL and 1×10^{-4} mg/mL (see supporting information). While quantity of the nanoparticles increases with concentration, their absorption and PL spectra are hardly affected. The size distribution also remains approximately the same. We believe that the filtration by using 0.45 µm pore size membrane allows only small-size nanoparticles to pass through.

It is important to note that the variation of CPN photophysical properties is not due to the difference of their size. It has been observed in other systems that an increase of CPN size causes a red shift of PL spectra [23,30]. In our system, the CPN prepared from DCM exhibits much larger size compared to that of the THF system. Its PL spectrum, however, shifts to higher energy region. The conjugation length of chromophores within extended MEH-PPV backbone constitutes about 10 to 17 repeat units [43], which is shorter than the dimension of nanoparticles. The free volume required for segmental aggregation is also smaller. Therefore, the chain collapse and segmental aggregation causing the change of conjugation length can occur within the nanoparticles. In previous study where the size of MEH-PPV nanoparticles is about 5 to 10 nm, the aggregation is still detected [29].

Table 2 Spectroscopic properties of conjugated polymers in different forms

	Initial solvents			
Samples	λ_{max} of absorption spectra		λ_{max} of PL spectra	
	THF	DCM	THF	DCM
MEH-PPV				
Solution	503	507	553 (585)	559 (600)
Nanoparticle	515 (550)	420	590 (630)	535 ^a
Film	549	550	593 (632)	593 (631)
rr-P3OT				
Solution	448	450	566 (604)	572 (610)
Nanoparticle	512 (546, 593)	-	633 (686)	558 ^b
Film	546 (610)	565 (615)	635 (663)	635 (662)

Our results clearly show that the initial solvent plays a very important role on the formation and hence photophysical properties of the MEH-PPV nanoparticles. Table 2 summarizes the photophysical properties of MEH-PPV in different forms. The MEH-PPV nanoparticles prepared from DCM and THF exhibit green ($\lambda_{\text{max}} = 535 \text{ nm})$ and red $(\lambda_{max} = 594 \text{ nm})$ photoemission, respectively. To further explore the origin of our major finding, we prepare thin films of the conjugated polymer by drop casting from 1 mg/mL THF and DCM solutions. This method allows self-assembling process of the conjugated polymer to take place without perturbing the individual chain conformation. The absorption patterns of resultant films are quite different from those of the nanoparticles. The change of solvents hardly affects their photophysical properties. The absorption spectra of both films exhibit λ_{max} at about 550 nm, accompanied with a broad low-energy tail extending above 600 nm. The significant red shift of the whole spectra to 550 nm indicates the presence of high aggregate fraction within the thin films. The appearance of low-energy tail is attributed to electronic absorption of other types of aggregates with relatively low HOMU-LUMO energy gap [44]. It has been shown that aggregates can exist in different forms depending on the stacking configuration of chromophores [45,46]. The PL spectra of both films are also similar exhibiting λ_{max} at about 593 nm. The slight difference of their pattern is within error bar of the measurements. In our recent study where MEH-PPV chains in DCM and THF are forced to assemble into particles by addition of cyclohexane (nonsolvent), we observe different aggregation mechanism [35]. At the very high fraction of cyclohexane, the use of DCM as initial solvent results in higher fraction of aggregates compared to that of the THF system.

An opposite result is obtained in this study where water is used as a poor solvent to drive the assembling of MEH-PPV chains into nanoparticles. Fig. 3 compares the amount of aggregates in each system by plotting ratio of absorbance at 550/500 nm. The aggregate fractions in thin films prepared by using the two solvents are comparable. In nanoparticles, however, the use of THF as an initial solvent leads to much higher fraction of aggregates. The nanoparticles prepared from DCM also contain large fraction of collapsed coils. The discrepancies of segmental aggregation and chain conformation lead to drastic difference of their PL spectra. This fundamental knowledge can be utilized to control properties of the nanoparticles without changing the structure or composition of the constituent polymers. Our results clearly demonstrate that the nanoparticles with different sizes and properties can be fabricated by varying type of the initial solvent. We also note that the nanoparticles contain lesser amount of aggregates compared to the drop cast films. This is attributed to the confinement of polymer chains within a small volume that hinders the appropriate stacking of some chromophores. However, the intensity of low energy peak (~630 nm) in PL spectra of the nanoparticle prepared from THF is higher than that of the thin film. Previous study shows that the photoemission of excimer contributes to the intensity of this peak [47]. Our observation suggests that the molecular packing within the nanoparticle favor the excimer formation.

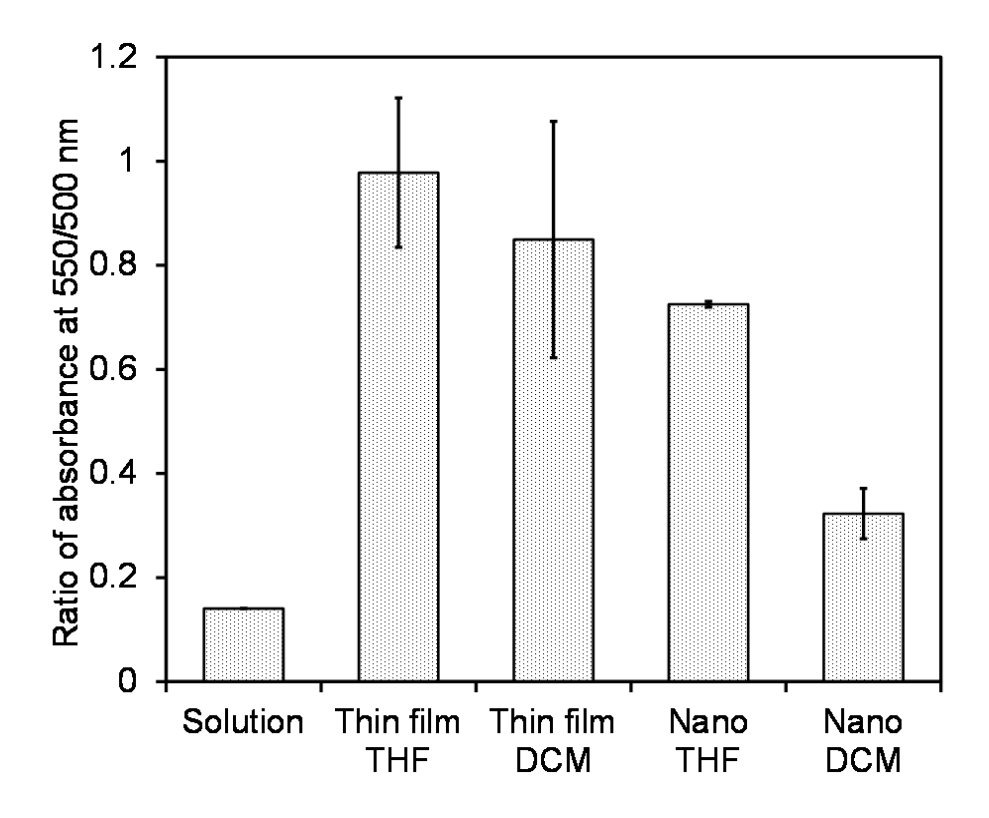


Fig. 3 Ratios of absorbance at 550/500 nm reflecting the aggregate fraction of MEH-PPV in different forms

Photophysical properties of the MEH-PPV nanoparticles are further explored by varying excitation wavelength as shown in Fig. 4. The variation of excitation energy allows electronic transition of various chromophores with different conjugation length. However, the PL spectra of nanoparticles prepared by using THF as an initial solvent exhibit the same pattern (see Fig. 4a). This result indicates that the photoemission process occurs via one type of chromophores. In this system, the fraction of aggregates, possessing the lowest HOMO-LUMO gap, is relatively high. The excited chromophores, therefore, can effectively transfer energy to aggregated sites before the photoemission

process takes place. The PL pattern only reflects electronic energy levels of aggregates. The measurements of photoluminescence excitation (PLE) spectra at different emission wavelengths provide consistent results. The PLE pattern is similar to the absorption spectrum and independent of the detecting emission wavelength as shown in Fig 4b. This behavior is similar to systems of thin films where aggregate fraction is also quite high. The result is quite different in the system of nanoparticles prepared by using DCM as an initial solvent. Fig. 4c shows that the PL spectra systematically shift to low-energy region upon increasing excitation wavelength. Since the nanoparticles constitute collapsed chains and contain less amount of aggregates, the energy transfer process is less efficient compared to the system of THF. Therefore, this system allows photoemission of different chromophores upon varying the excitation energy. This observation is consistent with our previous studies where the multiple photoemissions are detected in the system of collapsed coils [33,42]. The measurement of PLE spectrum by fixing emission wavelength at 500 nm detects the absorption at high-energy region with λ_{max} at about 395 nm (see Fig. 4d). This corresponds to the excitation of relatively short chromophores within the system. When the detecting emission wavelength is increased to 590 nm, the excitation band at about 435 nm grows significantly.

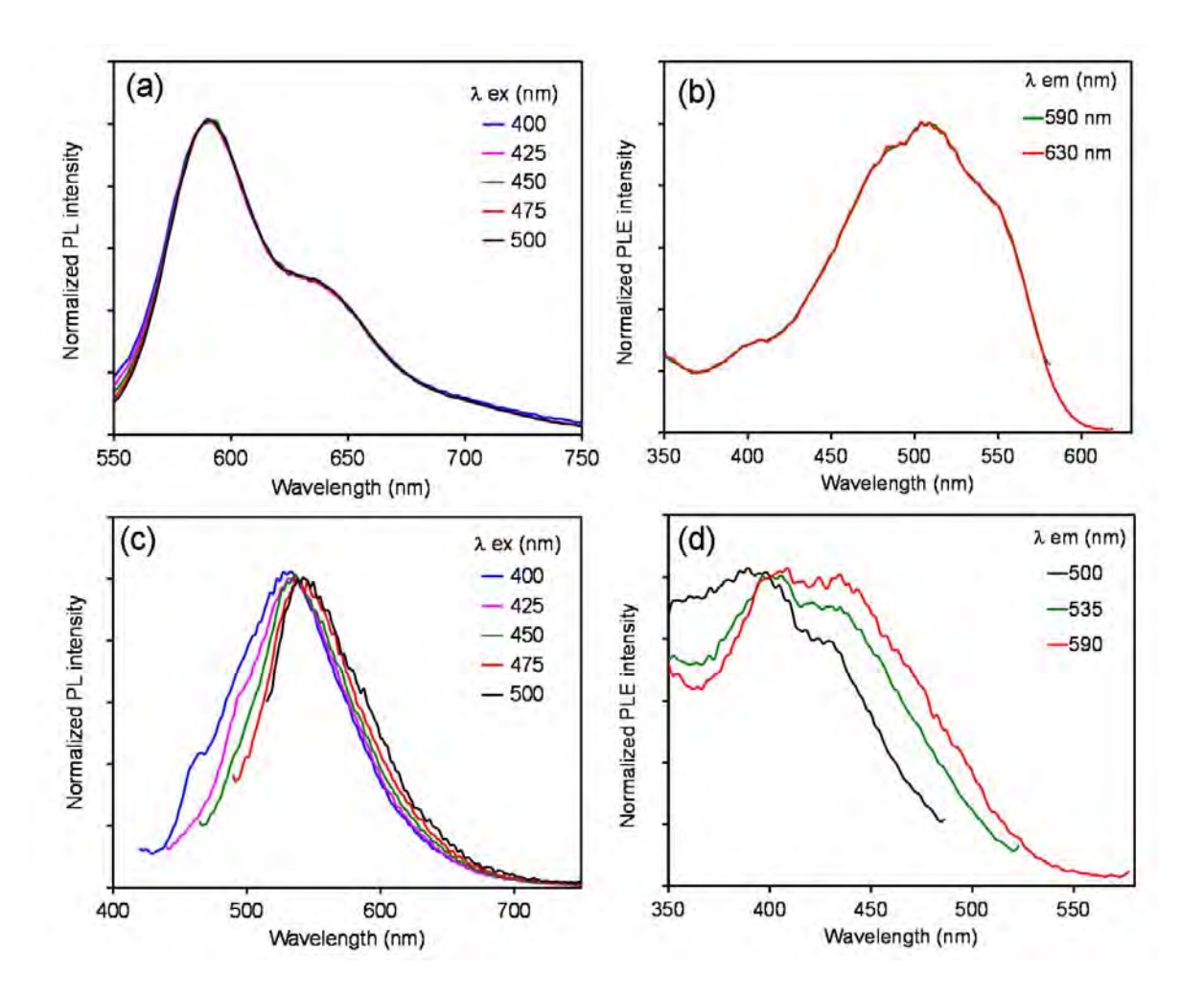


Fig. 4 (a,c) PL spectra and (b,d) PLE spectra of MEH-PPV nanoparticles measured at different excitation wavelengths (Ex λ) and emission wavelengths (Em λ), respectively. The nanoparticles were prepared from (a,b) THF and (c,d) DCM initial solvents.

From the aforementioned results, we propose mechanism for the formation of MEH-PPV nanoparticles in Fig. 5. Recent study by Cossiello et.al estimates solubility parameter (δ) of MEH-PPV and their components (δ_d (dispersion), δ_p (polar) and δ_h (hydrogen bonding)) as $\delta=18.7~J^{1/2}cm^{-3/2}$, $\delta_d=18.0~J^{1/2}cm^{-3/2}$, $\delta_p=4.0~J^{1/2}cm^{-3/2}$ and $\delta_h=18.0~J^{1/2}cm^{-3/2}$

 $3.0~J^{1/2}cm^{-3/2}$ [48]. They also observe that dispersion interaction between MEH-PPV and solvent is a major factor dictating the chain conformation and its photophysical properties. The absorption and PL spectra of MEH-PPV systematically blue shifts upon decreasing δ_d value of solvents, which corresponds to the decrease of conjugation length. Solubility parameters of solvents used in this study are listed in Table 3 [49]. The δ_d value of DCM, $18.2~J^{1/2}cm^{-3/2}$, is very close to that of MEH-PPV, providing strong dispersion interaction. Therefore, the chain adopts extended conformation in this solvent. The dispersion interaction between MEH-PPV and THF ($\delta_d = 16.8~J^{1/2}cm^{-3/2}$) is weaker forcing the chain shrinkage, which leads to the decrease of conjugation length. Table 2 shows that λ_{max} of the absorption and PL spectra of MEH-PPV in THF solvent is shorter than that of the DCM system.

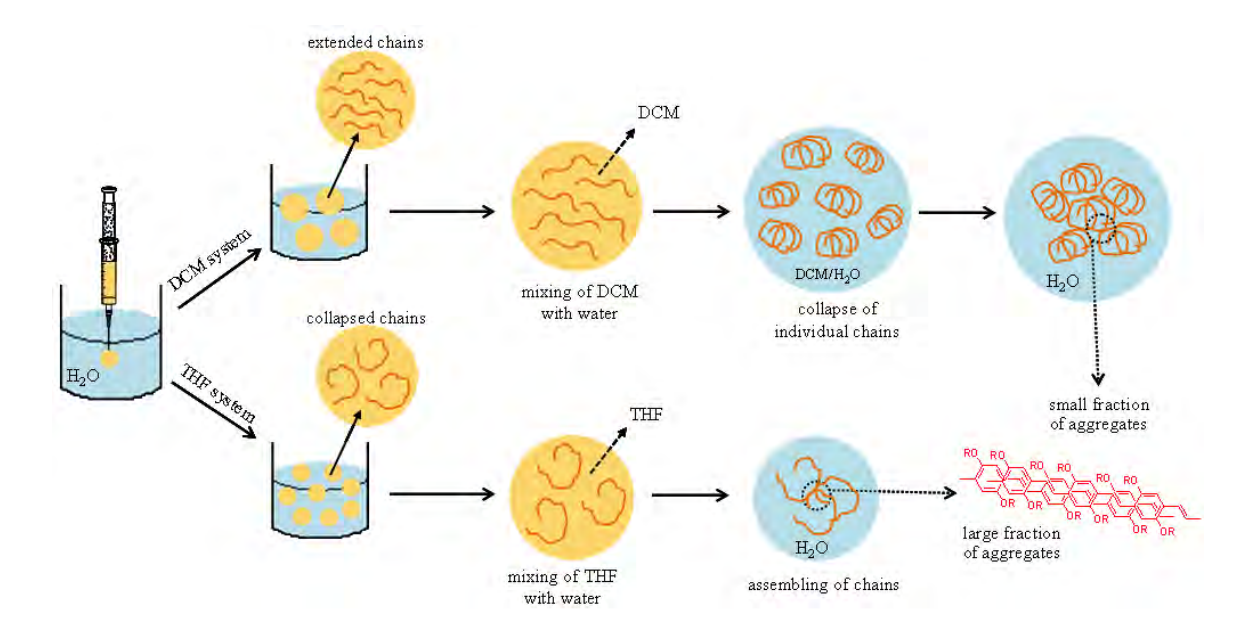


Fig. 5 Proposed mechanisms for the formation of MEH-PPV nanoparticles prepared by using (top) DCM and (bottom) THF as initial solvents

Table 3 Solubility parameter of solvents and conjugated polymers and their components [48,49,52]

Sample	$\delta (J^{1/2} cm^{-3/2})$	$\delta_{\rm d} ({\rm J}^{1/2} {\rm cm}^{-3/2})$	$\delta_{\rm p} ({\rm J}^{1/2} {\rm cm}^{-3/2})$	$\delta_h (J^{1/2} cm^{-3/2})$
DCM	20.3	18.2	6.3	6.1
THF	19.4	16.8	5.7	8.0
Water	47.8	15.5	16.0	42.3
MEH-PPV	18.7	18.0	4.0	3.0
rr-P3OT	18.2	-	-	-

When the polymer solutions in DCM or THF are injected into water medium, the interactions between the solvents play a crucial role on the formation of nanoparticles. Water is a nonsolvent for MEH-PPV. It has relatively high δ value (47.8 J^{1/2}cm^{-3/2}). The THF is miscible with water while the aqueous solubility of DCM is limited at 17.6 g/L. In the preparation process of nanoparticle, the initial droplets of THF or DCM solutions are disintegrated by continuous ultrasonication. Since the THF has favorable interactions with water, the solution is spontaneously broken into small droplets with narrow size distribution. The DCM, on the other hand, has weaker interactions with water, which in turn resist the breaking process. Therefore, the resultant DCM droplets exhibit larger size compared to that of the THF system. This hypothesis is supported by the size of obtained nanoparticles. The use of DCM as an initial solvent provides the nanoparticles with much larger size as shown in Table 1. This result is similar to the system of polymer blend where the size of polymer droplet increases with decreasing polymer-polymer interactions [50].

The mixing of THF with water is also relatively fast, which in turn drives the assembling of MEH-PPV molecules into nanoparticles with minimal change of individual chain conformation. The stacking of some conjugated segments occurs within the nanoparticles as indicated by the appearance of red-shift peak in absorption spectrum (see Fig. 2). The mixing of DCM with water probably takes place in a slower fashion, allowing the collapse of individual chains. When the mixing process is complete, the collapsed chains assemble into nanoparticles to minimize interaction with water medium. Since the collapsed chains constitute many kinks or physical defects, it is more difficult to form aggregates. Therefore, the photophysical properties of collapsed chains are dominant in this type of nanoparticles. The packing of collapsed chains may be responsible for the rough surface of nanoparticles as revealed by TEM in Fig. 1b. It is worthwhile to point out that the aggregation of MEH-PPV chains in DCM is very high when nonsolvent, cyclohexane, is added [35]. In this system, the high miscibility of DCM and cyclohexane does not allow the collapse of MEH-PPV prior to the assembling process.

3.2. Nanoparticles of rr-P3OT

In this section, we further investigate the role of initial solvent on the formation of nanoparticles by using rr-P3OT. Our result from solvent-nonsolvent titration shows that the solubility of rr-P3OT in THF is higher compared to that of the DCM system. This result conforms to the solubility parameter (δ) of rr-P3OT and solvents. The solubility of polymer in solvent is promoted when the difference between their δ values is small [49,51]. The δ values of rr-P3OT, THF and DCM are 18.2 J^{1/2}cm^{-3/2} [52], 19.4 J^{1/2}cm^{-3/2}

and 20.3 J^{1/2}cm^{-3/2}, respectively. Therefore, the THF is a better solvent for rr-P3OT, which is opposite to the MEH-PPV system. This discrepancy probably arises from the presence of s atoms in rr-P3OT backbone, which affects local interactions with the solvents. This result also indicates that the dispersion interaction between rr-P3OT and solvent is not a major factor that controls the solubility and conformation of rr-P3OT. We expect that rr-P3OT has very different solubility parameter components compared to those of the MEH-PPV. However, we still observe similar results. Fig. 6 shows SEM and TEM images of rr-P3OT nanoparticles. The use of THF as an initial solvent provides spherical nanoparticles with average size of about 50 nm, which is comparable to that of the MEH-PPV nanoparticles (see Table 1). When the DCM is used, the average size increases significantly. This result supports our hypothesis that the size of nanoparticles is mainly dictated by the water solubility of initial solvent. However, the internal morphology of rr-P3OT nanoparticles is hardly affected. The high resolution TEM images show that the nanoparticles prepared from both solvents exhibit homogenous internal density and smooth surface.

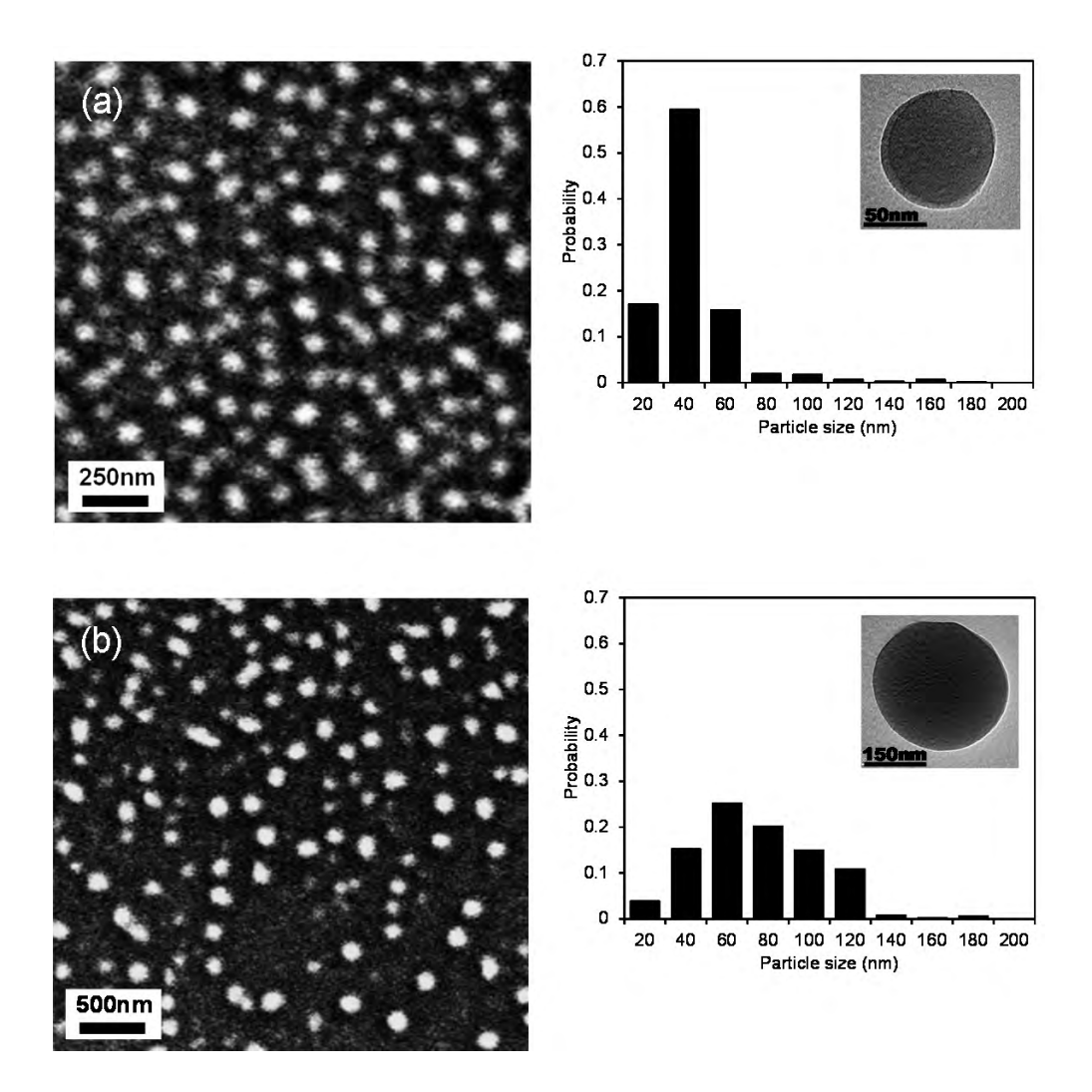


Fig. 6 SEM images of *rr*-P3OT prepared from different initial solvents, (a) THF and (b) DCM. Their size distributions are presented at the right side. High resolution TEM images of these nanoparticles are shown in the insets.

The photophysical properties of rr-P3OT in different forms are shown in Fig. 7. The isolated chain in THF solution exhibits a broad absorption pattern with λ_{max} at about 450 nm. Similar to MEH-PPV system, the PL spectrum constitutes peak and vibronic shoulder at 572 nm and 615 nm, respectively, reflecting electronic energy levels of the

longest chromophore within the conjugated backbone [53]. When the rr-P3OT forms nanoparticles by using THF as an initial solvent, the absorption spectrum drastically shifts to low-energy region. Three distinct red-shift peaks are clearly observed at about 515 nm, 550 nm and 605 nm. Previous studies have shown that the appearance of these peaks corresponds to the formation of aggregates within the nanoparticles [54,55]. These aggregates emit light at much lower energy region compared to the isolated chain. Their PL spectrum exhibits a well-defined pattern with λ_{max} and vibronic shoulder at about 638 nm and 695 nm, respectively.

In the system of DCM, absorption spectrum of the rr-P3OT nanoparticles still shifts to low-energy region. The three red-shift peaks, however, are obscured. A rise of absorbance at high-energy region is also observed. These results indicate that the molecular packing and individual chain conformation of rr-P3OT within the nanoparticles are different from the THF system. Fig. 8 compares the aggregate fraction in each system by plotting the ratio of absorbance at 550/440 nm. It is clear that the nanoparticles prepared from DCM solution contain lesser amount of aggregates. The measurement of PL spectrum provides a supportive result. PL spectrum of the nanoparticles shifts to relatively high-energy region, which is similar to the MEH-PPV system. It exhibits featureless pattern with λ_{max} at about 565 nm. The blue shift of PL spectrum indicates the collapse of conjugated chains within the nanoparticles [56]. Although relatively high amount of aggregates exists in this system, their PL peak at 638 nm is not observed. The photoemission of collapsed chains is still dominant. We suggest that the aggregate formed in the DCM system is a non-emissive species. We also note

that the blue shift of PL spectrum of *rr*-P3OT is smaller than that of the MEH-PPV. This is attributed to the difference in chain rigidity of the two polymers.

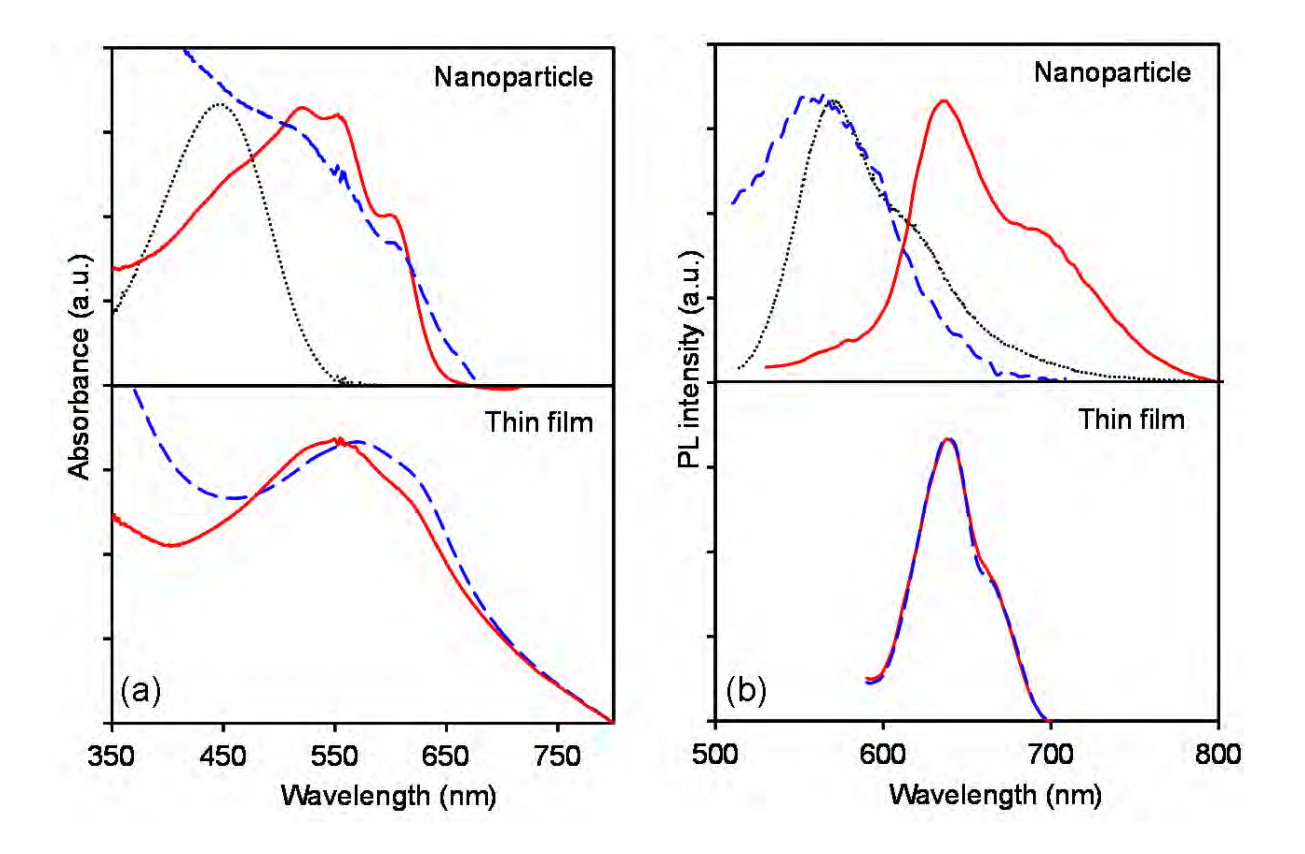


Fig. 7 (a) UV-vis absorption and (b) PL spectra of *rr*-P3OT in different forms, (top) nanoparticles and (bottom) drop-cast films. The samples were prepared by using (solid lines) THF and (dashed lines) DCM as initial solvents. The spectra of *rr*-P3OT dilute solution in THF (dotted lines) are included for comparison.

The absorption and PL spectra of drop cast films prepared from THF and DCM solutions exhibit similar pattern. The spectra significantly shift to lower energy region compared to those of the isolated chain indicating the presence of high aggregate fraction. Unlike the system of nanoparticles prepared from THF, we do not detect the three distinct

red-shift peaks in the absorption spectra. This observation suggests that local structures of aggregates formed in the nanoparticles and thin films are different. The measurements of PL spectra also detect the discrepancy in pattern. The λ_{max} values of PL spectra measured from the nanoparticles and thin films are comparable. Interestingly, the vibronic shoulder is detected at different wavelengths, about 695 nm and 665 nm for the nanoparticles and thin films, respectively. This indicates the variation of vibrational energy levels of aggregates in the two systems. The separation between peak and vibronic shoulder, corresponding to vibrational energy gap of the aggregates in ground state, increases from about 25 nm in thin films to about 55 nm in the nanoparticles. The increase of vibrational energy gap is attributed to the increase of confinement within the nanoparticles which may resist the vibration of polymer segments. We note that the change of vibrational energy levels is also observed but less pronounced in the MEH-PPV system.

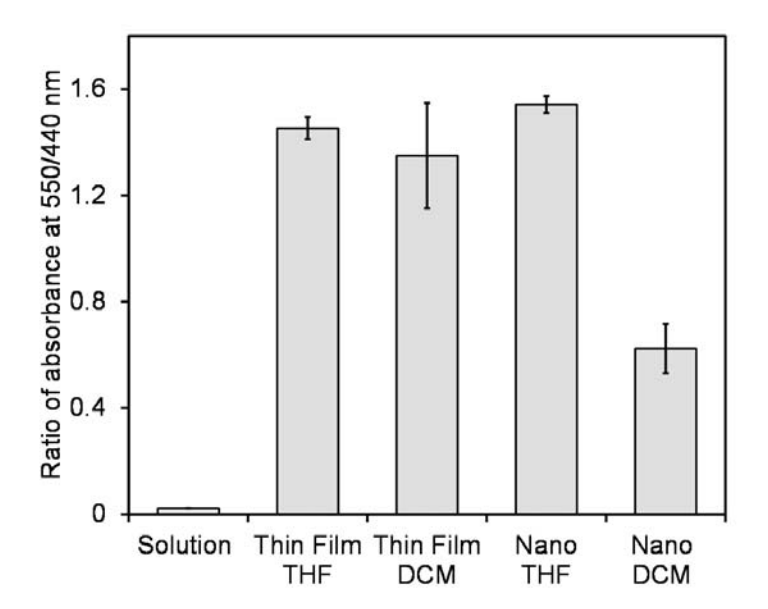


Fig. 8 Ratio of absorbance at 550/440 nm reflecting the aggregate fraction of *rr*-P3OT prepared in different forms

4. Conclusion

Our results in this study demonstrate that the mechanism of CPN formation in water is strongly influenced by properties of the initial solvents. We show that the solubility of initial solvent in water is a major factor dictating the conformational change and segmental aggregation of conjugated polymers within the CPNs. When the water solubility of initial solvent is relatively low, the collapse of conjugated chains occurs prior to the assembling process. The resultant CPNs contain large fraction of collapsed coils. Therefore, the photophysical properties of collapsed coils, which absorb and emit light at high-energy region, are dominant in this type of CPNs. When the initial solvent is miscible with water, the mixing process is relatively fast. The conjugated polymers are driven to assemble into CPNs with minimal change of individual chain conformation. This type of CPNs contains large fraction of aggregates and exhibits smaller size. Their absorption and PL spectra occur at low-energy region. The CPNs of MEH-PPV and rr-P3OT prepared in this study by using DCM and THF as initial solvents exhibit rather different photophysical properties. The difference in λ_{max} position of PL spectra is more than 50 nm. Our study shows that a careful choice of the solvent can be used to produce the CPNs with desired chain arrangement and photophysical properties, suitable for particular device application.

Acknowledgements

This research is financially supported by the Thailand Research Fund, Ministry of Higher Education and Naresuan University (Grant RMU5380017). RP thanks the Office of Higher Education Commission for supporting her Ph.D. scholarship under the program Strategic Scholarships for Frontier Research Network. RT thanks NANOTEC-MU Excellence Center on Intelligent Materials and Systems and Center for Innovation in Chemistry (PERCH-CIC) for supporting some research facilities.

References

- [1] X. Gong, D. Moses, A.J. Heeger, in: K.Müllen, U. Scherf (Eds.), Polymer-Based Light-Emitting Diodes (PLEDs) and Displays Fabricated from Arrays of PLEDs, Wiley-VCH, Weinheim, 2006, p. 151.
- [2] A. Facchetti, Chem. Mater. 23 (2011) 733-758.
- [3] H. Spanggaard, F. C. Krebs, Sol. Energy Mater. Sol. Cells 83 (2004) 125-146.
- [4] C. J. Brabec, N. S. Sariciftci, J. C. Hummelen, Adv. Funct. Mater. 11 (2001) 15-26.
- [5] G. Horowitz, Adv. Mater. 10 (1998) 365-377.
- [6] X. Zhan, Z. Tan, B. Domercq, Z. An, X. Zhang, S. Barlow, Y. Li, D. Zhu, B. Kippelen, S. R. Marder, J. Am. Chem. Soc. 129 (2007) 7246-7247.
- [7] C.Y. Yang, F. Hide, M.A. Díaz-García, A.J. Heeger, Polymer 39 (1998) 2299-2304.
- [8] B.J. Schwartz, Annu. Rev. Phys. Chem. 54 (2003) 141-172.
- [9] M. Brinkmann, J. Polym. Sci. Part B: Polym. Phys. 49 (2011) 1218-1233.
- [10] B.R. Saunders, M.L. Turner, Adv. Colloid Interface Sci. 138 (2008) 1-23.

- [11] C. Wu, B. Bull, K. Christensen, J. McNeill, Angew. Chem., Int. Ed. 121 (2009) 2779-2783.
- [12] J. H. Moon, P. MacLean, W. McDaniel, L. F. Hancock, Chem. Commun. (2007), 4910-4912.
- [13] C. Wu, B. Bull, C. Szymanski, K. Christensen, J. McNeill, ACS Nano 2 (2008) 2415-2423.
- [14] C. Wu, C. Szymanski, Z. Cain, J. McNeill, J. Am. Chem. Soc. 129 (2007) 12904-12905.
- [15] M. Green, P. Howes, C. Berry, O. Argyros, M. Thanou, Proc. R. Soc. A 465 (2009) 2751-2759.
- [16] M. Bruchez, M. Moronne, P. Gin, S. Weiss, A. P. Alivisatos, Science 281 (1998) 2013-2016.
- [17] K. Landfester, A. Musyanovych, V. Mailänder, J. Polym. Sci. Part A: Polym. Chem. 48 (2010) 493-515.
- [18] D. Tuncel, H. V. Demir, Nanoscale 2 (2010) 484-494.
- [19] A. Kaeser, A. P. H. J. Schenning, Adv. Mater. 22 (2010) 2985-2997.
- [20] C. Wu, C. Szymanski, J. McNeill, Langmuir 22 (2006) 2956-2960.
- [21] J. M. Lee, S. J. Lee, Y. J. Jung, J. H. Kim, Curr. Appl. Phys. 8 (2008) 659-663.
- [22] S. J. Lee, J. M. Lee, I. W. Cheong, H. Lee, J. H. Kim, J. Polym. Sci. Part A: Polym. Chem. 46 (2008) 2097-2107.
- [23] S. J. Lee, J. M. Lee, H.-Z. Cho, W. G. Koh, I. W. Cheong, J. H. Kim, Macromolecules 43 (2010) 2484-2489.
- [24] X.-G. Li, J. Li, M.-R. Huang, Chem. Eur. J. 15 (2009) 6446-6455.

- [25] Z. Wang, Y. Wang, D. Xu, E. S.-W. Kong, Y. Zhang, Synth. Met. 160 (2010) 921-926.
- [26] X.-G. Li, J. Li, Q.-K. Meng, M.-R. Huang, J. Phys. Chem. B 113 (2009) 9718-9727.
- [27] J. Pecher, S. Mecking, Chem. Rev. 110 (2010) 6260-6279.
- [28] E.-J. Park, T. Erdem, V. Ibrahimova, S. Nizamoglu, H. V. Demir, D. Tuncel, ACS Nano 5 (2011) 2483-2492.
- [29] C. Szymanski, C. Wu, J. Hooper, M. A. Salazar, A. Perdomo, A. Dukes, J. McNeill, J. Phys. Chem. B 109 (2005) 8543-8546.
- [30] O. Pras, D. Chaussy, O. Stephan, Y. Rharbi, P. Piette, D. Beneventi, Langmuir 26 (2010) 14437-14442.
- [31] B. G. Sumpter, P. Kumar, A. Mehta, M. D. Barnes, W. A. Shelton, R. J. Harrison, J. Phys. Chem. B 109 (2005) 7671-7685.
- [32] T.-Q. Nguyen, V. Doan, B. J. Schwartz, J. Chem. Phys. 110 (1999) 4068-4078.
- [33] R. Traiphol, N. Charoenthai, T. Srikhirin, T. Kerdcharoen, T. Osotchan, T. Maturos, Polymer 48 (2007) 813-826.
- [34] P. Kumar, A. Mehta, S. M. Mahurin, S. Dai, M. D. Dadmun, B. G. Sumpter, M. D. Barnes, Macromolecules 37 (2004) 6132-6140.
- [35] R. Traiphol, R. Potai, N. Charoenthai, T. Srikhirin, T. Kerdcharoen, T. Osotchan, J. Polym. Sci. Part B: Polym. Phys. 48 (2010) 894-904.
- [36] R. Traiphol, N. Charoenthai, Synth. Met. 158 (2008) 135-142.

- [37] "Physical Constants of Organic Compounds", in CRC Handbook of Chemistry and Physics, Internet Version 2005, David R. Lide, ed., http://www.hbcpnetbase.com, CRC Press, Boca Raton, FL, 2005, pp 84.
- [38] B. Valeur, Molecular Fluorescence: Principles and Applications, 1st ed., Wiley-VCH, Weinheim, 2001, p. 51.
- [39] P. F. Barbara, A. J. Gesquiere, S.-J. Park, Y. J. Lee, Acc. Chem. Res. 38 (2005) 602-610.
- [40] Z. Yu, P. F. Barbara, J. Phys. Chem. B 108 (2004) 11321-11326.
- [41] D. Hu, J. Yu, G. Padmanaban, S. Ramakrishnan, P. F. Barbara, Nano Lett. 2 (2002) 1121-1124.
- [42] R. Traiphol, P. Sanguansat, T. Srikhirin, T. Kerdcharoen, T. Osotchan, Macromolecules 39 (2006) 1165-1172.
- [43] H. S. Woo, O. Lhost, S. C. Graham, D. D. C. Bradley, R. H. Friend, C. Quattrocchi, J. L. Brédas, R. Schenk, K. Müllen, Synth. Met. 59 (1993) 13-28.
- [44] R. Traiphol, N. Charoenthai, P. Manorat, T. Pattanatornchai, T. Srikhirin, T. Kerdcharoen, T. Osotchan, Synth. Met. 159 (2009) 1224-1233.
- [45] S. Tretiak, A. Saxena, R.L. Martin, A.R. Bishop, J. Phys. Chem. B 104 (2000) 7029-7037.
- [46] S. Siddiqui, F.C. Spano, Chem. Phys. Lett. 308 (1999) 99-105.
- [47] R. Jakubiak, C. J. Collison, W. C. Wan, L. J. Rothberg, B. R. Hsieh, J. Phys. Chem. A 103 (1999) 2394-2398.
- [48] R. F.Cossiello, M. D. Susman, P. F. Aramendía, T. D. Z. Atvars, J. Lumin. 130 (2010) 415-423.

- [49] A. F. M. Barton, Chem.Rev. 75 (1975) 731-753.
- [50] A. R. Kamdar, Y. S. Hu, P. Ansems, S. P. Chum, A. Hiltner, E. Baer, Macromolecules 39 (2006) 1496-1506.
- [51] S. Samitsu, T. Shimomura, S. Heike, T. Hashizume, K. Ito, Macromolecules 41 (2008) 8000-8010.
- [52] A. Zen, M. Saphiannikova, D. Neher, U. Asawapirom, U. Scherf, Chem. Mater. 17 (2005) 781-786.
- [53] R. Palacios, P. Barbara, J. Fluoresc. 17 (2007) 749-757.
- [54] N. Kiriy, E. Jähne, H.-J. Adler, M. Schneider, A. Kiriy, G. Gorodyska, S. Minko,D. Jehnichen, P. Simon, A. A. Fokin, M. Stamm, Nano Lett. 3 (2003) 707-712.
- [55] C. Scharsich, R. H. Lohwasser, M. Sommer, U. Asawapirom, U. Scherf, M. Thelakkat, D. Neher, A. Köhler, J. Polym. Sci. Part B: Polym. Phys. 50 (2012) 442-453.
- [56] Y.-J. Ko, E. Mendez, J. H. Moon, Macromolecules 44 (2011) 5527-5530.

ผลลัพธ์ที่ได้รับจากงานวิจัย

- 1. Potai, R.; Traiphol, R.* "Controlling chain organization and photophysical properties of conjugated polymer nanoparticles prepared by reprecipitation method: The effect of initial solvent" *J. Colloid Interface Sci.* **2013**, *43*, 58-66. (IF = 3.07)
- 2. Potai, R.; Kamphan, A.; Traiphol, R.* "Conformational Change, Intrachain Aggregation and Photophysical Properties of Regionegular Poly(3-octylthiophene) in Alkanes" *J. Polym. Sci.: Part B polymer physics.* **2013 in press** doi:10.1002/polb.23326 (IF = 1.531)
- 3. Potai, R.; Kamphan, A.; Traiphol, R.* "On the formation and photophysical properties of emissive and non-emissive aggregates of regionegular poly(3-octylthiophene) in different local environments" (in preparation)
- 4. Invited Talk: "Chain organization and Photophysical Properties of Various Conjugated Polymers in Solution and Thin Films", September 30, 2012, 1st Thai-Taiwan Colloquium: Frontier Research in Science and Technology, Naresuan University, Phitsanulok, Thailand
- Potai, R.; Charoenthai, N.; Traiphol, R.* "Effect of solvents on photophysical properties of conjugated polymer nanoparticles in aqueous dispersion" Polymers for Advanced Technologies 2011 (PAT 2011), 2-5 October, 2011, Lodz, Poland (Oral presentation)
- 6. Potai, R.; Charoenthai, N.; Traiphol, R.* "Controlling photophysical properties of poly(3-octylthiophene-2,5-diyl) nanoparticles: Effects of regionegularities and

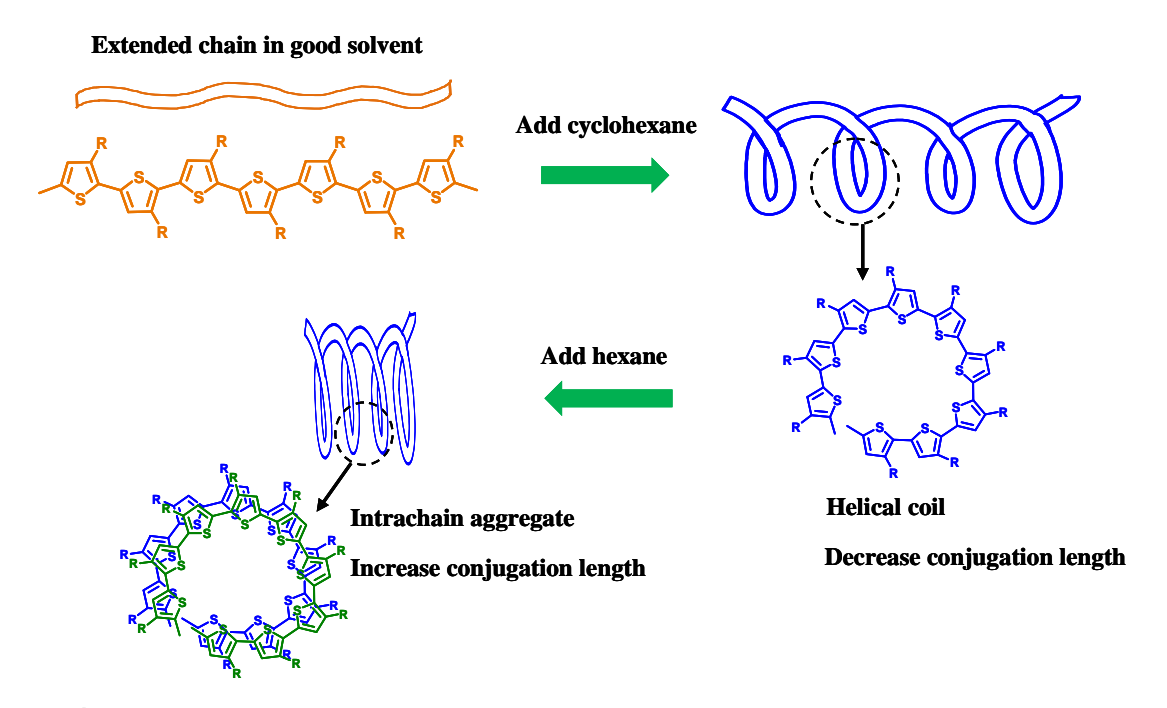
- solvents" Commission on Higher Education Congress IV: University Staff Development Consortium CHE-USDC Congress IV, 14-16 September, **2011**, Chonburi, Thailand (Poster presentation)
- 7. Kamphan, A.; Potai, R.; Charoenthai, N.; Traiphol, R.* "Chain organization and photophysical properties of regioregular poly(3-alkylthiophene)s in solutions: effects of solvent and alkyl length" The 6th Pure and Applied Chemistry International Conference 2012, 11-13 January, 2012, Chiangmai, Thailand (Poster presentation)
- 8. Kamphan, A.; Potai, R.; Charoenthai, N.; Traiphol, R.* "Effect of solvent and temperature on photophysical properties of regionegular poly(3-octylthiophene) in solutions" The 4th Science Research, 12-13 March, **2012**, Phitsanulok, Thailand (Poster presentation)
- 9. โครงการวิจัยนี้มีส่วนผลิตนักวิจัยระดับปริญญาเอก 2 คน คือ นางสาว รัตยาภรณ์ โพธิ์ใต้ และ นางสาว อโณทัย คำพันธ์

ภาคผนวก

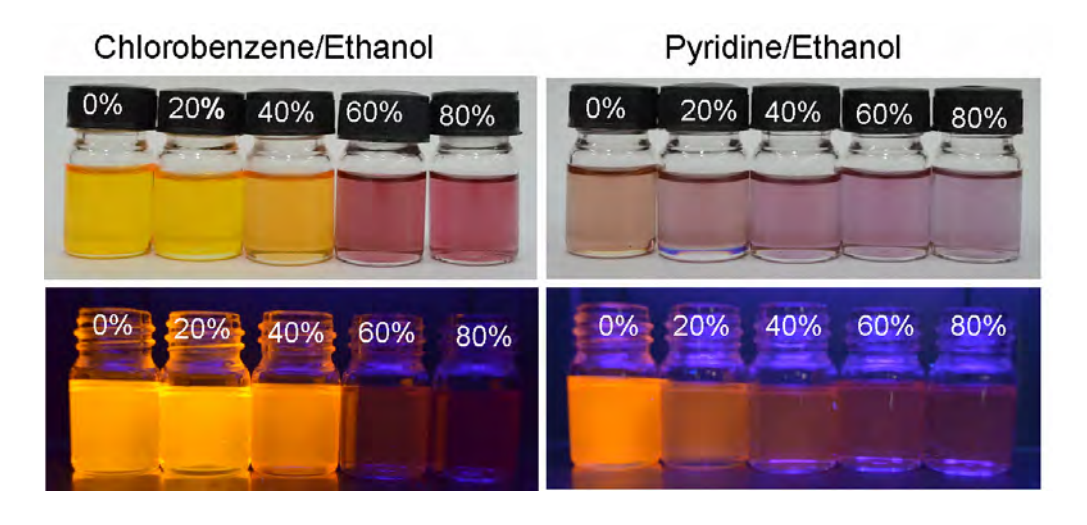
บทความสำหรับการเผยแพร่

กอนจูเกตพอลิเมอร์เป็นสารที่มีคุณสมบัติน่าสนใจหลายอย่าง สารเหล่านี้นอกจากสามารถนำ ไฟฟ้าได้แล้ว ยังสามารถเปล่งแสงได้ด้วยเมื่อถูกกระตุ้นด้วยพลังงานภายนอกเช่น พลังงานแสงและ พลังงานไฟฟ้า รวทั้งยังสามารถเปลี่ยนพลังงานแสงให้เป็นกระแสไฟฟ้าได้อีกด้วย จากคุณสมบัติเหล่านี้ ทำให้มีความเป็นไปได้ที่จะนำสารคอนจูเกตพอลิเมอร์ มาประยุกต์ใช้ในเทคโนโลยีแห่งอนาคตหลายๆ แบบ ยกตัวอย่างเช่นอาจมีการนำโมเลกุลของคอนจูเกตพอลิเมอร์มาใช้ทำเป็นเส้นลวดสำหรับการ ประดิษฐ์อุปกรณ์หรือหุ่นยนต์ขนาดเล็กได้ นอกจากนี้จากการที่คอนจูเกตพอลิเมอร์มีสมบัติการ เปล่งแสงที่ดี ทำให้สามารถนำมาประดิษฐ์เป็นจอภาพแสดงผลแบบแบนได้ด้วย (หรือที่รู้จักกันในชื่อ ของ Organic Light Emitting Diode, OLED) จอภาพแบบนี้มีข้อดีหลายอย่างเช่น สามารถทำให้ แบนเท่าความหนาของแผ่นกระดาษและมีลักษณะที่ยืดหยุ่นสามารถบิดงอได้ นอกจากนี้ยังสามารถทำ ให้มีลักษณะโปร่งใสได้ด้วย สารคอนจูเกตพอลิเมอร์ยังสามารถประยุกต์ในเทคโนโลยี Plastic Solar Cell (PSC) ได้อีกด้วย โดยสารเหล่านี้จะทำหน้าที่เปลี่ยนพลังงานแสงให้เป็นพลังงานไฟฟ้า

อย่างไรก็ตามในการที่จะทำให้จิตนาการเหล่านั้นกลายเป็นความจริงขึ้นมาได้ จำเป็นที่ต้อง เรียนรู้ถึงพฤติกรรมและสมบัติระคับโมเลกุลของสารคอนจูเกตพอลิเมอร์ ให้เข้าใจอย่างละเอียดลึกซึ้ง ยกตัวอย่างเช่น การพัฒนาให้ PSC มีประสิทธิภาพในการผลิตกระแสไฟฟ้าได้สูง ด้องสามารถที่จะ ควบคุมให้สารคอนจูเกตพอลิเมอร์เกิดการแยกประจุได้ดีที่สุด ซึ่งสมบัตินี้ขึ้นอยู่กับการจัดเรียงตัวของ คอนจูเกตพอลิเมอร์ในสภาวะฟิล์มบาง โดยจากการศึกษาที่ผ่านมาพบว่าการจับกันในลักษณะซ้อนทับ กันของโมเลกุลจะทำให้เกิดการแยกประจุได้ดีขึ้น ดังนั้นในงานวิจัยนี้จึงได้ทำการศึกษาปัจจัยต่างๆที่มี ผลต่อการเข้าจับกันของสารคอนจูเกตพอลิเมอร์ในกลุ่มของพอลิไธโอฟิน ซึ่งพบว่าเมื่อทำการเหนี่ยวนำ ให้สารพอลิไธโอฟินเสิงและการคายแสง เกิดขึ้นในช่วงพลังงานสูงขึ้น(ดูรูปที่ 1) แต่เมื่อเกิดการเข้าซ้อนทับกันของสายโซ่โมเลกุลกลับพบว่า สมบัติการดูดกลืนแสงเกิดขึ้นที่พลังงานต่ำลงดังจะเห็นได้จากการเปลี่ยนสีของสารที่เกิดขึ้น(ดูรูปที่ 2) ส่วนประสิทธิภาพการคายแสง โดยการจับกันแบบหลวมๆจะทำให้สารไม่เกิดการคายแสง แต่เมื่อสารเกิดการจับกันแบบแน่นมากขึ้นจะทำให้เกิดการคายแสงที่ช่วงพลังงานต่ำลง การเปลี่ยนชนิดของตัวทำละลายที่ ใช้ยังมีผลต่อปริมาณของการเข้าจับของพอลิเมอร์และสมบัติทางแสงด้วย องค์ความรู้ที่ได้จากการศึกษา เหล่านี้จะมีความสำคัญอย่างมากต่อการพัฒนาเทคโนโลยี PSC ให้สามารถผลิตกระแสไฟฟ้าได้มากขึ้น



รูปที่ 1 แสดงการเปลี่ยนแปลงรูปร่างพอลิไซ โอฟีนเมื่อมีการเติมไซ โคลเฮกเซนและเฮกเซนเข้าไปใน ระบบ โดยจะเกิดการม้วนตัวก่อนแล้วค่อยเกิดการเข้าซ้อนทับกันของสายโซ่โมเลกุล



ร**ูปที่ 2** (บน) แสดงการเปลี่ยนสีของพอลิไธโอฟืนในตัวทำละลายผสมคลอเบนซีนกับเอทธานอลและ ไพริดีนกับเอทธานอล (ล่าง) แสดงสมบัติการเปล่งแสงภายใต้การฉายแสง จะเห็นว่าสารเกิดการ เปล่งแสงได้น้อยลงเมื่อเกิดการเข้าจับกัน

Provided for non-commercial research and education use. Not for reproduction, distribution or commercial use.



This article appeared in a journal published by Elsevier. The attached copy is furnished to the author for internal non-commercial research and education use, including for instruction at the authors institution and sharing with colleagues.

Other uses, including reproduction and distribution, or selling or licensing copies, or posting to personal, institutional or third party websites are prohibited.

In most cases authors are permitted to post their version of the article (e.g. in Word or Tex form) to their personal website or institutional repository. Authors requiring further information regarding Elsevier's archiving and manuscript policies are encouraged to visit:

http://www.elsevier.com/authorsrights

Author's personal copy

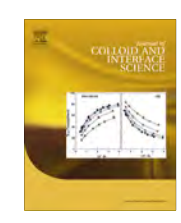
Journal of Colloid and Interface Science 403 (2013) 58-66



Contents lists available at SciVerse ScienceDirect

Journal of Colloid and Interface Science

www.elsevier.com/locate/jcis



Editor's Choice

Controlling chain organization and photophysical properties of conjugated polymer nanoparticles prepared by reprecipitation method: The effect of initial solvent

Ruttayapon Potai a, Rakchart Traiphol a,b,*

- ^a Laboratory of Advanced Polymers and Nanomaterials, Department of Chemistry and Center for Innovation in Chemistry, Faculty of Science, Naresuan University, Phitsanulok 65000, Thailand
- b NANOTEC-MU Excellence Center on Intelligent Materials and Systems, Faculty of Science, Rama 6 Road, Ratchathewi, Bangkok 10400, Thailand

ARTICLE INFO

Article history: Received 6 March 2013 Accepted 15 April 2013 Available online 26 April 2013

Keywords: Conformational change Aggregation Self-assembling Molecular packing Photophysics

ABSTRACT

This study explores roles of initial solvent on the formation of conjugated polymer nanoparticles (CPNs) and their photophysical properties. Stable aqueous CPN dispersion of poly(2-methoxy-5-(2'-ethylhexyloxy)-1,4-phenylvinylene)(MEH-PPV) and regioregular poly(3-octylthiophene)(rr-P3OT) are prepared via reprecipitation technique. This preparation method involves the injection of polymer solution in organic solvents into an excess amount of water. We demonstrate that water solubility of the initial solvent is a major factor dictating mechanism of the CPN formation. Dichloromethane (DCM) and tetrahydrofuran (THF), possessing very different water solubilities, are used as initial solvents in this work. The resultant CPNs exhibit quite different sizes and photophysical properties. The preparation of MEH-PPV nanoparticles from DCM solution provides average size of about 127 nm. Their absorption and photoluminescence (PL) spectra shift to higher energy region compared to those of the isolated chain. When the THF solution is used, opposite results are observed. Average size of the nanoparticles decreases to about 40 nm. Significant redshift of their absorption and PL spectra is also detected. Detailed data analysis indicates that the individual chain conformation and degree of segmental aggregation within the CPNs are quite different. This leads to drastic discrepancies of their photophysical properties. The use of DCM and THF as initial solvents provides the MEH-PPV nanoparticles with green (λ_{max} = 535 nm) and red (λ_{max} = 590 nm) photoemission, respectively. The investigation of rr-P3OT provides consistent results. Our study offers a new and simple route to control size and photophysical properties of CPNs by careful selection of the initial solvents.

© 2013 Elsevier Inc. All rights reserved.

1. Introduction

Conjugated polymer is a class of material that has received tremendous attention from scientific community in the past few decades. Major applications of conjugated polymers, which exhibit electroluminescent and semiconducting properties, involve organic electronic technologies such as organic light emitting diode (OLED) [1,2], organic solar cell (OSC) [3,4], and organic field emission transistor [5,6]. Poly[2-methoxy-5-(2'-ethylhexyloxy)-1,4-phenylenevinylene] (MEH-PPV) and regioregular poly(3-alkylthiophenes) (*rr*-P3ATs) are well-known conjugated polymers that have been extensively studied. The presence of branched side chains in MEH-PPV causes high fraction of amorphous region in thin film,

are usually fabricated into nanoparticle form. Compared to other types of nanoparticles such as liposomes and micelles, conjugated polymer nanoparticles (CPNs) possess an increased colloidal stability and a better chemical resistance [17]. The fabrication process is usually easier as well. Moreover, the higher biocompatibility and less toxicity of CPNs compared to inorganic nanoparticles are desir-

which in turn enhances the fluorescent intensity [7,8]. The *rr*-P3ATs, on the other hand, are more crystalline materials with relatively high charge carrier mobility, while their fluorescent intensity in thin film is rather weak [9,10]. Therefore, the MEH-PPV is more suitable for OLED application, while the *rr*-PATs are normally utilized as active materials in OSC [1,10].

Conjugated polymer is also a potential material for being uti-

lized in biotechnologies such as fluorescent sensor [11,12], biolog-

ical fluorescent imaging [13,14], and biological label [15,16]. To

utilize conjugated polymers in these biotechnologies, the polymers

able properties for using these materials in the biotechnologies

[18,19]. Because each CPN contains a number of chromophores, it

^{*} Corresponding author at: Laboratory of Advanced Polymers and Nanomaterials, Department of Chemistry and Center for Innovation in Chemistry, Faculty of Science, Naresuan University, Phitsanulok 65000, Thailand. Fax: +66 55261025.

E-mail address: rakchartt@nu.ac.th (R. Traiphol).

normally exhibits higher brightness and better photostability compared to molecular dyes [13,20]. Their photoluminescent properties can also be tuned by varying particles size, composition, and type of conjugated polymers [19].

CPNs can be prepared by using different methods such as oxidative polymerization, miniemulsion, and reprecipitation. The oxidative polymerization process requires catalyst/oxidant such as FeCl₃/H₂O₂ and appropriate surfactants [21-24]. The polymerization of monomers is allowed to take place inside small droplets of the reaction medium stabilized by surfactant. The properties of CPNs can be optimized by varying the surfactant/oxidant/monomer ratio, polymer concentration, polymerization temperature, and reaction time [24–26]. However, there are several problems involving this method such as poor water solubility of polymer, low oxidizing activity of catalysts, and extremely low conversion [21,26]. For miniemulsion method, the conjugated polymer dissolved in organic solvent is injected into an aqueous medium containing surfactant molecules [17]. The process generates stablecolloidal droplets of the polymer solution. The CPNs are obtained after evaporating the organic solvent. However, the surfactant molecules still remain in the system. The reprecipitation method can produce pure CNPs with controllable size [18,27]. The process requires the addition of small amount of dilute conjugated polymer solution into an excess volume of water. The sudden decrease in solubility drives the conjugated polymers to form nanoparticle. The reprecipitation method is a popular technique because it is quite simple, cheap and does not require any surfactant or template. The particle size can be simply controlled by adjusting the polymer concentration [13,19,28]. Moreover, this method can be applied to a wide variety of conjugated polymers that are soluble in organic solvents.

The preparation and photophysical properties of CPNs have been reported by several research groups. McNeill and co-workers have prepared various CPNs by using reprecipitation method. The injection of a dilute solution of MEH-PPV in tetrahydrofuran (THF) into aqueous medium provides CPNs with particle size ranging from 5 to 10 nm [29]. The use of other conjugated polymers such as polyfluorene, polyphenyleneethynylene and their copolymers also yield the CPNs with similar size [13,19]. They have demonstrated in these studies that the photoluminescent (PL) color of CPNs varies with types of the conjugated polymers. The size of CPNs also affects their PL properties. The CPNs of 2,7-poly(9,9-dialkylfluorene-co-fluorenone) exhibit systematic shift of PL spectra to low-energy region when their size is increased from 5 to 500 nm [30]. The CPNs of polythiophene shows similar behavior. Their PL color changes from blue to red upon increasing the size from 12 to 51 nm [23].

In this work, we present a new and versatile method for controlling the photophysical properties of CPNs. Previous studies have shown that conjugated polymer such as MEH-PPV in solution adopts different conformations depending on the strength of local polymer-solvent interactions [31-35]. The MEH-PPV chain is extended in a good solvent, dichloromethane (DCM), while the chain forms collapsed coil in a poor solvent, THF [31,34]. The decrease in solvent quality by addition of nonsolvent forces the MEH-PPV chains into aggregated state, which in turn causes the redshift of absorption and PL spectra [33,35,36]. In our recent study, we observe that the variation of initial solvents affects the degree of segmental aggregation in the solvent-nonsolvent system [35]. Since the preparation of CPNs via reprecipitation method also induces the assembling of polymer chains by decreasing solvent quality, the initial solvents are expected to play important role on their aggregation behavior. In this study, we use DCM and THF as initial solvents to prepare CPNs of MEH-PPV and regioregular poly(3octylthiophene)(rr-P3OT) in aqueous medium. The difference of initial polymer conformations is expected to influence of chain

Table 1Physical properties of solvents [37] and size of conjugated polymer nanoparticles prepared by using different solvents.

Solvents	Boiling point	Dielectric constant	Solubility in water (g/L,	Average particle size (nm)	
	(°C)		25 °C)	MEH-PPV	rr-P3OT
THF DCM	66.0 39.8	7.52 8.93	Miscible 17.6	49.1 ± 17.5 127.2 ± 29.8	49.4 ± 13.1 99.6 ± 64.5

packing within CPNs. In addition, the miscibility of DCM and THF with water is quite different [37] (see Table 1), which may also play important role on the formation of CPNs. In fact, the CPNs obtained by using the DCM and THF exhibit quite different photophysical properties. Our approach provides a simple method for controlling photophysical properties of CPNs without modifying chemical structure and/or composition of the conjugated polymer.

2. Experimental

The conjugated polymers, MEH-PPV and rr-P3OT, were purchased from Sigma–Aldrich. Number average molecular weight (M_n) and polydispersity (M_w/M_n) of the polymers determined by gel permeation chromatography (GPC) with polystyrene standard are 120,000 g/mol $(M_w/M_n = 4.3)$ for MEH-PPV and 58,300 g/mol $(M_w/M_n = 2.3)$ for rr-P3OT. THF was used as a solvent in the GPC measurement. The solvents, THF (anhydrous 99%) and DCM (AR grade), were purchased from Sigma–Aldrich. Physical properties of these solvents are shown in Table 1.

Nanoparticles of all conjugated polymers were prepared by a reprecipitation method adapted from the literature [13,14,19]. The conjugated polymers were fully dissolved in THF and DCM solvents and then diluted to concentration of 0.001 mg/mL. This concentration is lower than that of McNeill's study. However, the concentration is appropriate for the measurements of PL spectra with minimal influence of an inner-filtered effect. To prepare CPNs, each of 0.2 mL polymer solution was injected in a step-wise process into 32 mL of deionized water, while the mixtures were under continuous ultrasonication at 60 °C. The 0.2 mL addition of solution is equivalence to 8.3 g/L concentration of the organic solvents in water. This concentration is still lower than their water solubility (see Table 1). The mixtures appeared clear to naked eyes indicating complete miscibility. The time interval between each step was about 2 min, allowing the evaporation of organic solvents. The sum volume of polymer solution was 8 mL requiring the addition time of about 1.5 h. The ultrasonication process was continued for 30 min to ensure complete evaporation of the organic solvents. The resultant aqueous suspensions were filtered through 0.45 µm pore size cellulose acetate membrane. The CPN aqueous suspensions were clear and stable for months with no sign of agglomeration. Thin films of conjugated polymers were prepared by dropcasting from 1 mg/mL solution onto quartz slide. The solution droplet was allowed to dry in a clean atmosphere under ambient condition. Atomic force microscopy reveals that the films exhibit rough surface with thickness ranging from about 30 to 400 nm. Absorbance of all films is less than 0.1.

The UV-vis absorption spectra of CPNs were recorded by employing Analytic Specord 100 spectrometer with 10 cm thick quartz cuvette, while the PL spectra were measured by using Perkin-Elmer LS55 spectrometer. Absorbance of the CPN aqueous suspensions is less than 0.4 (equivalence to 0.04 for 1 cm thick cuvette). Since the absorbance of conjugated polymer is very low, an inner-filtered effect in the PL measurement is negligible in all systems [38]. Morphology and size distribution of the CPNs were characterized by transmission electron microscopy (TEM, Tecnai

12, D291) and scanning electron microscopy (SEM, LEO 1455 VP). The samples for TEM were prepared by drop-casting from CPN aqueous suspensions onto copper grids coated with carbon film. For SEM samples, one drop of CPN aqueous suspensions was deposited on a polished silicon substrate. After the evaporation of water, the samples were coated with gold.

3. Results and discussion

3.1. Nanoparticles of MEH-PPV

Morphologies and size distribution of MEH-PPV nanoparticles revealed by TEM are shown in Fig. 1. The nanoparticles prepared from both THF and DCM solvents exhibit spherical shape. Their size, however, varies significantly with type of the solvents. The use of THF as an initial solvent provides the nanoparticles with smaller size. The majority of nanoparticles exhibit diameter of about 40 nm. When the DCM is used as an initial solvent, average size of the nanoparticles significantly increases to about 120 nm. Their size distribution also becomes much broader. Furthermore, the packing of polymer chains within nanoparticles is affected by the variation of initial solvents. The nanoparticles prepared from DCM exhibit a rougher surface compared to that of the THF system. The interior density of each nanoparticle is also less homogeneous in the DCM system. These results indicate that mechanism for the nanoparticle formation strongly depends on type of the initial solvent. We note that the nanoparticles prepared from THF can be filtered through 200 nm pore size cellulose acetate membrane. Therefore, the agglomeration of nanoparticles in Fig. 1a is likely to occur during the preparation process for TEM measurement. The SEM images also detect large fraction of isolated nanoparticles. The nanoparticles obtained in this study exhibit larger size compared to the previous reports [13,18,29]. This is attributed to the difference in preparation conditions such as power of the ultrasonication and volume of the added solution in each step.

Photophysical properties of the MEH-PPV nanoparticles vary significantly with type of the initial solvent. Fig. 2 illustrates absorption and PL spectra of the MEH-PPV in different forms. The isolated chains in dilute THF solution exhibit a broad absorption spectrum with λ_{max} at about 504 nm. The broad pattern corresponds to electronic transition of various chromophores, possessing different conjugation lengths, within the conjugated chains. The photoemission process normally takes place via chromophores with the lowest HOMO-LUMO energy gap due to the high efficiency of energy transfer process [39-41]. The PL spectrum showing a well-defined pattern with λ_{max} and vibronic shoulder at about 554 nm and 594 nm, respectively, reflects energy levels of the longest chromophore within the system. When the MEH-PPV chains are forced to densely pack into nanoparticles by injecting the solution into an excess amount of water, the absorption and PL patterns change drastically. The absorption spectrum of nanoparticles prepared from THF solution shifts to lower energy region where the λ_{max} is detected at 515 nm. New redshift peak is also observed at about 550 nm. The appearance of this redshift peak indicates the formation of inter- and/or intrachain aggregates where some

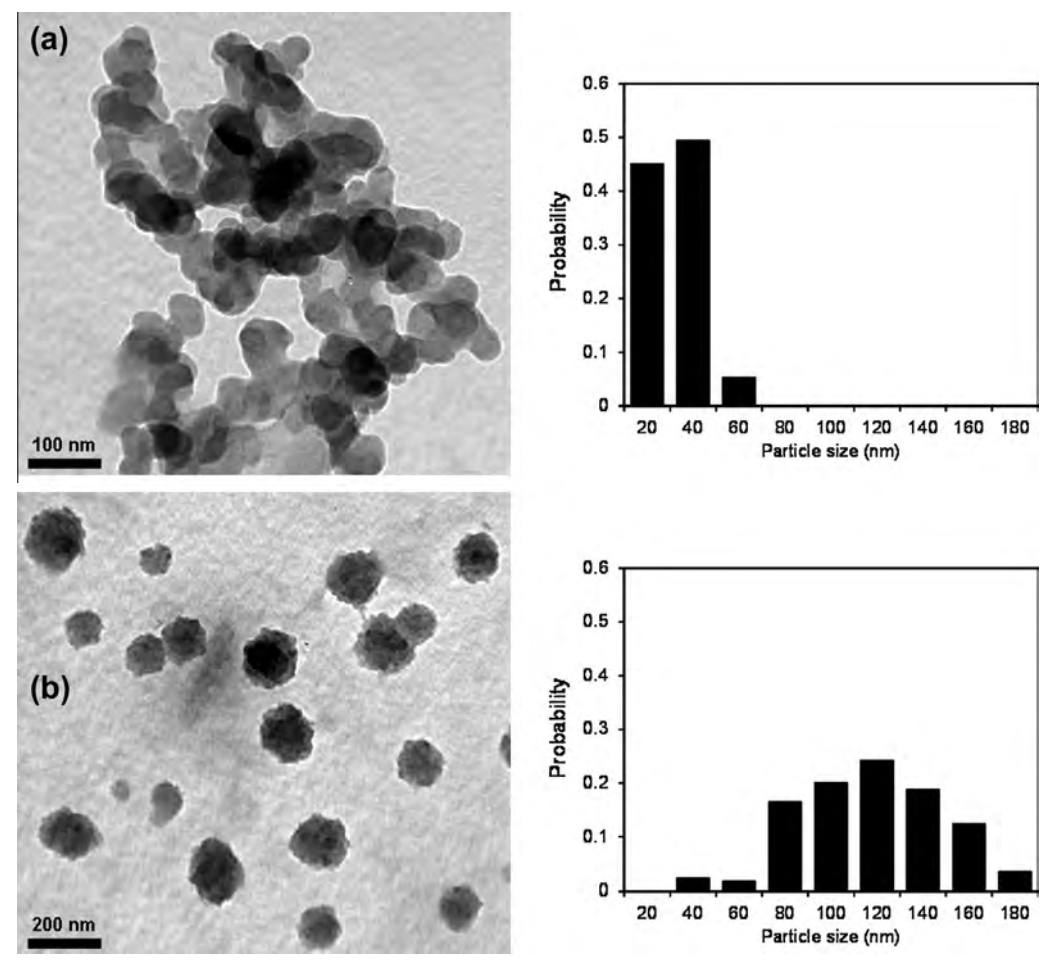


Fig. 1. TEM images of MEH-PPV nanoparticles prepared from different initial solvents, (a) THF and (b) DCM. Their size distributions are presented at the right side.

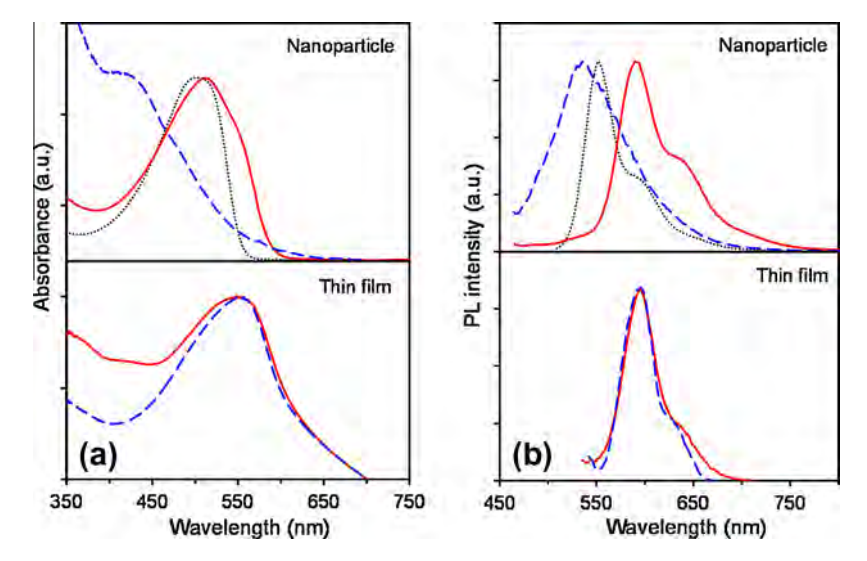


Fig. 2. (a) UV-vis absorption and (b) PL spectra of MEH-PPV in different forms, (top) nanoparticles and (bottom) drop-cast films. The samples were prepared by using (solid lines) THF and (dashed lines) DCM as initial solvents. The spectra of MEH-PPV dilute solution in THF (dotted lines) are included for comparison.

conjugated segments or chromophores stack on top of each other. The appropriate overlapping of Π -orbitals within the aggregates allows the formation of new electronic species with lower HOMO–LUMO energy gap. PL spectrum of the nanoparticles, reflecting electronic energy levels of the aggregates, exhibits $\lambda_{\rm max}$ and vibronic shoulder at about 594 nm and 640 nm, respectively. It is important to note that some conjugated segments do not form aggregates within the nanoparticles. The packing of these segments during the addition of water occurs in a random fashion, which do not allow the overlapping of Π -orbitals. Absorption spectra of these segments remain unaltered. Therefore, fraction of the aggregates within the system is proportional to the ratio of absorbance at 550/500 nm. Detailed discussion of this topic is given in our previous reports [33,35].

The MEH-PPV nanoparticles prepared by using DCM as an initial solvent exhibit quite different photophysical properties. Interestingly, the absorption spectrum shifts to higher energy region compared to that of the isolated chain. The absorbance at wavelength below 400 nm also rises significantly. Local λ_{max} is detected at about 420 nm. The significant blueshift of absorption spectrum indicates the collapse of MEH-PPV chains within the nanoparticles [31-34]. The drastic shrinkage of conjugated chains introduces kinks or physical defects within the backbone, which in turn limit local delocalization of Π electrons. In other words, the conjugation length of chromophores in the collapsed chain is reduced. Our previous studies have shown that the location of absorption spectra depends on the extent of chain collapse [42]. The absorption spectrum of isolated MEH-PPV chain systematically shifts to high-energy region upon increasing the polarity of alcohol solvents (i.e., decreasing solvent quality). In methanol, the MEH-PPV exhibits λ_{max} at about 445 nm. In this study, λ_{max} of the nanoparticles in water is detected at about 420 nm. This indicates higher magnitude of the chain collapse, which is attributed to the higher polarity of water medium. However, we also detect a broad shoulder at wavelength above 550 nm, corresponding to the aggregation of some chromophores within the nanoparticles. The measurement of PL spectrum indicates the collapse of MEH-PPV chain as well. The PL spectrum shifts to high-energy region and exhibits a featureless pattern. The PL peak is detected at about 535 nm, while the vibronic shoulder is not observed. The absence of the vibronic shoulder suggests that the vibrational energy levels of this system are not well-defined. We also prepare the MEH-PPV nanoparticles using polymer concentration at 1×10^{-2} mg/mL and $1\times10^{-4}\,\text{mg/mL}$ (see supporting information). While quantity of the nanoparticles increases with concentration, their absorption and PL spectra are hardly affected. The size distribution also remains approximately the same. We believe that the filtration by using 0.45 μm pore size membrane allows only small-size nanoparticles to pass through.

It is important to note that the variation of CPN photophysical properties is not due to the difference of their size. It has been observed in other systems that an increase in CPN size causes a redshift of PL spectra [23,30]. In our system, the CPN prepared from DCM exhibits much larger size compared to that of the THF system. Its PL spectrum, however, shifts to higher energy region. The conjugation length of chromophores within extended MEH-PPV backbone constitutes about 10–17 repeat units [43], which is shorter than the dimension of nanoparticles. The free volume required for segmental aggregation is also smaller. Therefore, the chain collapse and segmental aggregation causing the change of conjugation length can occur within the nanoparticles. In previous study where the size of MEH-PPV nanoparticles is about 5–10 nm, the aggregation is still detected [29].

Our results clearly show that the initial solvent plays a very important role on the formation and hence photophysical properties of the MEH-PPV nanoparticles. Table 2 summarizes the photophysical properties of MEH-PPV in different forms. The MEH-PPV nanoparticles prepared from DCM and THF exhibit green $(\lambda_{\rm max}$ = 535 nm) and red $(\lambda_{\rm max}$ = 594 nm) photoemission, respec-

Spectroscopic properties of conjugated polymers in different forms.

Samples	Initial solvents				
	λ_{\max} of absorption spectra		λ_{max} of PL spectra		
	THF	DCM	THF	DCM	
<i>MEH-PPV</i> Solution Nanoparticle Film	503 515 (550) 549	507 420 550	553 (585) 590 (630) 593 (632)	559 (600) 535 ^a 593 (631)	
rr-P3OT Solution Nanoparticle Film	448 512 (546, 593) 546 (610)	450 - 565 (615)	566 (604) 633 (686) 635 (663)	572 (610) 558 ^b 635 (662)	

Note: The excitation wavelength for PL measurements was ^a450 nm and ^b400 nm. Numbers in parentheses represent the location of shoulders in spectra.

tively. To further explore the origin of our major finding, we prepare thin films of the conjugated polymer by drop-casting from 1 mg/mL THF and DCM solutions. This method allows self-assembling process of the conjugated polymer to take place without perturbing the individual chain conformation. The absorption patterns of resultant films are quite different from those of the nanoparticles. The change of solvents hardly affects their photophysical properties. The absorption spectra of both films exhibit λ_{max} at about 550 nm, accompanied with a broad low-energy tail extending above 600 nm. The significant redshift of the whole spectra to 550 nm indicates the presence of high aggregate fraction within the thin films. The appearance of low-energy tail is attributed to electronic absorption of other types of aggregates with relatively low HOMU-LUMO energy gap [44]. It has been shown that aggregates can exist in different forms depending on the stacking configuration of chromophores [45,46]. The PL spectra of both films are also similar exhibiting λ_{max} at about 593 nm. The slight difference of their pattern is within error bar of the measurements. In our recent study where MEH-PPV chains in DCM and THF are forced to assemble into particles by addition of cyclohexane (nonsolvent), we observe different aggregation mechanisms [35]. At the very high fraction of cyclohexane, the use of DCM as initial solvent results in higher fraction of aggregates compared to that of the THF system.

An opposite result is obtained in this study where water is used as a poor solvent to drive the assembling of MEH-PPV chains into nanoparticles. Fig. 3 compares the amount of aggregates in each system by plotting ratio of absorbance at 550/500 nm. The aggregate fractions in thin films prepared by using the two solvents are comparable. In nanoparticles, however, the use of THF as an initial solvent leads to much higher fraction of aggregates. The nanoparticles prepared from DCM also contain large fraction of collapsed coils. The discrepancies of segmental aggregation and chain conformation lead to drastic difference of their PL spectra. This fundamental knowledge can be utilized to control properties of the nanoparticles without changing the structure or composition of the constituent polymers. Our results clearly demonstrate that the nanoparticles with different sizes and properties can be fabricated by varying type of the initial solvent. We also note that the nanoparticles contain lesser amount of aggregates compared to the drop-cast films. This is attributed to the confinement of polymer chains within a small volume that hinders the appropriate stacking of some chromophores. However, the intensity of low-energy peak (~630 nm) in PL spectra of the nanoparticle prepared from THF is higher than that of the thin film. Previous study shows that the photoemission of excimer contributes to the intensity of this peak [47]. Our observation suggests that the molecular packing within the nanoparticle favors the excimer formation.

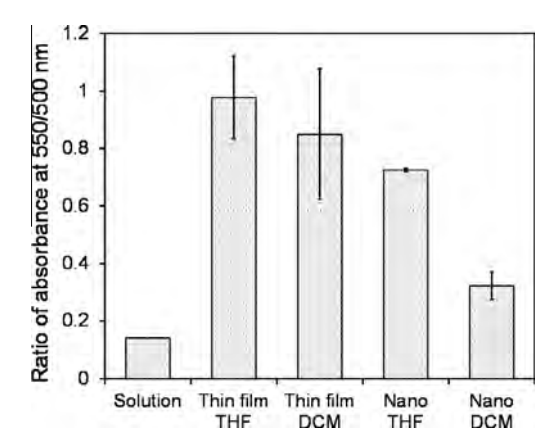


Fig. 3. Ratios of absorbance at 550/500 nm reflecting the aggregate fraction of MFH-PPV in different forms

Photophysical properties of the MEH-PPV nanoparticles are further explored by varying excitation wavelength as shown in Fig. 4. The variation of excitation energy allows electronic transition of various chromophores with different conjugation lengths. However, the PL spectra of nanoparticles prepared by using THF as an initial solvent exhibit the same pattern (see Fig. 4a). This result indicates that the photoemission process occurs via one type of chromophores. In this system, the fraction of aggregates, possessing the lowest HOMO-LUMO gap, is relatively high. The excited chromophores, therefore, can effectively transfer energy to aggregated sites before the photoemission process takes place. The PL pattern only reflects electronic energy levels of aggregates. The measurements of photoluminescence excitation (PLE) spectra at different emission wavelengths provide consistent results. The PLE pattern is similar to the absorption spectrum and independent of the detecting emission wavelength as shown in Fig 4b. This behavior is similar to systems of thin films where aggregate fraction is also quite high. The result is quite different in the system of nanoparticles prepared by using DCM as an initial solvent. Fig. 4c shows that the PL spectra systematically shift to low-energy region upon increasing excitation wavelength. Since the nanoparticles constitute collapsed chains and contain less amount of aggregates, the energy transfer process is less efficient compared to the system of THF. Therefore, this system allows photoemission of different chromophores upon varying the excitation energy. This observation is consistent with our previous studies where the multiple photoemissions are detected in the system of collapsed coils [33,42]. The measurement of PLE spectrum by fixing emission wavelength at 500 nm detects the absorption at high-energy region with λ_{max} at about 395 nm (see Fig. 4d). This corresponds to the excitation of relatively short chromophores within the system. When the detecting emission wavelength is increased to 590 nm, the excitation band at about 435 nm grows significantly.

From the aforementioned results, we propose mechanism for the formation of MEH-PPV nanoparticles in Fig. 5. Recent study by Cossiello et al. estimates solubility parameter (δ) of MEH-PPV and their components ($\delta_{\rm d}$ (dispersion), $\delta_{\rm p}$ (polar) and $\delta_{\rm h}$ (hydrogen bonding)) as $\delta = 18.7 \, \mathrm{J}^{1/2} \, \mathrm{cm}^{-3/2}$, $\delta_{\rm d} = 18.0 \, \mathrm{J}^{1/2} \, \mathrm{cm}^{-3/2}$, $\delta_{\rm p} = 4.0 \, \mathrm{J}^{1/2} \, \mathrm{cm}^{-3/2}$, and $\delta_{\rm h} = 3.0 \, \mathrm{J}^{1/2} \, \mathrm{cm}^{-3/2}$ [48]. They also observe that dispersion interaction between MEH-PPV and solvent is a major factor dictating the chain conformation and its photophysical properties. The absorption and PL spectra of MEH-PPV systematically blueshifts upon decreasing δ_d value of solvents, which corresponds to the decrease in conjugation length. Solubility parameters of solvents used in this study are listed in Table 3 [49]. The δ_d value of DCM, 18.2 J^{1/2} cm^{-3/2}, is very close to that of MEH-PPV, providing strong dispersion interaction. Therefore, the chain adopts extended conformation in this solvent. The dispersion interaction between MEH-PPV and THF ($\delta_d = 16.8 \, \text{J}^{1/2} \, \text{cm}^{-3/2}$) is weaker forcing the chain shrinkage, which leads to the decrease in conjugation length. Table 2 shows that λ_{max} of the absorption and PL spectra of MEH-PPV in THF solvent are shorter than that of the DCM system.

When the polymer solutions in DCM or THF are injected into water medium, the interactions between the solvents play a crucial role on the formation of nanoparticles. Water is a nonsolvent for MEH-PPV. It has relatively high δ value (47.8 $J^{1/2}$ cm $^{-3/2}$). The THF is miscible with water, while the aqueous solubility of DCM is limited at 17.6 g/L. In the preparation process of nanoparticle, the initial droplets of THF or DCM solutions are disintegrated by continuous ultrasonication. Since the THF has favorable interactions with water, the solution is spontaneously broken into small droplets with narrow size distribution. The DCM, on the other hand, has weaker interactions with water, which in turn resist the breaking process. Therefore, the resultant DCM droplets exhibit larger size compared to that of the THF system. This hypothesis is supported by the size of obtained nanoparticles. The use of DCM as

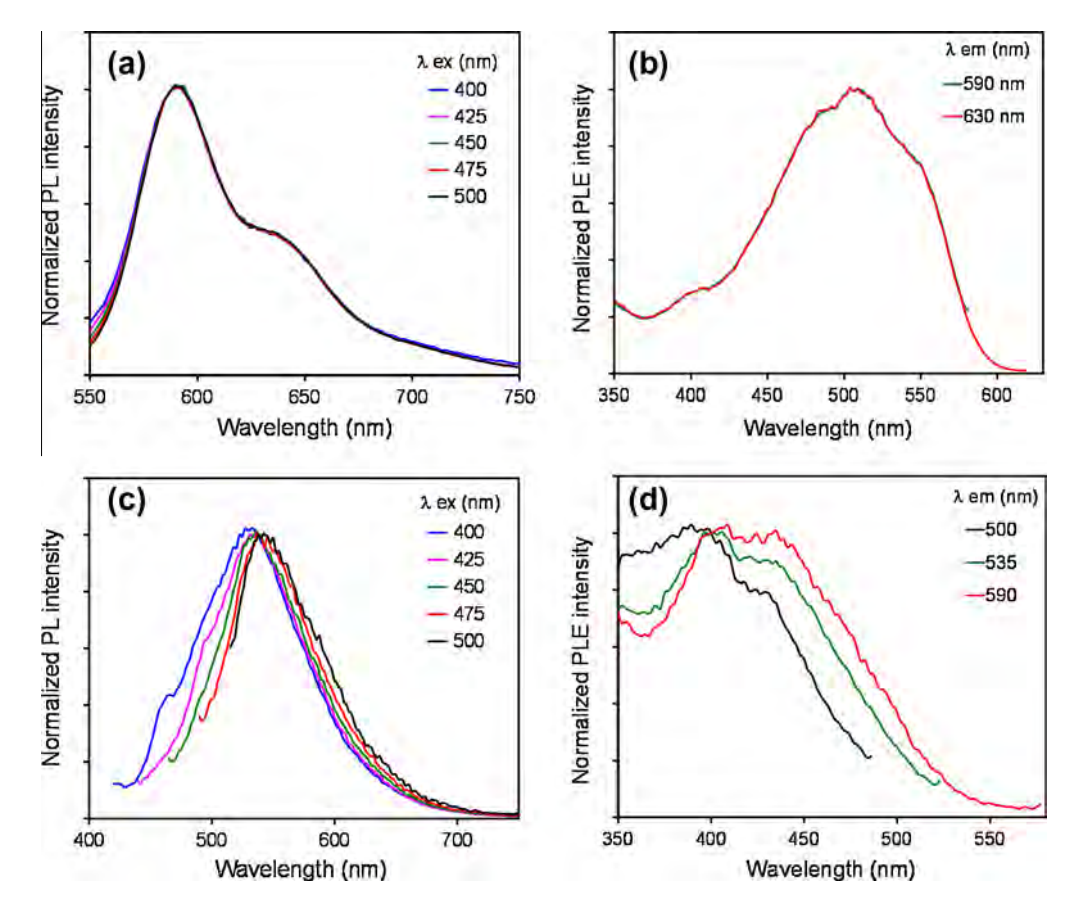


Fig. 4. (a and c) PL spectra and (b and d) PLE spectra of MEH-PPV nanoparticles measured at different excitation wavelengths (Ex λ) and emission wavelengths (Em λ), respectively. The nanoparticles were prepared from (a and b) THF and (c and d) DCM initial solvents.

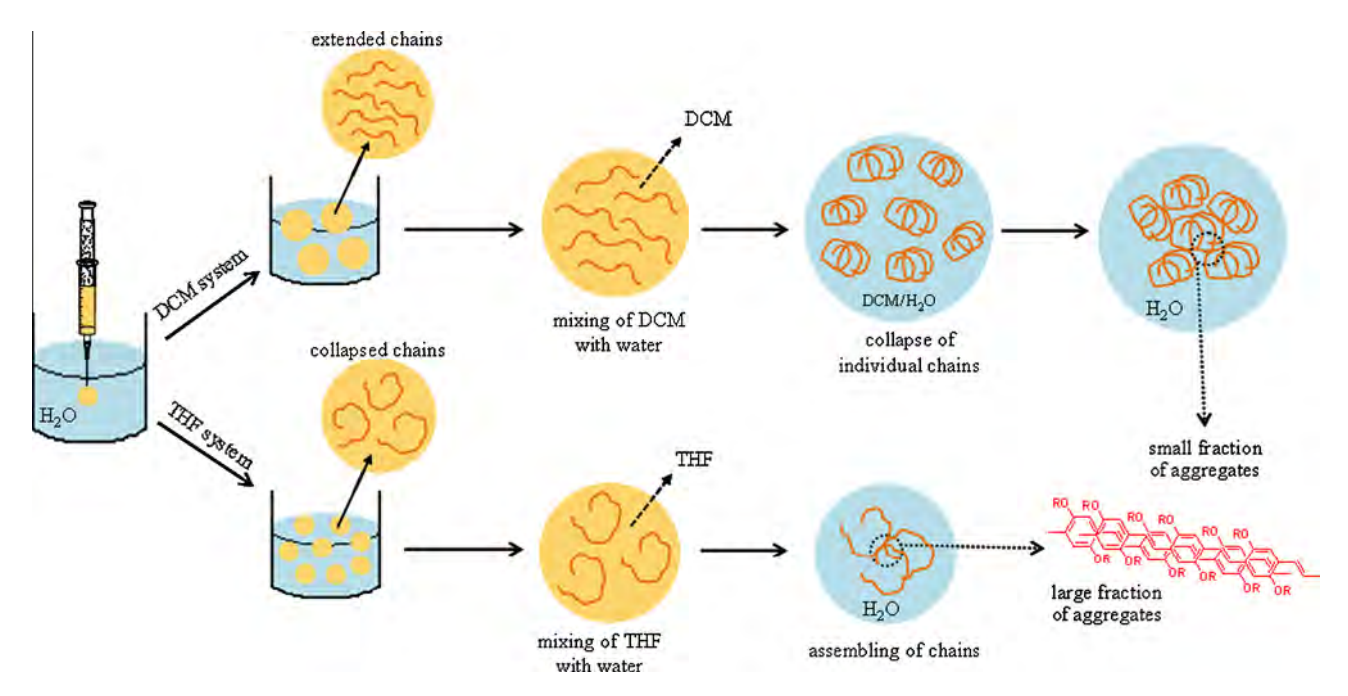


Fig. 5. Proposed mechanisms for the formation of MEH-PPV nanoparticles prepared by using (top) DCM and (bottom) THF as initial solvents.

an initial solvent provides the nanoparticles with much larger size as shown in Table 1. This result is similar to the system of polymer blend where the size of polymer droplet increases with decreasing polymer–polymer interactions [50].

The mixing of THF with water is also relatively fast, which in turn drives the assembling of MEH-PPV molecules into nanoparticles with minimal change of individual chain conformation. The stacking of some conjugated segments occurs within the nanopar-

Table 3Solubility parameter of solvents and conjugated polymers and their components [48,49,52].

Sample	$\delta (J^{1/2} \mathrm{cm}^{-3/2})$	$\delta_{\rm d}~({\rm J}^{1/2}~{\rm cm}^{-3/2})$	$\delta_{\rm p} ({\rm J}^{1/2} {\rm cm}^{-3/2})$	$\delta_{\rm h}~({\rm J}^{1/2}~{\rm cm}^{-3/2})$
DCM	20.3	18.2	6.3	6.1
THF	19.4	16.8	5.7	8.0
Water	47.8	15.5	16.0	42.3
MEH-PPV	18.7	18.0	4.0	3.0
rr-P3OT	18.2	=	=	-

ticles as indicated by the appearance of redshift peak in absorption spectrum (see Fig. 2). The mixing of DCM with water probably takes place in a slower fashion, allowing the collapse of individual chains. When the mixing process is complete, the collapsed chains assemble into nanoparticles to minimize interaction with water medium. Since the collapsed chains constitute many kinks or physical defects, it is more difficult to form aggregates. Therefore, the photophysical properties of collapsed chains are dominant in this type of nanoparticles. The packing of collapsed chains may be responsible for the rough surface of nanoparticles as revealed by TEM in Fig. 1b. It is worthwhile to point out that the aggregation of MEH-PPV chains in DCM is very high when nonsolvent, cyclohexane, is added [35]. In this system, the high miscibility of DCM and cyclohexane does not allow the collapse of MEH-PPV prior to the assembling process.

3.2. Nanoparticles of rr-P3OT

In this section, we further investigate the role of initial solvent on the formation of nanoparticles by using rr-P3OT. Our result from solvent-nonsolvent titration shows that the solubility of rr-P3OT in THF is higher compared to that of the DCM system. This result conforms to the solubility parameter (δ) of rr-P3OT and solvents. The solubility of polymer in solvent is promoted when the difference between their δ values is small [49,51]. The δ values of *rr*-P3OT, THF, and DCM are $18.2 \,\mathrm{J}^{1/2} \,\mathrm{cm}^{-3/2}$ [52], $19.4 \,\mathrm{J}^{1/2} \,\mathrm{cm}^{-3/2}$, and 20.3 $I^{1/2}$ cm^{-3/2}, respectively. Therefore, the THF is a better solvent for rr-P3OT, which is opposite to the MEH-PPV system. This discrepancy probably arises from the presence of s atoms in rr-P3OT backbone, which affects local interactions with the solvents. This result also indicates that the dispersion interaction between rr-P3OT and solvent is not a major factor that controls the solubility and conformation of rr-P3OT. We expect that rr-P3OT has very different solubility parameter components compared to those of the MEH-PPV. However, we still observe similar results. Fig. 6 shows SEM and TEM images of rr-P3OT nanoparticles. The use of THF as an initial solvent provides spherical nanoparticles with average size of about 50 nm, which is comparable to that of the MEH-PPV nanoparticles (see Table 1). When the DCM is used, the average size increases significantly. This result supports our hypothesis that the size of nanoparticles is mainly dictated by the water solubility of initial solvent. However, the internal morphology of rr-P3OT nanoparticles is hardly affected. The high

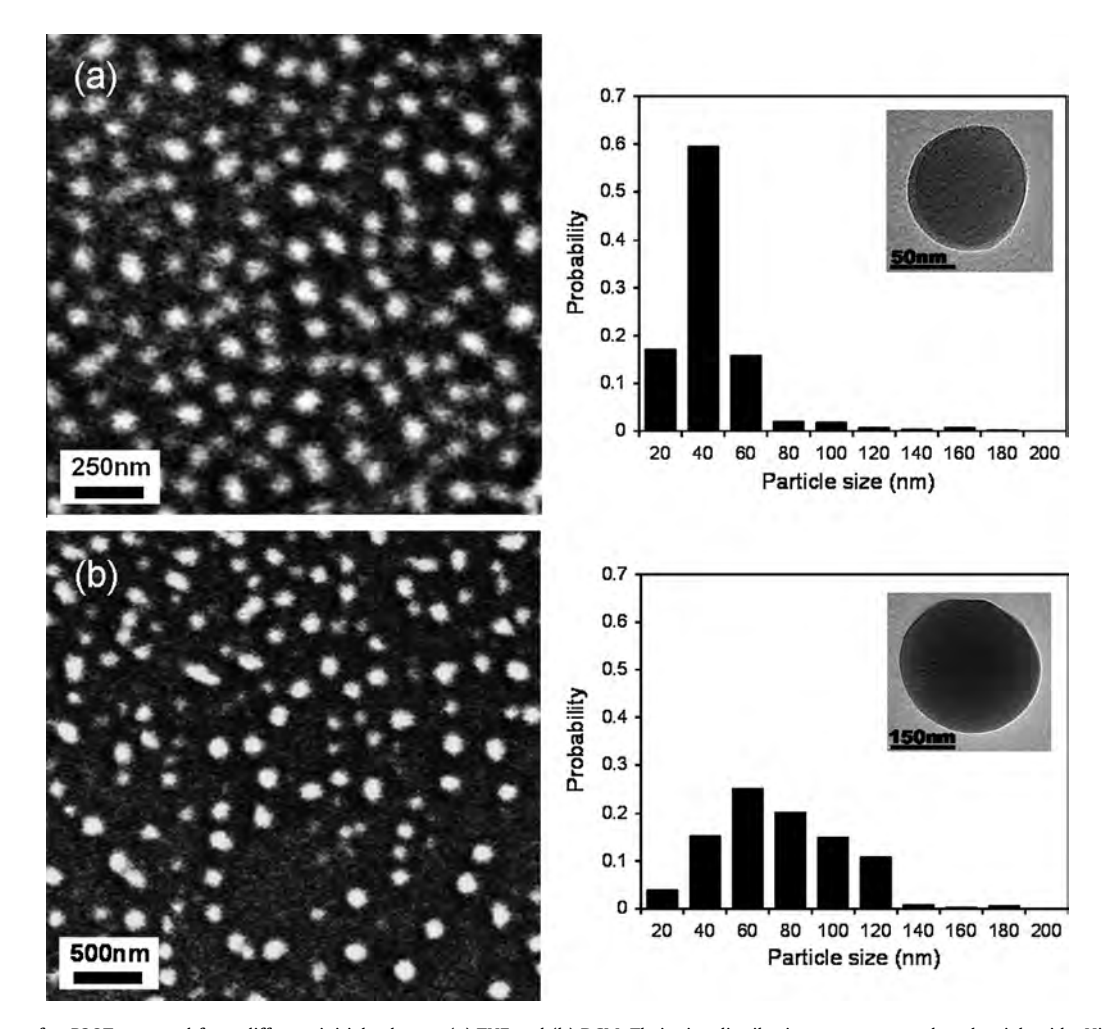


Fig. 6. SEM images of rr-P3OT prepared from different initial solvents, (a) THF and (b) DCM. Their size distributions are presented at the right side. High resolution TEM images of these nanoparticles are shown in the insets.

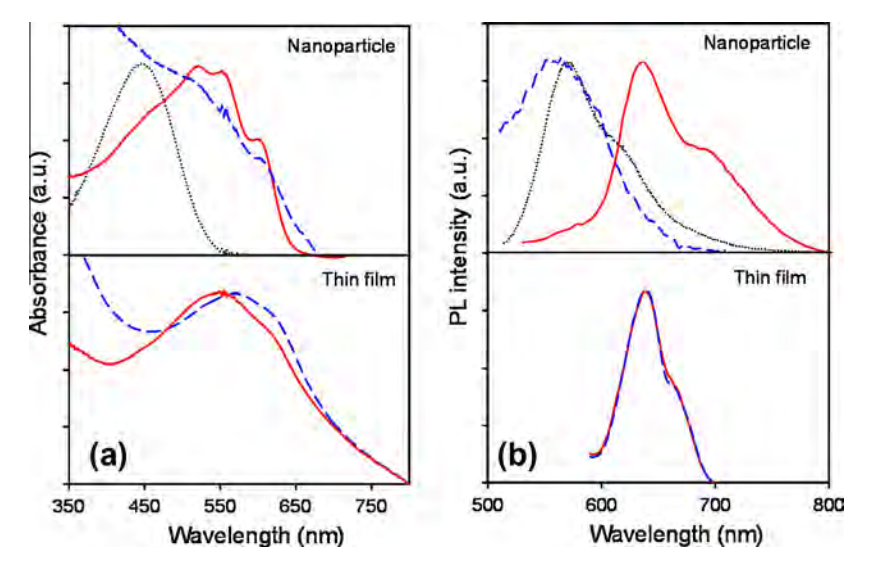


Fig. 7. (a) UV-vis absorption and (b) PL spectra of *rr*-P3OT in different forms, (top) nanoparticles and (bottom) drop-cast films. The samples were prepared by using (solid lines) THF and (dashed lines) DCM as initial solvents. The spectra of *rr*-P3OT dilute solution in THF (dotted lines) are included for comparison.

resolution TEM images show that the nanoparticles prepared from both solvents exhibit homogenous internal density and smooth surface.

The photophysical properties of rr-P3OT in different forms are shown in Fig. 7. The isolated chain in THF solution exhibits a broad absorption pattern with $\lambda_{\rm max}$ at about 450 nm. Similar to MEH-PPV system, the PL spectrum constitutes peak and vibronic shoulder at 572 nm and 615 nm, respectively, reflecting electronic energy levels of the longest chromophore within the conjugated backbone [53]. When the rr-P3OT forms nanoparticles by using THF as an initial solvent, the absorption spectrum drastically shifts to low-energy region. Three distinct redshift peaks are clearly observed at about 515 nm, 550 nm, and 605 nm. Previous studies have shown that the appearance of these peaks corresponds to the formation of aggregates within the nanoparticles [54,55]. These aggregates emit light at much lower energy region compared to the isolated chain. Their PL spectrum exhibits a well-defined pattern with $\lambda_{\rm max}$ and vibronic shoulder at about 638 nm and 695 nm, respectively.

In the system of DCM, absorption spectrum of the *rr*-P3OT nanoparticles still shifts to low-energy region. The three redshift peaks, however, are obscured. A rise of absorbance at high-energy region is also observed. These results indicate that the molecular packing and individual chain conformation of *rr*-P3OT within the nanoparticles are different from the THF system. Fig. 8 compares

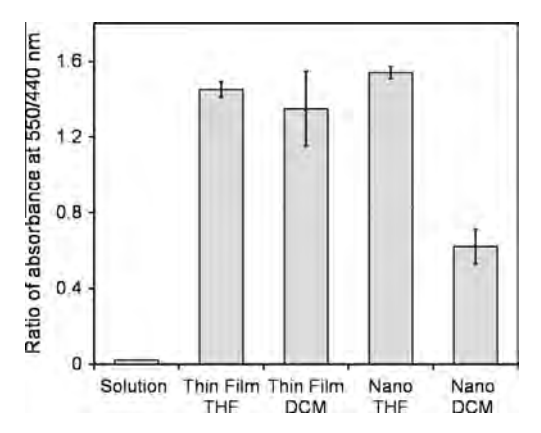


Fig. 8. Ratio of absorbance at $550/440\,\mathrm{nm}$ reflecting the aggregate fraction of rr-P3OT prepared in different forms.

the aggregate fraction in each system by plotting the ratio of absorbance at 550/440 nm. It is clear that the nanoparticles prepared from DCM solution contain lesser amount of aggregates. The measurement of PL spectrum provides a supportive result. PL spectrum of the nanoparticles shifts to relatively high-energy region, which is similar to the MEH-PPV system. It exhibits featureless pattern with $\lambda_{\rm max}$ at about 565 nm. The blueshift of PL spectrum indicates the collapse of conjugated chains within the nanoparticles [56]. Although relatively high amount of aggregates exists in this system, their PL peak at 638 nm is not observed. The photoemission of collapsed chains is still dominant. We suggest that the aggregate formed in the DCM system is a non-emissive species. We also note that the blueshift of PL spectrum of rr-P3OT is smaller than that of the MEH-PPV. This is attributed to the difference in chain rigidity of the two polymers.

The absorption and PL spectra of drop-cast films prepared from THF and DCM solutions exhibit similar pattern. The spectra significantly shift to lower energy region compared to those of the isolated chain indicating the presence of high aggregate fraction. Unlike the system of nanoparticles prepared from THF, we do not detect the three distinct redshift peaks in the absorption spectra. This observation suggests that local structures of aggregates formed in the nanoparticles and thin films are different. The measurements of PL spectra also detect the discrepancy in pattern. The λ_{max} values of PL spectra measured from the nanoparticles, and thin films are comparable. Interestingly, the vibronic shoulder is detected at different wavelengths, about 695 nm and 665 nm for the nanoparticles and thin films, respectively. This indicates the variation of vibrational energy levels of aggregates in the two systems. The separation between peak and vibronic shoulder, corresponding to vibrational energy gap of the aggregates in ground state, increases from about 25 nm in thin films to about 55 nm in the nanoparticles. The increase in vibrational energy gap is attributed to the increase in confinement within the nanoparticles which may resist the vibration of polymer segments. We note that the change of vibrational energy levels is also observed but less pronounced in the MEH-PPV system.

4. Conclusion

Our results in this study demonstrate that the mechanism of CPN formation in water is strongly influenced by properties of the initial solvents. We show that the solubility of initial solvent in water is a major factor dictating the conformational change and segmental aggregation of conjugated polymers within the CPNs. When the water solubility of initial solvent is relatively low, the collapse of conjugated chains occurs prior to the assembling process. The resultant CPNs contain large fraction of collapsed coils. Therefore, the photophysical properties of collapsed coils, which absorb and emit light at high-energy region, are dominant in this type of CPNs. When the initial solvent is miscible with water, the mixing process is relatively fast. The conjugated polymers are driven to assemble into CPNs with minimal change of individual chain conformation. This type of CPNs contains large fraction of aggregates and exhibits smaller size. Their absorption and PL spectra occur at low-energy region. The CPNs of MEH-PPV and rr-P3OT prepared in this study by using DCM and THF as initial solvents exhibit rather different photophysical properties. The difference in λ_{max} position of PL spectra is more than 50 nm. Our study shows that a careful choice of the solvent can be used to produce the CPNs with desired chain arrangement and photophysical properties, suitable for particular device application.

Acknowledgments

This research is financially supported by the Thailand Research Fund, Ministry of Higher Education and Naresuan University (Grant RMU5380017). RP thanks the Office of Higher Education Commission for supporting her Ph.D. scholarship under the program Strategic Scholarships for Frontier Research Network. RT thanks NANOTEC-MU Excellence Center on Intelligent Materials and Systems and Center for Innovation in Chemistry (PERCH-CIC) for supporting some research facilities.

Appendix A. Supplementary material

Supplementary data associated with this article can be found, in the online version, at http://dx.doi.org/10.1016/j.jcis.2013.04.022.

References

- [1] X. Gong, D. Moses, A.J. Heeger, in: K. Müllen, U. Scherf (Eds.), Polymer-Based Light-Emitting Diodes (PLEDs) and Displays Fabricated from Arrays of PLEDs, Wiley-VCH, Weinheim, 2006, p. 151.
- A. Facchetti, Chem. Mater. 23 (2011) 733-758.
- [3] H. Spanggaard, F.C. Krebs, Sol. Energy Mater. Sol. Cells 83 (2004) 125–146. [4] C.J. Brabec, N.S. Sariciftci, J.C. Hummelen, Adv. Funct. Mater. 11 (2001) 15–26.
- [5] G. Horowitz, Adv. Mater. 10 (1998) 365-377.
- [6] X. Zhan, Z. Tan, B. Domercq, Z. An, X. Zhang, S. Barlow, Y. Li, D. Zhu, B. Kippelen, S.R. Marder, J. Am. Chem. Soc. 129 (2007) 7246-7247.
- [7] C.Y. Yang, F. Hide, M.A. Díaz-García, A.J. Heeger, Polymer 39 (1998) 2299–2304.
- [8] B.J. Schwartz, Annu. Rev. Phys. Chem. 54 (2003) 141-172.
- [9] M. Brinkmann, J. Polym. Sci. Part B: Polym. Phys. 49 (2011) 1218-1233.
- [10] B.R. Saunders, M.L. Turner, Adv. Colloid Interface Sci. 138 (2008) 1-23.
- [11] C. Wu, B. Bull, K. Christensen, J. McNeill, Angew. Chem., Int. Ed. 121 (2009) 2779-2783.
- [12] J.H. Moon, P. MacLean, W. McDaniel, L.F. Hancock, Chem. Commun. (2007) 4910-4912.
- [13] C. Wu, B. Bull, C. Szymanski, K. Christensen, J. McNeill, ACS Nano 2 (2008) 2415-2423.
- [14] C. Wu, C. Szymanski, Z. Cain, J. McNeill, J. Am. Chem. Soc. 129 (2007) 12904-12905.

- [15] M. Green, P. Howes, C. Berry, O. Argyros, M. Thanou, Proc. R. Soc. London, A 465 (2009) 2751-2759.
- [16] M. Bruchez, M. Moronne, P. Gin, S. Weiss, A.P. Alivisatos, Science 281 (1998) 2013-2016.
- [17] K. Landfester, A. Musyanovych, V. Mailänder, J. Polym. Sci. Part A: Polym. Chem. 48 (2010) 493-515.
- [18] D. Tuncel, H.V. Demir, Nanoscale 2 (2010) 484-494.
- [19] A. Kaeser, A.P.H.J. Schenning, Adv. Mater. 22 (2010) 2985–2997.
- [20] C. Wu, C. Szymanski, J. McNeill, Langmuir 22 (2006) 2956–2960.
- [21] J.M. Lee, S.J. Lee, Y.J. Jung, J.H. Kim, Curr. Appl. Phys. 8 (2008) 659-663. [22] S.J. Lee, J.M. Lee, I.W. Cheong, H. Lee, J.H. Kim, J. Polym. Sci. Part A: Polym. Chem. 46 (2008) 2097-2107.
- [23] S.J. Lee, J.M. Lee, H.-Z. Cho, W.G. Koh, I.W. Cheong, J.H. Kim, Macromolecules 43 (2010) 2484-2489.
- [24] X.-G. Li, J. Li, M.-R. Huang, Chem. Eur. J. 15 (2009) 6446–6455.
- [25] Z. Wang, Y. Wang, D. Xu, E.S.-W. Kong, Y. Zhang, Synth. Met. 160 (2010) 921-
- [26] X.-G. Li, J. Li, Q.-K. Meng, M.-R. Huang, J. Phys. Chem. B 113 (2009) 9718-9727.
- [27] J. Pecher, S. Mecking, Chem. Rev. 110 (2010) 6260-6279.
- [28] E.-J. Park, T. Erdem, V. Ibrahimova, S. Nizamoglu, H.V. Demir, D. Tuncel, ACS Nano 5 (2011) 2483–2492. [29] C. Szymanski, C. Wu, J. Hooper, M.A. Salazar, A. Perdomo, A. Dukes, J. McNeill, J.
- Phys. Chem. B 109 (2005) 8543-8546.
- [30] O. Pras, D. Chaussy, O. Stephan, Y. Rharbi, P. Piette, D. Beneventi, Langmuir 26 (2010) 14437-14442.
- [31] B.G. Sumpter, P. Kumar, A. Mehta, M.D. Barnes, W.A. Shelton, R.J. Harrison, J. Phys. Chem. B 109 (2005) 7671-7685.
- [32] T.-Q. Nguyen, V. Doan, B.J. Schwartz, J. Chem. Phys. 110 (1999) 4068-4078.
- [33] R. Traiphol, N. Charoenthai, T. Srikhirin, T. Kerdcharoen, T. Osotchan, T. Maturos, Polymer 48 (2007) 813-826.
- [34] P. Kumar, A. Mehta, S.M. Mahurin, S. Dai, M.D. Dadmun, B.G. Sumpter, M.D. Barnes, Macromolecules 37 (2004) 6132-6140.
- [35] R. Traiphol, R. Potai, N. Charoenthai, T. Srikhirin, T. Kerdcharoen, T. Osotchan, J. Polym. Sci. Part B: Polym. Phys. 48 (2010) 894-904.
- [36] R. Traiphol, N. Charoenthai, Synth. Met. 158 (2008) 135-142.
- [37] Physical Constants of Organic Compounds, in CRC Handbook of Chemistry and Physics, Internet Version 2005, David R. Lide, (Ed.), www.hbcpnetbase.com>, CRC Press, Boca Raton, FL, 2005, p. 84.
- [38] B. Valeur, Molecular Fluorescence: Principles and Applications, first ed., Wiley-VCH, Weinheim, 2001. p. 51.
- [39] P.F. Barbara, A.J. Gesquiere, S.-J. Park, Y.J. Lee, Acc. Chem. Res. 38 (2005) 602-
- [40] Z. Yu, P.F. Barbara, J. Phys. Chem. B 108 (2004) 11321-11326.
- [41] D. Hu, J. Yu, G. Padmanaban, S. Ramakrishnan, P.F. Barbara, Nano Lett. 2 (2002) 1121-1124.
- [42] R. Traiphol, P. Sanguansat, T. Srikhirin, T. Kerdcharoen, T. Osotchan, Macromolecules 39 (2006) 1165–1172.
- [43] H.S. Woo, O. Lhost, S.C. Graham, D.D.C. Bradley, R.H. Friend, C. Quattrocchi, J.L. Brédas, R. Schenk, K. Müllen, Synth. Met. 59 (1993) 13-28.
- [44] R. Traiphol, N. Charoenthai, P. Manorat, T. Pattanatornchai, T. Srikhirin, T. Kerdcharoen, T. Osotchan, Synth. Met. 159 (2009) 1224-1233.
- [45] S. Tretiak, A. Saxena, R.L. Martin, A.R. Bishop, J. Phys. Chem. B 104 (2000) 7029-7037.
- [46] S. Siddiqui, F.C. Spano, Chem. Phys. Lett. 308 (1999) 99-105.
- [47] R. Jakubiak, C.J. Collison, W.C. Wan, L.J. Rothberg, B.R. Hsieh, J. Phys. Chem. A 103 (1999) 2394-2398.
- [48] R.F. Cossiello, M.D. Susman, P.F. Aramendía, T.D.Z. Atvars, J. Lumin. 130 (2010) 415-423
- [49] A.F.M. Barton, Chem. Rev. 75 (1975) 731-753.
- [50] A.R. Kamdar, Y.S. Hu, P. Ansems, S.P. Chum, A. Hiltner, E. Baer, Macromolecules 39 (2006) 1496-1506.
- [51] S. Samitsu, T. Shimomura, S. Heike, T. Hashizume, K. Ito, Macromolecules 41 (2008) 8000-8010.
- [52] A. Zen, M. Saphiannikova, D. Neher, U. Asawapirom, U. Scherf, Chem. Mater. 17 (2005) 781-786.
- [53] R. Palacios, P. Barbara, J. Fluoresc, 17 (2007) 749–757.
- [54] N. Kiriy, E. Jähne, H.-J. Adler, M. Schneider, A. Kiriy, G. Gorodyska, S. Minko, D. Jehnichen, P. Simon, A.A. Fokin, M. Stamm, Nano Lett. 3 (2003) 707-712.
- [55] C. Scharsich, R.H. Lohwasser, M. Sommer, U. Asawapirom, U. Scherf, M. Thelakkat, D. Neher, A. Köhler, J. Polym. Sci. Part B: Polym. Phys. 50 (2012) 442-453.
- [56] Y.-J. Ko, E. Mendez, J.H. Moon, Macromolecules 44 (2011) 5527-5530.



Conformational Change, Intrachain Aggregation and Photophysical Properties of Regioregular Poly(3-octylthiophene) in Alkanes

Ruttayapon Potai, ¹ Anothai Kamphan, ¹ Rakchart Traiphol^{1,2}

¹Laboratory of Advanced Polymers and Nanomaterials, Department of Chemistry and Center for Innovation in Chemistry, Faculty of Science, Naresuan University, Phitsanulok 65000, Thailand

²NANOTEC-MU Excellence Center on Intelligent Materials and Systems, Faculty of Science, Rama 6 Road, Ratchathewi, Bangkok 10400, Thailand

Correspondence to: R. Traiphol (E-mail: rakchartt@nu.ac.th)

Received 13 March 2013; revised 1 May 2013; accepted 17 May 2013; published online

DOI: 10.1002/polb.23326

ABSTACT: This study explores the role of segmental solubility of regioregular poly(3-octylthiophene) (rr-P3OT) on chain organization and its photophysical properties. In good solvent chlorobenzene (CRB), rr-P3OT chain adopts an extended conformation, allowing long conjugation length of π -electrons. Cyclohexane is a good solvent for octyl side chain but a poor solvent for the thiophene backbone. The selective segmental interactions of rr-P3OT with this solvent induce conformational change of the polymer. Addition of cyclohexane into the CRB solution leads to chain coiling, which in turn causes significant decrease of the conjugation length. Absorption and photoluminescence spectra of the rr-P3OT in cyclohexane exhibit a blueshift of about 16 nm compared to those of the CRB solution. The change of chain conformation is also detectable by monitoring the variation of quantum yield upon increasing

cyclohexane ratio. The quantum yield drops from 0.17 \pm 0.01 to 0.11 \pm 0.01 when the extended $\it rr$ -P3OT chain transforms into coiled conformation. Hexane is a nonsolvent for $\it rr$ -P3OT due to its relatively low solubility parameter. The addition of hexane into $\it rr$ -P3OT solution in cyclohexane forces dense packing of thiophene rings within the coiled chain. An intrachain aggregation occurs in this system, leading to the appearance of three distinct redshift peaks in absorption spectra and the drastic drop of quantum yield. Correlation between the growth of redshift peaks and the decrease of quantum yield is clearly observed. © 2013 Wiley Periodicals, Inc. J. Polym. Sci., Part B: Polym. Phys. 2013, $\it voleta$ 00, 000–000

KEYWORDS: conformational analysis; conjugated polymer; chain organization; photophysics; solvent effect

INTRODUCTION Structural-property relationship of conjugated polymers has been a subject of interest in the past few decades. This is mainly due to their potential applications in various advanced technologies such as organic light-emitting diodes, 1,2 plastic solar cells, 3,4 and organic field-effect transistors.^{5,6} Poly(3-alkylthiophene)s (P3ATs) is one class of conjugated polymer that receives tremendous attention. Advantages of the P3AT include high environmental stability and well-ordered semicrystalline structure.^{7,8} The close packing of conjugated backbone in their crystalline domains allows the overlap of π -orbitals, promoting charge carrier mobility. 9,10 This characteristic is particularly important for plastic solar cell application where high degree of charge separation upon photoirradiation is desired. 3,4,11 The presence of alkyl side chains also allows high solubility in common organic solvents, which facilitates the fabrication of P3AT thin films in the devices via wet processes.^{7,8}

It has been demonstrated that properties of conjugated polymers can be controlled by structural modification of main

chain and/or side chains.^{8,9,11-13} To optimize efficiency of the aforementioned devices, tremendous effort has been dedicated for synthesizing new classes of conjugated polymers. However, other molecular parameters such as interchain/intrachain aggregation and individual chain conformation also affect their properties significantly.9,10 The stacking of conjugated backbone within aggregates promotes the overlap of π -orbitals, which in turn facilitates intersegmental delocalization of π electrons. The aggregation of conjugated polymers normally leads to the formation of new electronic species with lower HOMO-LUMO energy gap compared to that of the isolated chain. As the existence of aggregates strongly affects important properties of conjugated polymers such as charge carrier mobility, 9,10,14 photo/electroluminescence intensity and color,1,9 it is essential to understand molecular and experimental parameters dictating the aggregate formation. Previous studies reported by different groups have shown that the aggregation of P3AT leads to the growth of three distinct redshift peaks in absorption spectrum. 15-21 The quantum yield also decreases significantly.16

© 2013 Wiley Periodicals, Inc.



TABLE 1 Properties of Solvents and Polymers 31,32,63,64

Sample	Dielectric constant	δ (J ^{1/2} cm ^{-3/2})
Chlorobenzene	5.7	19.6
Pyridine	13.3	21.8
Cyclohexane	2.0	16.8
<i>n</i> -Hexane	1.8	14.9
n-Octane	1.9	15.5
Thiophene	2.7	20.2
rr-P3OT	-	18.2

The change of individual chain conformation affects π electron delocalization along conjugated backbone. Roles of chain conformation on photophysical properties have been extensively investigated in the system of well-known poly[2-methoxy-5-(2'-ethylhexyloxy)-1,4-phenylenevinylene] (MEH-PPV).²²⁻²⁷ In good solvent, the conjugated polymer normally prefers extended conformation owning to its rigid backbone. 24,25 The conjugated chain folds or collapses in poor solvent to minimize local interactions. The presence of physical defects or kinks along the conjugated backbone of collapsed chain interrupts the delocalization of π electrons.^{26,27} In other words, the conjugation length decreases when conjugated chain adopts folded or collapsed conformation, causing a blueshift in absorption and photoluminescence (PL) spectra. In previous studies by one of the authors, the blueshift of absorption spectrum as much as 60 nm is detected when the extended MEH-PPV chain is forced to collapse in very poor solvent.²⁷ In the system of P3AT, however, the blueshift of absorption and PL spectra is never detected in poor solvent. The decrease of solvent quality normally leads to the growth of new redshift peaks, arising from interchain and/or intrachain aggregation. 10,15,19-21 Some authors also suggest the planarization of each individual chain in poor solvent. 18,28

In this study, we systematically induce conformational change of regioregular poly(3-octylthiophene) (rr-P3OT) using cyclohexane and hexane as poor solvents. The solubility parameters (δ) of these solvents are much lower than that of rr-P3OT (see Table 1). However, the δ values are close to that of the octyl side chain, providing selective local polymer–solvent interactions. The hexane can only dissolve a trace amount of the polymer. The solubility of rr-P3OT increases significantly in cyclohexane, attributed to its higher δ value. Therefore, cyclohexane can be used to induce chain coiling without intrachain aggregation. Atomic force microscopy (AFM) is used to follow conformational change in each system. In our study, we detect a significant blueshift in absorption and PL spectra.

EXPERIMENTAL

The rr-P30T was purchased from Sigma-Aldrich. The number average molecular weight (M_n) determined by gel permeation chromatography (GPC) with polystyrene standard is

58,300 g mol^{-1} ($M_{\text{w}}/M_{\text{n}} = 2.3$). It has been known that the GPC measurement of rigid rod polymer usually overestimates the absolute molecular weight by a factor of about 2- $2.3.^{29,30}$ By comparing the $M_{\rm n}$ of GPC with MALDI-TOF data, the contour length of rr-P3OT in this study is \sim 51 nm.² The regionegularity of P30T provided by the supplier is about 98%. Solutions of rr-P30T were prepared by dissolving powder sample in chlorobenzene (CRB) and pyridine (PRD), assisted by mechanical stirring and ultrasonication. All solvents used in this study are analytical grade. In PRD solvent, the polymer solution was stirred for several days to achieve complete dissolution. The solution appears clear to naked eyes. To vary local polymer-solvent interactions, poor solvents were added into the systems. In this study, the dissolved polymer solutions in solvents were injected into a mixture of solvent-nonsolvent under stirring. Concentration of the polymer was kept constant at 0.001 mg mL^{-1} . An inner-filtered effect is negligible at this concentration. When cyclohexane was used as a poor solvent, the ratio of the cyclohexane was varied from 0 to 100% v/v. In this system, the properties of solution are independent of aging time. To induce larger extent of chain coiling, a nonsolvent, hexane, was added into the rr-P30T solution in cyclohexane. Ratio of the hexane was increased up to 90% v/v. When the hexane ratio was above 50% v/v, it was important to use freshly prepared solutions to avoid the polymer precipitation. Absorption spectra of polymer solutions were recorded by using Analytica Specord 100 UV/vis spectrometer with 4and 10-cm-thick quartz cuvettes, depending on the polymer concentration. The measurements of PL emission spectra were carried out on Perkin-Elmer LS55 spectrometer.

The quantum yield of rr-P3OT (Φ_X) was measured by using 0.1 M NaOH aqueous solution of fluorescien (Φ_{ST} =0.79) as a standard. A series of solution exhibiting absorbance less than 0.1 was used. The calculation was performed by using the following equation.

$$\Phi_X = \Phi_{ST} \left(\frac{slope_X}{slope_{ST}} \right) \left(\frac{\eta_X^2}{\eta_{ST}^2} \right)$$

The slopes (slope_X and slope_{ST}) were obtained from the plots between integrated area of PL spectra and absorbance at the excitation wavelength. The refractive indices of solvent (η_X) and standard (η_{ST}) were taken into account in the calculation. In the system of mixtures, refractive indices were estimated by interpolation from those of the pure solvents.

Samples for AFM measurement were prepared by drop casting from 0.05 mg mL $^{-1}$ solutions. The solution droplet was allowed to dry in a clean atmosphere under ambient condition. Three samples were prepared for each condition. Polished silicon wafer, used as a substrate, was freshly cleaned before the deposition. The substrate was soaked in a piranha solution (7:3 v/v of conc. $\rm H_2SO_4$ and 30% $\rm H_2O_2$) at 80 °C for 1 h. It was rinsed by using deionized water and dried with nitrogen gas. Morphology of self-assembled $\it rr$ -P30T films was explored by AFM (SPI3800N Nanoscope II, Seiko Instrument, Japan) operating in a dynamic contact mode. The

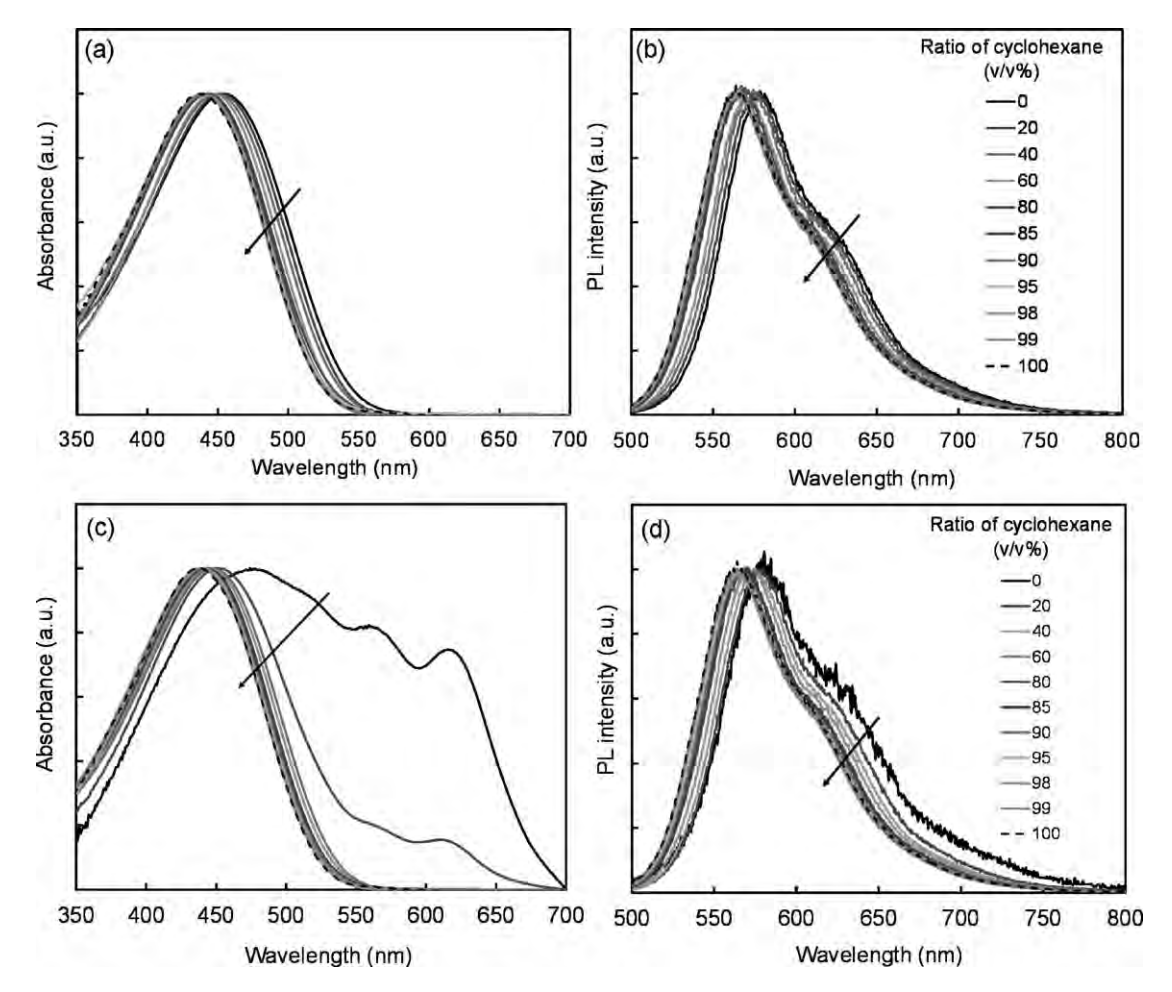


FIGURE 1 (Left) Absorption and (right) PL spectra of 0.001 mg mL⁻¹ *rr*-P3OT in (a,b) mixture of chlorobenzene and cyclohexane and (c,d) mixture of pyridine and cyclohexane. Arrows indicate the change of spectra upon increasing ratio of cyclohexane. All spectra are normalized for clarity.

cantilever was fabricated from $\mathrm{Si}_3\mathrm{N}_4$ with a spring constant of about 15 N m $^{-1}$. At least three areas were scanned for each sample. To minimize the line broadening effect due to a finite shape of AFM tip, the width of nanostructures was measured as full width at half height.

RESULTS AND DISCUSSION

Conformational Change in Cyclohexane

Solubility parameters (δ) and dielectric constant of all solvents and rr-P30T are listed in Table 1. The comparison of these δ values can provide an insight about local interactions between the solvent and each segment of rr-P30T. The difference between solubility parameters of CRB and rr-P30T is relatively small. This suggests strong polymer–solvent interactions, resulting in high solubility. PRD is a more polar solvent with higher δ value. Therefore, the PRD is a poorer solvent compared to the CRB. The weaker polymer–solvent interaction in PRD system is indicated by the decrease of polymer solubility. Cyclohexane is a nonpolar solvent. It is a poor solvent for thiophene group due to the large difference of their δ values. However, the octyl side

chain of rr-P3OT has strong dispersion interaction with this solvent. The disparity of these segmental interactions leads to the change of chain conformation.

Absorption and PL spectra of rr-P30T in pure CRB and their mixtures with cyclohexane are shown in Figure 1(a,b). In good solvent CRB, the rr-P30T chain adopts an extended conformation where dihedral angles between thiophene rings are relatively small. $^{34-36}$ This allows large extent of π orbital overlapping along conjugated backbone, resulting in relatively long conjugation length. Absorption spectrum of rr-P3OT in this solvent exhibits a broad pattern with λ_{max} at 454 nm, assigned to π - π transition within conjugated backbone of the isolated chain. 37,38 The PL spectrum exhibits a peak at 574 nm accompanied with vibronic shoulder at about 615 nm. When the cyclohexane is added into this system, local environment around rr-P30T chain is altered. The absorption and PL spectra systematically shift to high-energy region upon increasing the cyclohexane ratio. The change takes place in a continuous fashion while the shape of spectra remains the same. The blueshift of about 16 nm is detected when the cyclohexane ratio reaches 100%. The position of maximum absorption and PL emission are at 438 and 558 nm, respectively. The variation of λ_{max} value as a function of cyclohexane ratio is shown in Figure 2. It is important to note that the blueshift of absorption and PL spectra in cyclohexane is not due to the change of dielectric constant of solvent. The use of nonpolar toluene as a solvent for rr-P30T does not provide the same result.

The blueshift of absorption and PL spectra is attributed to the conformational change of rr-P30T in cyclohexane. Previous studies by Kiriy et al. suggest that rr-P30T can form helical conformation in the system of mixed chloroform/ hexane.^{39,40} In this structure, the octyl side chain extends toward the nonpolar medium due to favorable dispersion interaction. The helical conformation also minimizes contact between the polar thiophene backbone and nonpolar hexane. In contrast to our result, the authors observed the growth of three distinct redshift peaks in absorption spectra upon increasing the hexane concentration. As the redshift peaks were still observed at extremely low polymer concentration, it was concluded that the planarization of rr-P30T backbone occurred at a single-molecule level, resulting in the increase of conjugation length. However, the possibility of intrachain aggregation was not considered in their discussion. We believe that the rr-P30T chain also forms helical conformation in cyclohexane. The twisting of thiophene group in the helix interrupts π -electron delocalization, causing the decrease of conjugation length. As the solubility of rr-P30T in cyclohexane is higher than that of the hexane, the magnitude of chain coiling and segmental packing along helical axis are expected to be lesser. Therefore, the intrachain aggregation along helical axis and/or planarization does not occur in this system.

Conjugated polymer in solution is a semiflexible chain. The chain can twist and fold causing physical defects or kinks along the conjugated backbone. Small angle neutron scattering measurements reveal that poly(3-butylthiophene) in nitrobenzene is a semiflexible chain with persistence length of about 14 thiophene units. 41 Study of poly(2,5-dinonyl-pphenyleneethynylene) in toluene also observes the chain bending in dilute concentration.⁴² As the presence of physical defects interrupts π electron delocalization, an effective conjugation length (ECL) of conjugated polymer is normally much shorter than the contour length. To further analyze our result, the ECL of rr-P30T in each solvent is estimated by utilizing optical properties of its oligomers. 43-46 Bidan et al. demonstrate that the absorption energy of regioregular oligo(3-octylthiophene)s (n = 1-6) varies linearly with reciprocal of the number of thiophene rings (n).⁴³ The obtained linear relationship is shown in eq (1).

$$E_{(eV)} = 2.54 + \frac{3.15}{n} \tag{1}$$

The ECL of rr-P3OT in CRB and cyclohexane is estimated by substituting the absorption energy (in eV unit) into (1). This calculation yields ECL of rr-P3OT in CRB and cyclohexane equivalent to about 17 and 11 thiophene units. However,

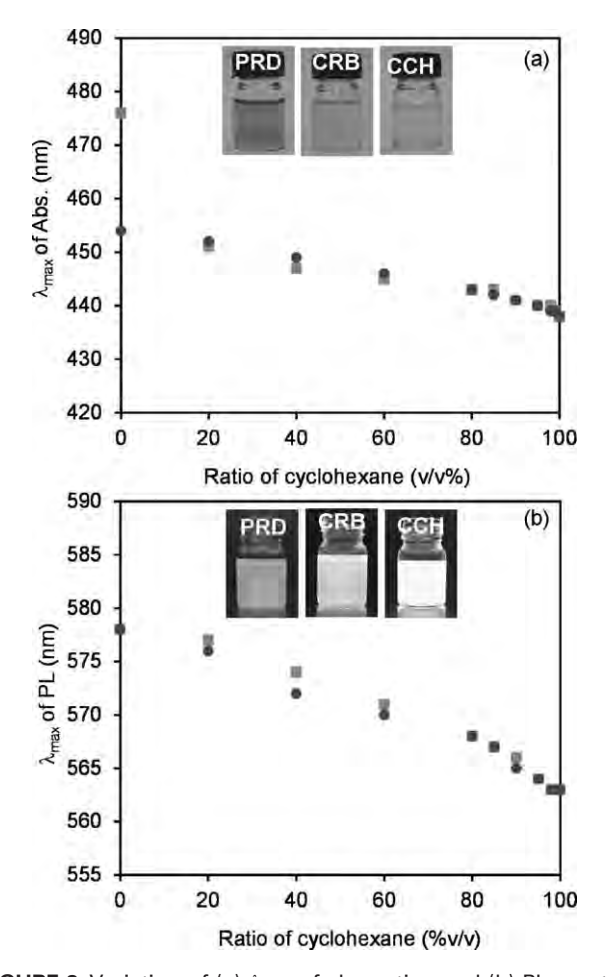


FIGURE 2 Variation of (a) $\lambda_{\rm max}$ of absorption and (b) PL spectra upon increasing ratio of cyclohexane (CCH) in *rr*-P3OT solutions. The initial solvents are (circle) chlorobenzene (CRB) and (square) pyridine (PRD). Insets show photographs of *rr*-P3OT in the pure solvents taken in (a) ambient condition and (b) under UV light irradiation.

several studies have shown that deviation from linear eq (1) occurs when the size of oligomers becomes relatively long. Height Meier suggests an exponential relationship between absorption energy and n as shown in eq (2), which takes into account the convergent behavior of $\lambda_{\rm max}$ of the long oligomers.

$$\lambda_{\max}(n) = (\lambda_{\infty} - \lambda_1)e^{-b(n-1)} \tag{2}$$

The λ_1 , $\lambda_{\rm max}(n)$, and λ_{∞} are the maximum absorption wavelength of monomer, oligomers, and polymer, respectively. The convergent factor b can be obtained by fitting optical properties of oligomers⁴³ and rr-P3OT ($\lambda_{\infty}=454$ nm), which provides the b value of 0.308 (regression coefficient = 0.99). The ECL is estimated by substituting b value into eq (3).

$$n_{ECL} = \frac{\ln(\lambda_{\infty} - \lambda_1)}{b} + 1 \tag{3}$$

The ECL of *rr*-P30T in CRB is equivalent to 18 thiophene units. For cyclohexane system, the ECL is estimated by

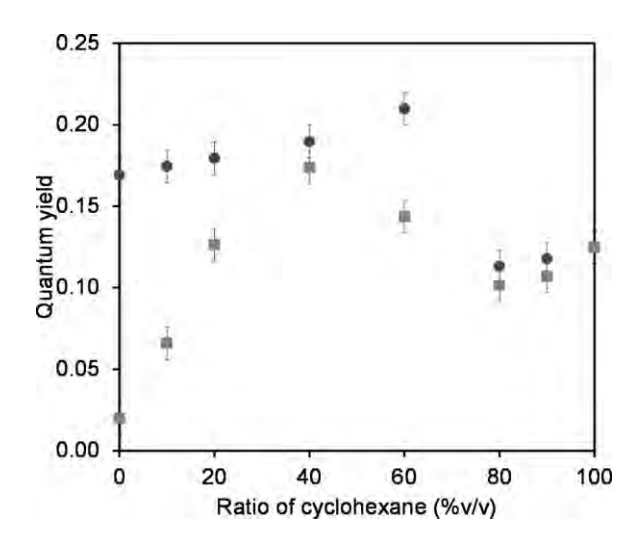


FIGURE 3 Variation of quantum yield of rr-P3OT in mixed solutions. (circle) Mixtures of chlorobenzene/cyclohexane and (square) mixtures of pyridine/cyclohexane.

substituting $\lambda_{\max}(n) = 438$ nm into eq (2), which yields n =9 thiophene units. These data analysis demonstrates significant decrease of ECL in cyclohexane due to the conformational change of rr-P30T.

In the system of PRD, the polymer-solvent interactions are relatively weak. The rr-P30T chains are forced to assemble into aggregates, indicated by the presence of three redshift peaks at about 515, 560, and 616 nm in absorption spectrum [see Fig. 1(c)]. Previous studies suggests that the improved π - π stacking causes the increase of conjugated length within aggregates. 9,24,26,29,47 The PL intensity also drops significantly compared to that of the CRB system. However, the shape and peak position of PL spectrum still resemble those of the isolated chain. This result suggests that the aggregates of rr-P30T in PRD are the nonemissive species. This type of aggregates was also observed in the system of poly(9,9-di(2-ethylhexyl)fluorene).⁴⁸ When a small amount of cyclohexane is added into the system, the redshift peaks in absorption spectrum decrease significantly. The λ_{max} also shifts from 476 to 452 nm. This observation indicates that the enhanced dispersion interaction between octyl side chain of rr-P30T and cyclohexane leads to the dissociation of aggregates. At 40% v/v of cyclohexane, the redshift peaks disappear and the shape of absorption spectrum is similar to that of the CRB system. At this stage, the rr-P30T chains separate from each other. The systematic blueshift of absorption and PL spectra occurs upon increasing cyclohexane ratio to 99% v/v, indicating the conformational change. The decrease of λ_{max} is comparable to the system of CRB (see Fig. 2). Therefore, the polarity of initial solvent hardly affects the magnitude of conformational change of rr-P30T.

The change of chain conformation significantly affects the quantum yield of rr-P3OT. The extended chain in CRB exhibits a quantum yield of about 0.17 \pm 0.01. The addition of cyclohexane ratio up to 60% v/v leads to continuous increase of quantum yield to 0.21 ± 0.01 (see Fig. 3). This is probably due to the change of local polymer-solvent interactions and conformational change of rr-P3OT, affecting the radiative de-excitation pathways of excited π electrons.⁴⁹ However, it is not trivial to separate these two effects because they are closely related. Interestingly, significant drop of quantum yield to 0.11 ± 0.01 occurs upon increasing the cyclohexane ratio to 80% v/v. The discontinuous change of quantum yield indicates an abrupt increase of nonradiative de-excitation processes within the system. This behavior cannot be attributed to the change of solvent composition because the quantum yield remains roughly constant at higher cyclohexane ratio. We believe that the magnitude of chain coiling or shrinking at this stage is relatively large, causing intrachain-segmental interactions. This leads to the drop of quantum yield similar to the effect of interchain/intrachain aggregation. However, the strength of segmental interactions within aggregates is much stronger, leading to the growth of new absorption peaks and further drop of quantum yield. The presence of aggregates in PRD system causes the decrease of quantum yield to about 0.02 ± 0.01. The aggregates dissociate upon increasing cyclohexane ratio, leading to systematic increase of quantum yield as shown in Figure 3. At 40% v/v of cyclohexane, the chains are in isolated conformation. Therefore, the quantum yield of rr-P30T at this stage is comparable to that of the CRB system. The significant drop of quantum yield is detected at higher cyclohexane ratio.

AFM is utilized to investigate the conformational change of rr-P30T. Samples are prepared by dropcasting from different solutions onto flat SiO_x/Si substrate where the isolated chains assemble into large domains. Although the AFM does not directly reveal the conformation of isolated chain, morphology of the assembled domains can reflect the conformation of individual chains. The self-assembling from pure CRB leads to the formation of nanoribbons and clusters [see Fig. 4(a)]. It has been observed in different types of conjugated polymers that their rigid rod nature drives the formation of nanoribbons. 18,50-52 In this structure, the main chains arrange parallel to each other perpendicular to the nanoribbon axis. 7,47,53-57 The width of nanoribbons is defined by contour length of conjugated backbone. The nanoribbons of rr-P3OT in this study exhibit a width of about 60.2 \pm 7.5 nm, consistent with its contour length. When the sample is prepared from PRD solution, spherical nanoparticles with large size distribution are observed as shown in Figure 4(b). We believe that these nanoparticles form in solution due to relatively weak polymer-solvent interactions. The segmental aggregation occurs within these nanoparticles. We note that micron-size particles are also detected in some areas of the sample. The addition of 50% v/v cyclohexane into CRB solution leads to the formation of flat sheet-like structure with homogeneous thickness of about 11.7 ± 1.8 nm [see Fig. 4(d)]. Width of the nanosheets is in a micron range. We suggest that the rr-P30T chains are still extended at this condition. These extended chains arrange into the nanosheets where their thickness depends on number of the stacked



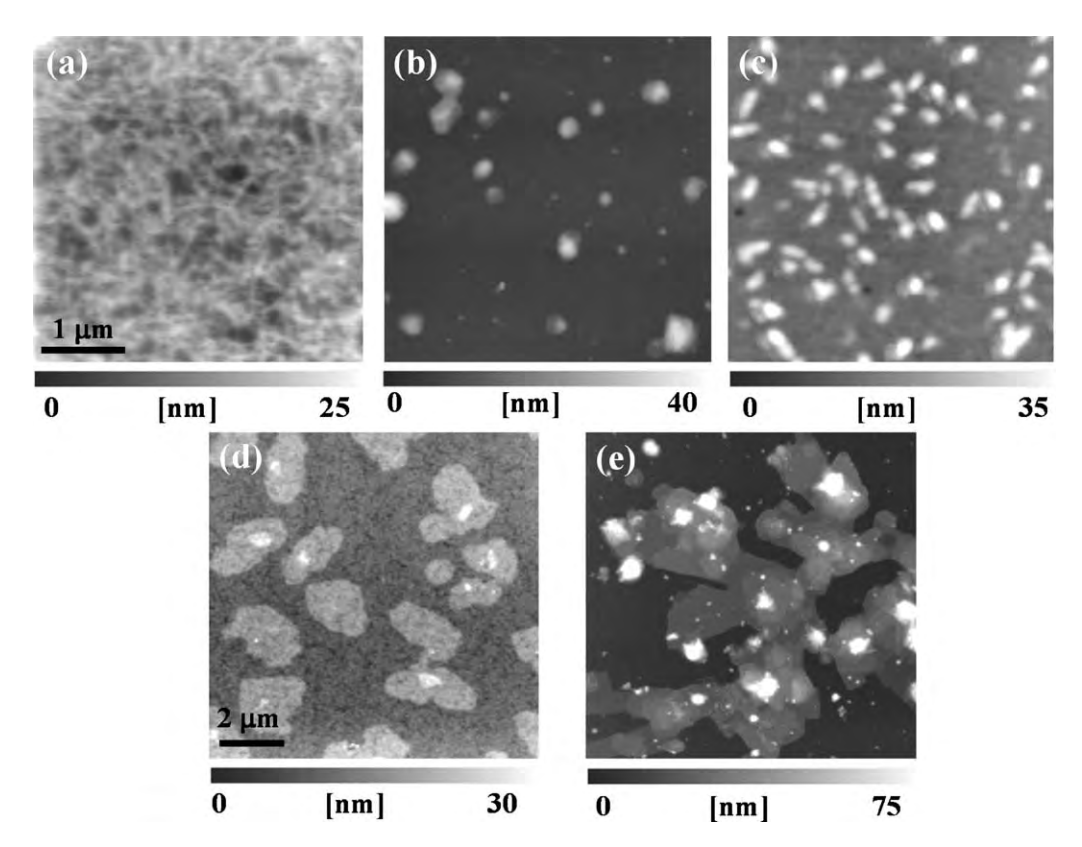


FIGURE 4 AFM topography images of rr-P3OT on silicon wafer prepared by drop casting from 0.05 mg mL⁻¹ solution in (a) chlorobenzene, (b) pyridine, (c) cyclohexane, (d) mixed chlorobenzene/cyclohexane (50:50 v/v %), and (e) mixed pyridine/cyclohexane (50:50 v/v %). Scale bars are 1 μm for (a,b,c) and 2 μm for (d,e).

rr-P30T layers. This hypothesis is parallel with molecular packing model suggested by previous works. 53-57 The width of nanosheets is much larger than that of the nanoribbons, attributed to the decrease of polymer solubility. In the system of PRD and 50% v/v cyclohexane, we also observe the formation of nanosheets [see Fig. 4(e)]. The sheet thickness, however, increases to about 17.7 \pm 2.2 nm. Some nanoparticles are still detected. This result indicates that the addition of 50% v/v cyclohexane causes the dissociation of aggregates. The chains also become extended before the assembling into nanosheets.

The preparation of thin films from rr-P30T solution in pure cyclohexane provides rather different morphology. We observe the formation of dot-like and rod-like structures [see Fig. 4(c)]. The width and thickness of these structures are quite uniform, about 135 \pm 6.8 and 21.8 \pm 3.3 nm, respectively. Some of the dots also arrange into nanorods. Previous studies by Kiriy et al. observe one-dimensional (1D) aggregation of rr-P30T and rr-P3HT in the mixtures of chloroform and hexane, yielding micron-long nanorods. 39,40 Based on the width of nanorods, the authors suggest that helical coils of the polymers aggregate in one dimensional direction. The width of nanorods in this study is much larger than that of the previous studies. It cannot be attributed to the diameter of single helical coil. However, we still observe the aggregation of nanodots in 1D direction. We suggest that multiple helical coils

assemble to form the nanodots and nanorods in this study. The formation of helical coil aggregates has been observed in the systems of polythiophene derivatives. 58-60 It is important to note that the self-assembling of rr-P30T in a random fashion will lead to the formation of nanoparticles as detected in the system of pure PRD.

Intrachain Aggregation in Hexane/Cyclohexane

In this section, the conformational change of rr-P30T is further induced by addition of hexane into the cyclohexane solution. From Table 1, the solubility parameters (δ) of rr-P30T, cyclohexane, and hexane are 18.2, 16.8, and 14.9 $I^{1/2}$ cm^{-3/2}, respectively. In general, the solubility of polymer in solvent is reduced when the difference between their δ values is large.³¹ The δ value of hexane is 1.9 $I^{1/2}$ cm^{-3/2} lower than that of the cyclohexane, which leads to the reduction of rr-P30T solubility. Therefore, the magnitude of helical coiling is expected to increase upon increasing the hexane ratio. Absorption and PL spectra of rr-P30T in cyclohexane/hexane mixtures are shown in Figure 5. The addition of 30% v/v hexane does not cause the blueshift of absorption and PL spectra, indicating that the conjugation length of rr-P30T still remains the same. An increase of hexane ratio to 40% v/v leads to the growth of redshift peaks. The absorbance of these new peaks increases systematically upon increasing the hexane ratio. At 90% v/v hexane, the redshift peaks are at about 525, 558, and 605 nm. As the redshift peaks are

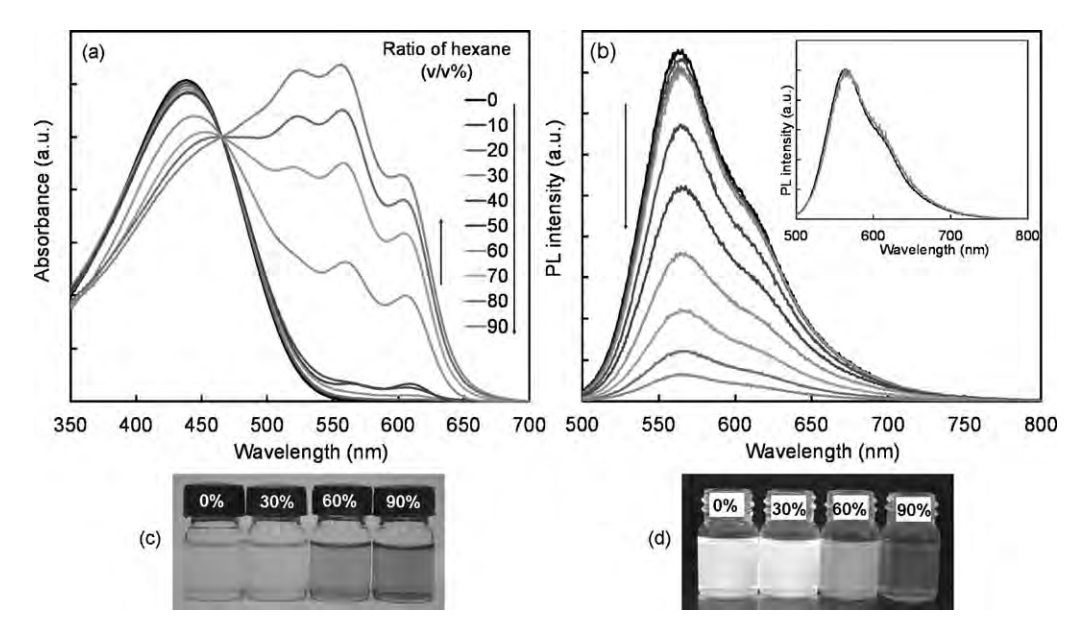


FIGURE 5 (a) Absorption and (b) PL spectra of 0.001 mg mL $^{-1}$ rr-P3OT in mixtures of cyclohexane and hexane. The inset compares PL spectra of rr-P3OT in pure cyclohexane and mixture with 90% v/v hexane. Photographs of rr-P3OT in mixtures of cyclohexane and hexane in (c) ambient condition and (d) under UV light irradiation.

still detected at extremely low concentration of the polymer (see Fig. 6), this phenomenon is likely to occur at a single-molecule level. Kiriy et al. suggests that the formation of helical coil causes planarization of the conjugated backbone, which in turn results in the increase of conjugation length. Their computational study shows that the dense packing of thiophene rings along helical axis limits the dihedral SCCS angle to about 1–6 °C. They also observe that it takes about 12 thiophene units to complete one turn of the helix. However, our calculation by utilizing eq (1) indicates that the fully extended rr-P30T chain $(n=\infty)$ yields $\lambda_{\rm max}$ of about 488 nm. This number is much lower than the detected

 $\lambda_{\rm max}$ values in mixed cyclohexane/hexane. Therefore, the backbone planarization is not a sole factor causing the growth of redshift peaks in absorption spectra. We suggest that the intrachain aggregation also contributes to the increase of conjugation length. The decrease of solvent quality forces the packing of main chain along helical axis, allowing the overlap of π orbitals. The enhanced π electron delocalization leads to the formation of new electronic species with lower HOMO–LUMO gap. The transition between two distinct electronic species is indicated by the observation of isosbestic point in Figure 5. However, it is not trivial to separate the effects from those two phenomena. This is mainly because the conjugated

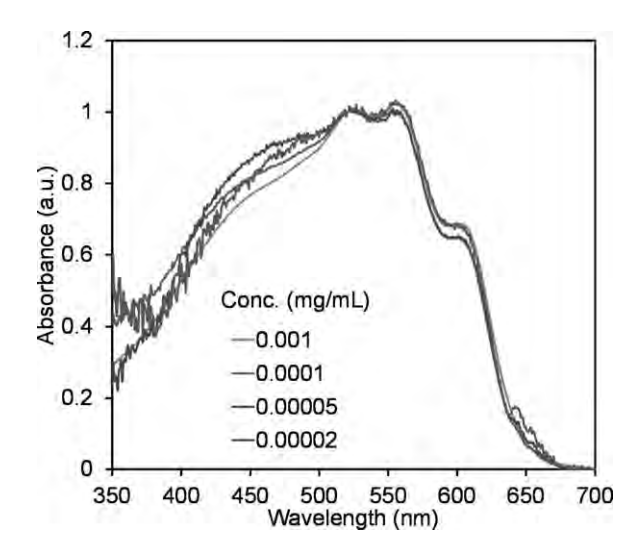


FIGURE 6 Normalized absorption spectra of rr-P3OT in mixture of cyclohexane and 90% v/v hexane. Polymer concentration ranges from 1×10^{-3} to 2×10^{-5} mg mL⁻¹.

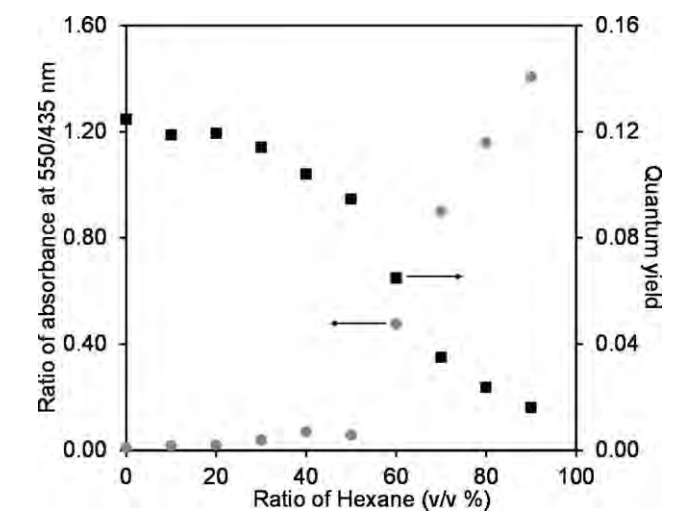


FIGURE 7 Variation of absorbance at 550/435 nm and quantum yield upon increasing hexane ratio. The error bars of quantum yield are omitted for clarity of presentation.



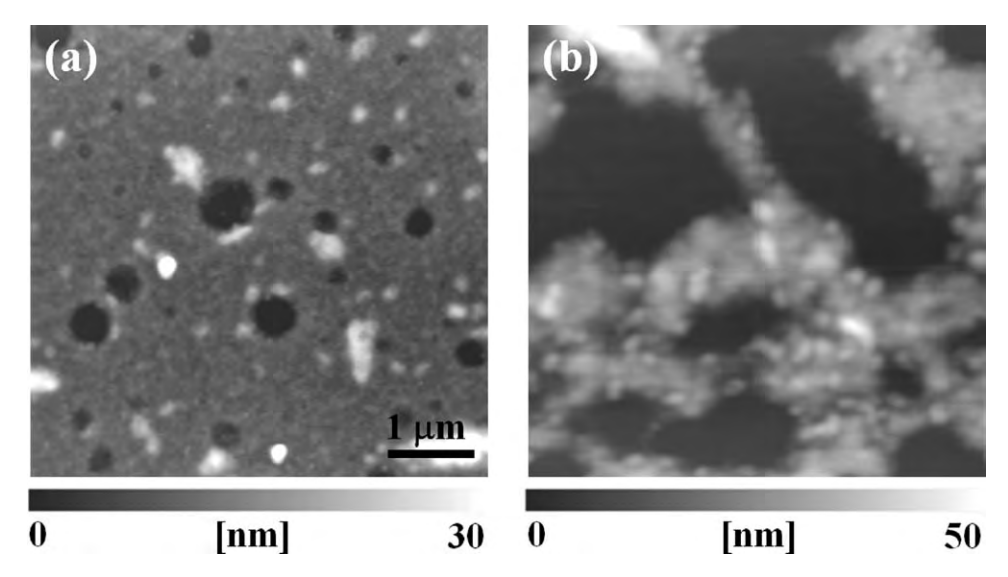


FIGURE 8 AFM topography images of *rr*-P3OT on silicon wafer prepared by drop casting from 0.05 mg mL⁻¹ solution in (a) mixed cyclohexane/hexane (60:40 v/v %) and (b) mixed cyclohexane/hexane (40:60 v/v %).

backbones become planar when they stack on top of each other to form aggregates. 18,21,56

The intrachain aggregation is also indicated by the decrease of quantum yield. Figure 5(b) shows systematic decrease of PL intensity upon increasing the hexane ratio. Correlation between the growth of redshift peaks and quantum yield of rr-P30T is illustrated in Figure 7. The ratio of absorbance at 550/435 nm reflects the aggregate fraction within the system. An increase of hexane ratio to 30% v/v hardly affects the absorption spectra and quantum yield of rr-P30T. The appearance of small redshift peaks at 50% v/v hexane causes slight decrease of the quantum yield. The aggregate fraction increases abruptly at higher hexane ratio, which in turn causes a sharp drop of quantum yield. At 90% v/v hexane, the quantum yield of rr-P30T is comparable to the system of pure PRD, also containing large aggregate fraction. AFM measurements also show supporting results (see Fig. 8). When the sample is prepared from the solution containing 40%v/v hexane, we observe sheet-like structure with thickness of about 8.1 ± 1.0 nm. Some nanoparticles are also detected. At 60% v/v hexane, the amount of these nanoparticles increases significantly. They assemble into large clusters in the thin film. We believe that the intrachain aggregation takes place within these nanoparticles. The formation of large cluster is an indication of sudden decrease of the polymer solubility. It is worthwhile to note that 1D aggregation is not observed in our system. This is probably due to the difference of solvent used in the previous study.

The PL pattern hardly changes upon increasing the hexane ratio (see inset of Fig. 5(b)]. This is in contrast to the results from absorption spectra, which detect a significant redshift. The PL spectrum of rr-P3OT solution containing 90%v/v hexane still exhibits λ_{max} at about 558 nm, which is the same as that of the pure cyclohexane system. This observation indicates that the aggregates in this system are the

nonemissive species. The observed PL intensity arises from the photoemission of nonaggregated segments within the system. We also observe that PL spectrum of rr-P3OT in PRD is detected at lower energy region compared to the system of mixed cyclohexane/hexane. The $\lambda_{\rm max}$ is detected at 574 nm. This $\lambda_{\rm max}$ value is equal to that of the extended rr-P3OT chain is pure CRB. Therefore, the conformation of nonaggregated chain does not change in the PRD. In system of cyclohexane/hexane, the chain form helical coil, resulting in the decrease of conjugation length, before the intrachain aggregation takes place.

CONCLUSIONS

In this study, we have shown that conformational change of rr-P30T chain occurs in cyclohexane solution. The unfavorable interaction between thiophene conjugated backbone and the nonpolar solvent induces chain coiling, which in turn causes the decrease of ECL. When the extended rr-P30T chain in CRB transforms into coiled conformation in cyclohexane, the decrease of ECL is comparable to the shortening of about 6-9 thiophene units. The chain coiling in cyclohexane also causes the drop of quantum yield. The extent of chain coiling is further induced by addition of a nonsolvent hexane. The dense packing of thiophene units within the coiled chain allows intrachain aggregation, which is responsible to appearance of three redshift peaks in absorption spectrum and the drastic drop of quantum yield. We also observe that the intrachain aggregates are the nonemissive species. Our study clearly distinguishes the effects of individual chain conformation and segmental aggregation on photophysical properties of polythiophene derivative.

ACKNOWLEDGMENTS

This research is financially supported by the Thailand Research Fund, Ministry of Higher Education, and Naresuan University (Grant RMU5380017). R. Potai thanks the Office of Higher Education Commission for supporting her PhD scholarship under the program Strategic Scholarships for Frontier Research Network. This work has partially been supported by the Nanotechnology Center (NANOTEC), Ministry of Science and Technology, Thailand, through its program of center of Excellence Network. R. Traiphol thanks Center for Innovation in Chemistry (PERCH-CIC) for supporting some research facilities.

REFERENCES AND NOTES

- 1 Y. Chen, D. Ma, J. Mater. Chem. 2012, 22, 18718-18734.
- **2** R. R. Søndergaard, M. Hösel, F. C. Krebs, *J. Polym. Sci. Part B: Polym. Phys.* **2013**, *51*, 16–34.
- **3** W. Cai, X. Gong, Y. Cao, *Sol. Energy Mater. Sol. Cells* **2010**, *94*, 114-127.
- **4** S. Günes, H. Neugebauer, N. S. Sariciftci, *Chem. Rev.* **2007**, *107*, 1324-1338.
- **5** C. Wang, H. Dong, W. Hu, Y. Liu, D. Zhu, *Chem. Rev.* **2011**, *112*, 2208-2267.
- **6** S. Kola, J. Sinha, H. E. Katz, *J. Polym. Sci. Part B: Polym. Phys.* **2012**, *50*, 1090-1120.
- 7 R. D. McCullough, Adv. Mater. 1998, 10, 93-116.
- 8 I. Osaka, R. D. McCullough, *Acc. Chem. Res.* 2008, 41, 1202-1214.
- **9** F. J. M. Hoeben, P. Jonkheijm, E. W. Meijer, A. P. H. J. Schenning, *Chem. Rev.* **2005**, *105*, 1491-1546.
- **10** O. A. Gus'kova, P.G. Khalatur, A. R. Khokhlov, *Macromol. Theory Simul.* **2009**, *18*, 219-246.
- 11 A. Facchetti, Chem. Mater. 2011, 23, 733-758.
- **12** Z. B. Henson, K. Müllen, G. C. Bazan, *Nat. Chem.* **2012**, *4*, 699-704.
- 13 M. Theander, O. Inganäs, W. Mammo, T. Olinga, M. Svensson, M. R. Andersson, *J. Phys. Chem. B* 1999, 103, 7771-7780.
- 14 J. D. Myers, J. Xue, Polym. Rev. 2012, 52, 1-37.
- **15** S. D. D. V. Rughooputh, S. Hotta, A. J. Heeger, F. Wudl, *J. Polym. Sci. Part B: Polym. Phys.* **1987**, *25*, 1071-1078.
- 16 G. Rumbles, I. D. W. Samuel, L. Magnani, K. A. Murray, A. J. DeMello, B. Crystall, S. C. Moratti, B. M. Stone, A. B. Holmes, R. H. Friend, *Synth. Met.* 1996, *76*, 47-51.
- 17 R. Potai, R. Traiphol, *J. Colloid Interface Sci.* (2013), Available at: http://dx.doi.org/10.1016/j.jcis.2013.04.022
- **18** S. Samitsu, T. Shimomura, S. Heike, T. Hashizume, K. Ito, *Macromolecules* **2008**, *41*, 8000-8010.
- **19** Y. D. Park, H. S. Lee, Y. J. Choi, D. Kwak, J. H. Cho, S. Lee, K. Cho, *Adv. Funct. Mater.* **2009**, *19*, 1200-1206.
- **20** S. Sun, T. Salim, L. H. Wong, Y. L. Foo, F. Boey, Y. M. Lam, *J. Mater. Chem.* **2011**, *21*, 377-386.
- **21** C. Scharsich, R. H. Lohwasser, M. Sommer, U. Asawapirom, U. Scherf, M. Thelakkat, D. Neher, A. Köhler, *J. Polym. Sci. Part B: Polym. Phys.* **2012**, *50*, 442-453.
- **22** T.-Q. Nguyen, I. B. Martini, J. Liu, B. J. Schwartz, *J. Phys. Chem. B* **1999**, *104*, 237-255.
- 23 R. Traiphol, R. Potai, N. Charoenthai, T. Srikhirin, T. Kerdcharoen, T. Osotchan, *J. Polym. Sci. Part B: Polym. Phys.* 2010, 48, 894-904.

- **24** P. Kumar, A. Mehta, S. M. Mahurin, S. Dai, M. D. Dadmun, B. G. Sumpter, M. D. Barnes, *Macromolecules* **2004**, *37*, 6132-6140.
- **25** B. G. Sumpter, P. Kumar, A. Mehta, M. D. Barnes, W. A. Shelton, R. J. Harrison, *J. Phys. Chem. B* **2005**, *109*, 7671-7685.
- 26 R. Traiphol, N. Charoenthai, T. Srikhirin, T. Kerdcharoen, T. Osotchan, T. Maturos, *Polymer* 2007, 48, 813-826.
- 27 R. Traiphol, P. Sanguansat, T. Srikhirin, T. Kerdcharoen, T. Osotchan, *Macromolecules* 2006, *39*, 1165-1172.
- **28** W. Xu, L. Li, H. Tang, H. Li, X. Zhao, X. Yang, *J. Phys. Chem. B* **2011**, *115*, 6412-6420.
- **29** J. Liu, R. S. Loewe, R. D. McCullough, *Macromolecules* **1999**, *32*, 5777-5785.
- **30** J. A. Merlo, C. D. Frisbie, *J. Phys. Chem. B* **2004**, *108*, 19169-19179.
- 31 A. F. M. Barton, Chem. Rev. 1975, 75, 731-753.
- **32** A. Zen, M. Saphiannikova, D. Neher, U. Asawapirom, U. Scherf, *Chem. Mater.* **2005**, *17*, 781-786.
- **33** L. Xue, X. Yu, Y. Han, *Colloid Surf. A: Physicochem. Eng. Asp.* **2011**, *380*, 334-340.
- **34** P. V. Shibaev, K. Schaumburg, T. Bjornholm, K. Norgaard, *Synth. Met.* **1998**, *97*, 97-104.
- 35 D. Curcó, C. Alemán, J. Comput. Chem. 2007, 28, 1743-1749.
- **36** M. Moreno, M. Casalegno, G. Raos, S. V. Meille, R. Po, *J. Phys. Chem. B* **2010**, *114*, 1591-1602.
- 37 X. Qiao, X. Wang, Z. Mo, Synth. Met. 2001, 118, 89-95.
- 38 R. Palacios, P. Barbara, J. Fluoresc. 2007, 17, 749-757.
- **39** N. Kiriy, E. Jähne, H.-J. Adler, M. Schneider, A. Kiriy, G. Gorodyska, S. Minko, D. Jehnichen, P. Simon, A. A. Fokin, M. Stamm, *Nano Lett.* **2003**, *3*, 707-712.
- **40** N. Kiriy, E. Jähne, A. Kiriy, H.-J. Adler, *Macromol. Symp.* **2004**, *210*, 359-367.
- 41 J. P. Aimé, F. Bargain, M. Schott, H. Eckhardt, G. G. Miller, R. L. Elsenbaumer, *Phys. Rev. Lett.* 1989, *62*, 55-58.
- **42** D. Perahia, X. Jiao, R. Traiphol, *J. Polym. Sci. Part B: Polym. Phys.* **2004**, *42*, 3165-3178.
- **43** G. Bidan, A. De Nicola, V. Enée, S. Guillerez, *Chem. Mater.* **1998**, *10*, 1052-1058.
- **44** C.-G. Wu, C.-Y. Lai, N.-L. Hsiao, *Eur. Polym. J.* **2009**, *45*, 879-887.
- 45 H. Meier, Angew. Chem. Int. Ed. 2005, 44, 2482-2506.
- **46** L. Zhang, N. S. Colella, F. Liu, S. Trahan, J. K. Baral, H. H. Winter, S. C. B. Mannsfeld, A. L. Briseno, *J. Am. Chem. Soc.* **2013**, *135*, 844-854.
- **47** J. Liu, Y. Sun, X. Gao, R. Xing, L. Zheng, S. Wu, Y. Geng, Y. Han, *Langmuir* **2011**, *27*, 4212-4219.
- **48** R. Traiphol, N. Charoenthai, P. Manorat, T. Pattanatornchai, T. Srikhirin, T. Kerdcharoen, T. Osotchan, *Synth. Met.* **2009**, *159*, 1224-1233.
- **49** B. Valeur, In Molecular Fluorescence: Principles and Applications; Wiley-VCH: Weinheim, **2001**; pp 8-11.
- **50** R. Traiphol, D. Perahia, *Thin Solid Films* **2006**, *515*, 2123-2129.
- **51** H. Dong, S. Jiang, L. Jiang, Y. Liu, H. Li, W. Hu, E. Wang, S. Yan, Z. Wei, W. Xu, X. Gong, *J. Am. Chem. Soc.* **2009**, *131*, 17315-17320.
- **52** R. Traiphol, N. Charoenthai, T. Srikhirin, D. Perahia, *Synth. Met.* **2010**, *160*, 1318-1324.
- 53 P. Arosio, M. Moreno, A. Famulari, G. Raos, M. Catellani, S. V. Meille, *Chem. Mater.* 2009, *21*, 78-87.



- **54** M. Brinkmann, P. Rannou, *Macromolecules* **2009**, *42*, 1125-1130.
- **55** N. Kayunkid, S. Uttiya, M. Brinkmann, *Macromolecules* **2010**, *43*, 4961-4967.
- **56** M. Brinkmann, *J. Polym. Sci. Part B: Polym. Phys.* **2011**, *49*, 1218-1233.
- **57** C. Melis, L. Colombo, A. Mattoni, *J. Phys. Chem. C* **2011**, *115*, 576-581.
- **58** S. Haraguchi, Y. Tsuchiya, T. Shiraki, K. Sugikawa, K. Sada, S. Shinkai, *Chem. Eur. J.* **2009**, *15*, 11221-11228.
- **59** J. D. Ripoll, A. Serna, D. Guerra, A. Restrepo, *J. Phys. Chem. A* **2010**, *114*, 10917-10921.

- **60** J. Torras, C. Sanchez-Navas, O. Bertran, C. Aleman, *Phys. Chem. Chem. Phys.* **2012**, *14*, 1881-1891.
- 61 S. Siddiqui, F.C. Spano, *Chem. Phys. Lett.* 1999, *308*, 99-105.
 62 S. Tretiak, A. Saxena, R.L. Martin, A.R. Bishop, *J. Phys. Chem. B* 2000, *104*, 7029-7037.
- **63** C. L. Yaws; K. Y. Li, In Thermophysical Properties of Chemicals and Hydrocarbons; C. L. Yaws, Eds.; William Andrew: Norwich, New York, **2008** Chapter 13.
- **64** C. Wohlfarth, In CRC Handbook of Chemistry and Physics; Internet Version 2005; D. R. Lide, Eds.; Available at: http://www.hbcpnetbase.com; CRC Press: Boca Raton, Florida, **2005**; Section 6.